UNIVERSITY OF CALIFORNIA,
IRVINE

Integrated Microfluidic Systems for Continuous Particle Sorting

DISSERTATION

submitted in partial satisfaction of the requirements
for the degree of

DOCTOR OF PHILOSOPHY

in Biomedical Engineering

by

Jason T. Luo

Dissertation Committee:
Professor Mark Bachman, Chair
Professor Guann-Pyng Li
Dr. Edward L. Nelson

2015

DEDICATION

For all my family and friends,

and the memory of my father

TABLE OF CONTENTS

LIST OF FIGURES

ACKNOWLEDGEMENTS

I met my advisor, Professor Mark Bachman, while searching for orders to blindly follow for the next several years. Professor Bachman immediately shot that notion down and told me that he wanted to cultivate decisive, independent leaders for the burgeoning biotech industry, not to bark at mindless pipette-slinging drones. I proved a challenge to him then: convinced that I could not accomplish anything without an authority figure holding my hand, I spent my early days in the lab collecting shaky inconclusive data to bring to my group meetings, along with the trembling question, "Uhh…well, this is what came out…what do you guys think?" Professor Bachman never gave up on me though, and instead gave me every possible chance, however undeserved, to succeed, from pulling late nights in the lab with me cobbling together last-minute ideas to inviting me to crash in his hotel room at various conferences. I will be forever in his debt for his patience, words of wisdom, and taking every opportunity to tell me that engineering is about technology second and about people first.

My co-advisor, Professor G.-P. Li, is the ultimate visionary. I will always be grateful for his ability to see the technological forest through the daily trees of debugging a piece of equipment, for predicting the impact that our work will have in the next several years to come, and for reminding me that innovating for a better tomorrow should be fun and exciting. A lowly graduate student has nearly no business even sharing a room with a man of his standing and ability, much less asking him for his assistance, yet I have not met anyone as generous with his time and energy as Professor Li. This includes meetings originally capped at half an hour that ended up running into the evening because he could not stop his own train of thought; I would sit there struggling to keep up with him, my mind racing and my body now several doses of caffeine behind schedule, yet Professor Li remained animated as ever to the end, leaving me every time with a hearty laugh and a "Good luck!" on his way to his next appointment.

I am especially grateful to our lab's partner in research, Dr. Edward Nelson, an inspiration of a medical scientist and easily the finest mentor-scientist for which a student can ask, for reminding me that we must always give our best efforts as scientists and engineers, because the world deserves that much from us. He easily reigns supreme as the most frightening person I will ever meet in my life, but receiving a good scare from Dr. Nelson simply means he believes in what you are doing and wants it, and you, to succeed. I would like to offer similar thanks to Amanda Laust, Nadia Reihanifan, Alis Asatryan, Kelly Biegler, Ruth Chang, Trisha Westerhof, and Jo Tucker of the Nelson Lab for their generosity in helping me with all things biology, including teaching me to be my own biggest skeptic.

The most personally enriching moments of these past several years were spent with a few special people who began as colleagues but grew into lifelong friends. Throughout my tenure in the lab, Dr. Lily Wu was the older sister I never had, celebrating with me during all the good times, offering optimism during the bad, and constantly reminding me that from whom much was given, much is expected. On a daily basis, Sara Saedinia, our Most Beautiful Girl in the Lab, in addition to her valuable insight on everything from microfluidic protein detection to power supplies for signal amplification, tolerated my antics, baked me birthday cakes, struggled together with me through bleary-eyed late nights of groping for experimental data, and in general provided smiles, hugs, and laughter at all the right times. Similarly, Renee Pham, our lab

manager extraordinaire who had the misfortune of sitting next to me for several years, grew into a formidable verbal sparring partner who never hesitated to first put me in my place, and then suggest yet another gluttonous expedition at the barbeque joint of her choice. Finally, Maryam Shakib's ongoing display of courage, grace, and tenacity in the face of adversity reminds me daily that we owe it to ourselves to make the most of every single day that we are for whatever reason alive in this universe.

I would like to acknowledge the many labmates and collaborators over the years with whom I was fortunate enough to cross paths and share ideas. They are, approximately in order of appearance: Austin Moy, Maulik Patel, Sameeran Kunche, Peng Zhang, Roger Shih, Mark Merlo, Nick Gunn, Jonas Tsai, Lifeng Zheng, Mindy Simon, Crystal Rapier, Muranami Akira, Sarkis Babikian, Kevin Limtao, Brian Soriano, Amanda Ngo, Nuthan Hegde, and Mike Klopfer. Richard Chang and Alan Jiang will forever boggle my mind with their magical talents for microfabrication, and I owe those two gentlemen all the beer they can drink for the rest of their lives. Adeela Syed, boss of all things optical, has saved me too many times to count with her expertise, not to mention the steady supply of revitalizing coffee and cookies on her desk.

From the Department of Biomedical Engineering here at UC Irvine, I would like to thank Professors Abraham Lee, Jered Haun, Steven George, and Noo Li Jeon for their words of wisdom, collaborative spirit, and for letting me work and train in their labs. I would also like to thank Cristina Surpless for putting out all my logistical fires and for being the department's resident cool aunt, and Karen Stephens for being a second mom to me and every other student in the department, and perhaps to a few faculty too.

None of this would have been possible without the support of my family. My mother has never hesitated to remind me that giving anything less than my all was to cheat both myself and everyone who had been counting on me. My sister Janet, twenty-seven months younger than me but years wiser in so many ways, loves letting me know that I can always work harder and complain less. Finally, my father always believed that to know a man, simply look at how well he fulfills his duties to his friends and family; he never failed to set the standard in this regard. In a slightly different world, perhaps one in which he might have enjoyed the same opportunities that he made possible for me, he would have been the first engineer in the family, and I the second. It is a shame that someone so passionate about gadgets had to miss the biotechnological revolution of which we stand on the cusp; he would have insisted on owning the world's first at-home handheld complete blood counter, for example, and perhaps some sort of all-purpose drug delivery injector from a certain science fiction franchise. He may be gone, but a bit of him will inevitably live on in everything I have built and will build in my life.

This research was supported in part by the National Science Foundation's IGERT program under Award No. 0549479, and in part by the National Cancer Institute of the National Institutes of Health under Award No. P30CA062203.

CURRICULUM VITAE

Jason Luo
Department of Biomedical Engineering
University of California, Irvine
Irvine, CA, 92617

Education

University of California, Irvine, Irvine, CA
Ph.D. in Biomedical Engineering 2015

University of California, Irvine, Irvine, CA
M.S. in Biomedical Engineering 2008

University of California, Berkeley, Berkeley, CA
B.S. in Bioengineering/Materials Science and Engineering 2007

Research

University of California, Irvine, Irvine, CA
MEMS-based microfluidic devices for blood-on-a-chip diagnostics, especially for rare cell detection, isolation, and retrieval.

Research Projects

Lab-on-PCB 2014-2015
Project lead

Adaptation of microfluidic technologies to standardized printed circuit board platform for easy scalability and implementation of existing auxiliary electronic components

Integration of microcomponents onto single platform for seamless connection between reagent input and data output

Collaborative effort with researchers from Department of Mechanical and Aerospace Engineering, University of California, Irvine

Dielectrophoresis for Blood Cell Sorting and Purification 2008-2014
Project lead

Design of a MEMS-based microfluidic system for dielectrophoretic sorting of various mammalian cells, including circulating tumor cells

Collaborative effort with researchers from Department of Medicine, Institute of Immunology, University of California, Irvine

Drug Delivery Contact Lens 2008
Project lead

Designed and fabricated a microfluidic drug delivery contact lens for cornea injury treatment

Mentored high school student assistant

University of California, Berkeley, Berkeley, CA
Pathway elucidation of myopia development in leghorn chicken model

Research Project

Effects of Various Chemical Inputs on Retinal Pigment Epithelium During Myopia Development 2004-2007
Undergraduate assistant

Assist in the design of experiments studying RPE cells extracted from myopic eyeballs

Maintain epithelial cell cultures

Care for live chicken models

Awards

NSF IGERT LifeChips Fellowship 2010-2012
Interdisciplinary training fellowship for research at the interface of nano/microtechnology and life science

Whitaker Foundation Fellowship 2007-2008
For first-year study in biomedical engineering at UC Irvine

Regents' and Chancellor's Scholarship 2003-2007
For undergraduate study at UC Berkeley

Teaching

Biomedical Engineering 121 2013
Quantitative Physiology: Organ Transport Systems

Biomedical Engineering 121 2012
Introduction to Biomedical Engineering

Biological Sciences 93 2008
DNA to Organisms

Biological Sciences 97 2008
Genetics

Publications and Presentations

Luo, Jason, et al. "Dielectrophoresis for the Sorting and Counting of Blood Cells." Lifechips2009 Symposium. UC Irvine, Irvine, CA, January 9-10, 2009 (Poster)

Luo, Jason, et al. "A Microfluidic Device for the Capture, Enumeration, and Isolation of Circulating Tumor Cells." ASME 5th Frontiers in Biomedical Devices Conference. Newport Beach, CA, USA, September 20-21, 2010. (Talk)

Luo, Jason, et al. "A Microfluidic Device for the Capture, Enumeration, and Isolation of Circulating Tumor Cells." LabAutomation 2011. Palm Springs, CA, USA, January 29-February 2, 2011. (Poster)

Luo, Jason, et al. "Dielectrophoretic Purification of Circulating Tumor Cells." 3rd Annual International Symposium on LifeChips. Irvine, CA, February 8-10, 2012. (Poster)

Luo, Jason, et al. "Lateral Dielectrophoretic Particle Sorting Using Gel Vertical Electrodes." BMES Annual Meeting. Atlanta, GA, October 24-27, 2012. (Poster)

Luo, Jason, et al. "Electronic-microfluidic system for sorting particles and whole blood using gel electrodes." Electronic Components & Technology Conference (ECTC) 2013. Las Vegas, NV, May 28-31, 2013. (Poster and conference paper)

Luo, Jason, et al. "Microfluidic Dielectrophoretic Sorter Using Gel Vertical Electrodes." CADMIM IAB Meeting. Irvine, CA, USA, Apr 10-11, 2014. (Poster)

Luo, Jason, et al. "Microfluidic Dielectrophoretic Sorter Using Gel Vertical Electrodes." Biomicrofluidics Vol. 8, No. 3, 2014. (Journal paper)

Luo, Jason, et al. "Lab-on-PCB Device Using Vertical Alloy Electrodes." IEEE Transactions on Components, Packaging and Manufacturing Technology 2015. (In prep)

Luo, Jason, et al. "Switchable Pick-and-Place Vertical Electrodes." Journal of Micromechanics and Microengineering 2015. (In prep)

Technical experience

Biological sciences

fluorescence microscopy, cell culture, tissue dissection, immunohistochemistry, cancer cell biology

Engineering

microfluidic device design, fabrication and operation, electronics for microfluidic devices, photolithography, soft lithography, simulation, data analysis, SEM, machining

ABSTRACT OF THE DISSERTATION

Integrated Microfluidic Systems for Continuous Particle Sorting

By

Jason T. Luo

Doctor of Philosophy in Biomedical Engineering

University of California, Irvine, 2015

Professor Mark Bachman, Chair

Particle sorting, counting, and separation are crucial precursor steps to a host of biomedical assays, and various macroscale tools have been developed over the past several decades in response. In more recent years, microfluidic technologies have gained significant popularity as a means of performing these same tasks and more, all at reduced power, reagent volume, time, and user difficulty. This raises the possibility that every fluidic, optical, and electronic system in a biomedical laboratory could soon be reduced to a microscale equivalent, and incorporated onto a single handheld device, a hypothetical lab-on-a-chip. However, while the sorting technologies at the heart of this new class of device have developed at a dramatic pace, the devices themselves remain costly to fabricate, difficult to manufacture at large scales, and poorly integrated with auxiliary systems such as power supplies and peristaltic pumps. As such, they rarely develop beyond the proof-of-concept stage and have yet to achieve any significant acceptance in the biomedical community. This work seeks to move microfluidic sorters beyond this obstacle. First, it was demonstrated that multiple components could be implemented onto a single platform, eliminating cumbersome external fluidics in the process. Next, methods from the mature microelectronics industry were used to build an electronic microfluidic cell sorter on a printed

circuit board platform, yielding a dramatic improvement in device manufacturability and user friendliness, as well as ease of integration with other electronics, micro or otherwise. Finally, building on this, a method was developed to manufacture large numbers of three-dimensional microelectrodes and then incorporate them into a microfluidic device using pick-and-place methods, again a technique adapted from the microelectronics industry. Together, this shifts microfluidics away from the established standard of cumbersome devices monolithically constructed using costly materials and methods and towards a novel standard of more manufacturable and user-friendly devices, and represents a step towards this class of device gaining mainstream acceptance in the biomedical community.

Chapter 1: Introduction

1.1 *Particle Detection and Sorting in Medicine and the Biological Sciences*

Particle detection, analysis, sorting, and capture play a critical role in any biological or chemical analysis.[1] For biomedical applications specifically, particle analysis is used in everything from diagnosing routine diseases to the development of novel drug delivery systems to cell biology studies towards personalized immunotherapies. An exhaustive review of particle analysis for biomedical applications is beyond the role of this introduction, but several examples are listed below to provide the reader context into the vital role the technology plays in medicine and the biological sciences.

1.1.1 Disease Diagnostics

Disease diagnosis often begins with the analysis of blood and its component cells.[2] For example, medical practitioners have used the presence, absence, and relative concentrations of erythrocytes, leukocytes, and platelets as indicative of certain diseases since the advent of light microscopy. These assays have only grown more sophisticated with increased technology and a modern understanding of immunology.

Additionally, various diseases can alter the physical properties of cells or even introduce whole different cell types into an environment; the detection of these modified cells can play a critical diagnostic role, and the recovery of these same cells might yield therapeutic benefits. A common example is malaria, in which diseased erythrocytes are rendered stiff and less mobile; a system for identifying and capturing these deformed cells might enable a clinician to better identify and treat the disease.[3]

Another common example is solid tumor metastasis, in which malignant cells somehow develop the ability to shed off a primary tumor, invade the patient's circulatory system, and form secondary tumors at distant sites.[4] Significant efforts have gone towards identifying and enumerating these so-called circulating tumor cells for diagnostic and prognostic purposes.[5] Additional, more ambitious efforts have now commenced towards capturing and culture these cells towards developing a more detailed understanding of the mutations behind metastasis, which in turn might lead to personalized chemotherapy.[6]

1.1.2 Molecular and Cell Biology

Particle sorting and analysis is ubiquitous in molecular and cell biology research. The observation of cells, stained or otherwise, under light microscopy was for centuries the backbone of molecular and cell biology.[7] In recent years, fluorescent probes, working in conjunction with FACS and fluorescent microscopy, have provided access into the cellular mechanisms never before observable.[8]

From a more applied perspective, research has progress from simply studying cells to actively harnessing them for therapeutic purposes. To this end, particle sorting plays a critical role. For example, a rare population of fetal bone marrow cells with hematopoietic precursors was identified based on the expression of certain cell surface markers.[9] Significant efforts are also underway to understand the varying paths of differentiation of a seemingly identical population of stem cells.[10]

1.1.3 Synthetic Particle Technologies

Particle sorting is not limited to mammalian cells, either. Polymeric beads have long been ubiquitous in the biomedical laboratory: a prime example is the Dynabead® line of magnetic beads, in use since the 1980s.[11] These superparamagnetic microspheres can undergo a variety of surface treatments, allowing them to target specific cell surface receptors, proteins, etc., both for enrichment and for depletion. A related technology is magnetic-activated cell sorting (MACS), in which nanoscale magnetic beads are functionalized to target specific antigens.[12] The fabrication and use of these technologies depend heavily on the ability to sort and analyze both the magnetic particles themselves and the complexes they form with target particles.

More recent work in droplet science has led to the development of a more exotic concept, that of microparticles for both the discovery and the delivery of therapeutics.[13] It is possible to form emulsions of immiscible phases in which the dispersed phase exists as droplets of very tightly distributed radii and composition. These precisely-fabricated droplets can then be used to deliver equally precise doses of drugs via both oral and injectable pathways. However, as a precursor step, the batch must be rigorously analyzed by various particle sorting technologies to ensure a sufficiently tight distribution.

For drug discovery, droplets have been developed to serve as a novel form of microreactor.[13] Using droplets as encapsulated chambers, researchers are able to combine very precise volumes of reagent for reaction assays. In addition to the expanded experimental capacity, researchers are able to both conserve reagent and better simulate the biochemical reactions within a mammalian cell, itself a sort of microreactor. However, various particle analysis technologies are required to observe and analyze the results of these reactions.

1.2 *Conventional Methods for Particle Detection, Sorting, and Recovery*

A host of technologies has come and gone over the past century to facilitate the study of bioparticles. Indeed, advances in the biomedical sciences are inextricably linked to synchronous advances in enabling technologies. While a complete review of conventional particle sorting techniques is beyond the scope of this document, a short discussion is included to provide the reader some context into the state of the technology and to highlight areas in which microfluidic devices might fill a niche.

1.2.1 Early Methods

Interest in bioparticles naturally began with the examination of blood.[2] Given the limits of nineteenth century technology, most initial technologies focused in visual inspections of samples on glass sides using light microscopy.[14] While crude by modern standards, these early technologies remain in use even today. For example, a complete blood count is occasionally performed by eye, albeit with the use of modern stains.[15] Additionally, the hemocytomer, invented by Louis-Charles Malassez in the nineteenth century, remain a popular method for conveniently estimating a cell count in a suspension.[16] For sorting and processing larger volumes, tools such as filtration and centrifugation became widespread. For example, mechanical filters mounted on standard conical vial are a cheap and easy way of eliminating particles above a certain size threshold, while Ficoll-Paque, a heavy polysaccharide solution for density-based separation, is the standard method for fractionating a sample of whole blood.[17], [18]

These methods, highly innovative for their time and, in some cases, still in widespread use, traded either speed, sensitivity, or both for their simplicity; it was not uncommon for researchers to spend inordinate amounts of time manually counting particles by eye under a microscope and

sorting them using criteria limited by what the human eye could perceive.[14] The advent of flow cytometry has made possible a level of sorting orders of magnitude more sensitive than previous technologies and is at least partially responsible for the surge in biomedical discoveries beginning in the 1980s.[19] Moldavan is credited by most sources as the pioneer behind flow cytometry, with a seminal work describing an electronic method for quantifying particles in a moving stream.[20] Subsequent work attempted to build on combining this with technologies from the inkjet printer industry[21] towards scanning streams of cells for variations in properties ranging from visual appearance to electrical impedance.[22]–[24] However, the truly breakthrough technology remained just out of reach until the end of the 1960s.

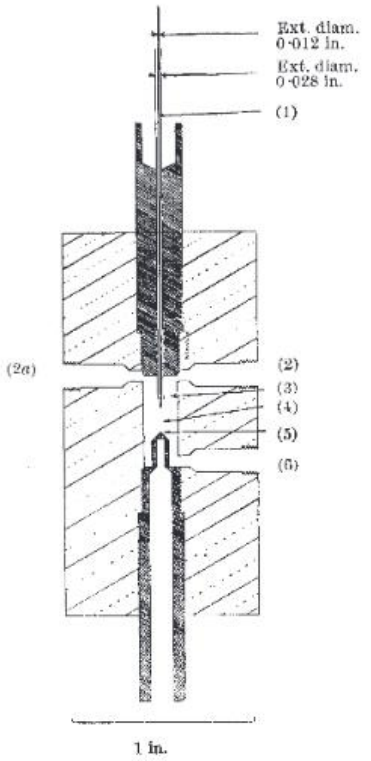

Figure 1.2.1 Early flow cytometry apparatus
Reprinted by permission from Macmillan Publishers Ltd:[22] , copyright 1953

1.2.2 Fluorescence-Activated Flow Cytometry

Today, a specific type of flow cytometry, fluorescence-activated cell sorting (FACS), is nearly synonymous with flow cytometry itself.[25] Invented By Len Herzenberg at Stanford University in the late 1960s[26], [27] and commercialized soon after by BD Dickinson[28], FACS came of age during a time of astonishing advancement across several fields, including computer science, optics, and immunology, all within the context of the War on Cancer.[29] The technology is elegant in its simplicity: briefly, particles are strategically stained with fluorescent dyes prior to flowing into the FACS system. Upon entering the system, they are hydrodynamically focused into a stream one particle wide by a sheath of buffer. Each particle is then passed through the apparatus of lasers; front and side scatter data is collected for each particle. A vibrating mechanism breaks the stream into droplets after scanning, each of which contains a single particle. Depending on that particle's scatter data, a certain electric charge is applied to the droplet. Downstream electromagnets then sort the particles into different batches by charge. All raw scatter data is collected and presented on a computerized display for analysis.

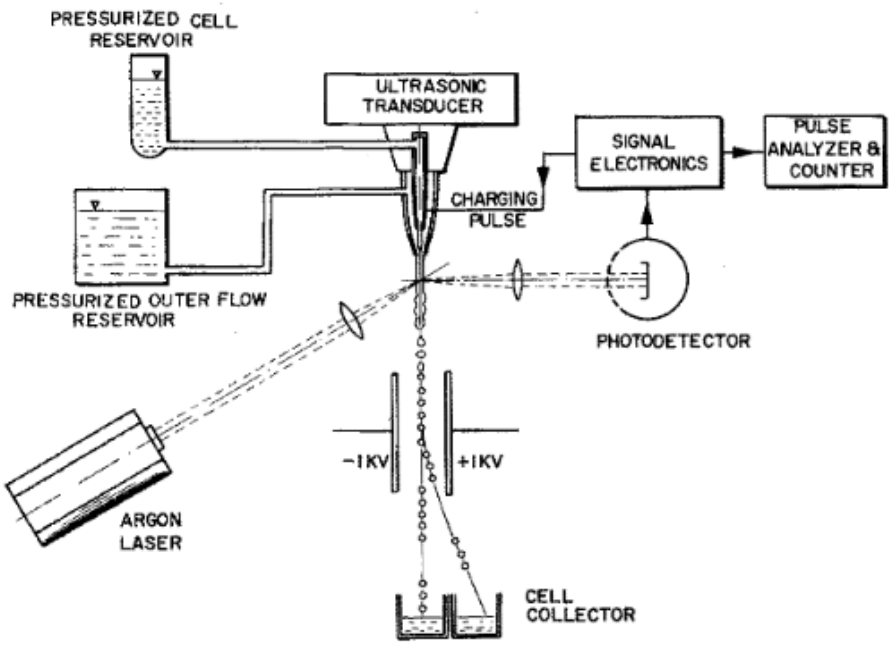

Figure 1.2.2 First FACS apparatus
Reprinted with permission from [27]. Copyright 2003, AIP Publishing LLC.

The impact of FACS on the biomedical community cannot be overstated. By giving researchers and clinicians the ability to perform single-cell analyses on large populations based on a host of parameters, from cell surface antigens to intracellular processes, FACS has revolutionized every facet of biomedical science, from pathology to molecular biology to immunology, and in 2015 is the cell sorting technology against which all others are compared.

However, the technology does leave some room for improvement, even after four decades of iteration.[30] Detection of rare molecules in intracellular compartments remains a challenge, as do the effects of cell autofluorescence and smearing across multiple emission spectra. Finally, FACS is by definition limited to stainable targets, and is of limited use should reagents for targeting a certain molecule be absent, or if the parameter in question is something that cannot be stained, e.g. a cell's electronic properties. Additionally, engineering obstacles persist, such as the

time required to accurately process a desired number of cells, the ability to recover a sufficiently large viable population. Finally FACS comes at a high cost, both in terms of initial setup and on a per-use basis.

1.3 *Summary*

The detection and analysis of rare cells has been crucial for biomedical assays dating back to the nineteenth century. To this end, a large number of technologies have been developed, culminating in FACS, the gold standard in 2015. FACS allows a user to stain for a large number of cellular markers and then rapidly sort them based on these stains. Most importantly, users are free to stain their particles using a limitless number of fluorescent cocktails and process tens of dyes in parallel with each other. Additionally, FACS detection sensitivity is such that a cell as rare as one in ten-thousand can be found. Finally, sorting is automated, and properties of the sample are conveniently displayed for data processing and analysis, thus greatly increasing the number of cells which users can process compared to previous methods.

Despite its advantages, however, FACS has a few drawbacks.[31] Most importantly, it is very costly[32], both in terms of initial setup, continuous maintenance, and on a per-use basis. It is dependent on the infrastructure of a modern biomedical laboratory and consequently cannot be used in remote settings. Additionally, due to spillover effects between colors, care must be taken to select dyes whose emission spectra lie far enough from each other, reducing the practical number of lasers that can be used in parallel, and, related to this, by definition, the use of FACS is limited to detecting "stainable" aspects of a cell; FACS cannot accurately detect variations in properties such as cellular deformability or dielectric constant. This becomes particularly pertinent in applications such as stem cells, which may lack any differentiating markers that can

be targeted by antibody-based stains. Finally, it is still a challenge to process large amounts of cells in a timely manner, and to recover large viable populations. While FACS is continually improving upon these limitations, a new class of device, microfluidics, has developed in the meantime to address these concerns from a whole new perspective.

Chapter 2: Introduction to Microfluidic Devices

2.1 *Microfluidics Overview*

A complete review of the past, present, and future of microfludic technology is beyond the scope of this document. However, a short discussion is included to provide the reader some context into the motivations behind the development of microfluidics, as well as the status of the technology and necessary steps to ensure its continued development in the next several years.

2.1.1 A Brief History

Microfluidic technologies trace their roots back to the golden age of the integrated circuit, when, in 1975, Terry, using methods from the IC industry, developed a silicon chip for gas chromatography.[33], [34] Micromachined out of silicon, this device consisted of an inlet valve, a thermoconductivity meter, and a channel over a meter long, and could separate simple mixtures.

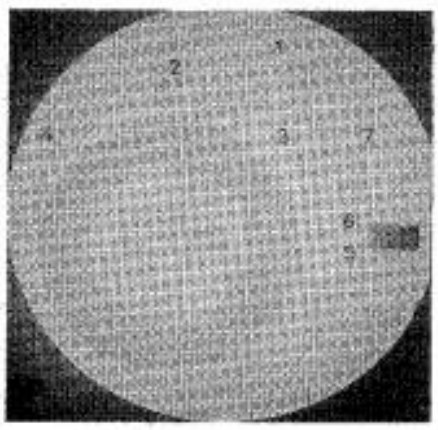

Figure 2.1.1 First microfluidic device
Stephen Terry's microfluidic gas chromatography device consisted of little more than channels wet-etched onto a silicon wafer. Lost to obscurity initially, it would find vindication two decades later. Reprinted with permission from [34] © 1979 IEEE

Terry's work opened the possibility of using semiconductor technologies in applications outside of computing, but in the absence of various other enabling technologies, the concept of microfludic technologies could not yet arrive. Instead, engineers, staying well within charted territories, directed their efforts towards building silicon-based micro-components for use in existing electronic devices.

By the end of the 1980s, however, these small developments in micromachining silicon had amassed enough interest that chemists finally rediscovered the notion of using microcomponents for fluidics, and 1990 saw the emergence of the concept of a microscale total analysis system, since dubbed μTAS. In his pioneering work, "Miniaturized Total Chemical Analysis Systems: A Novel Concept for Chemical Sensing," Manz envisioned miniaturized silicon devices for performing all the steps of common chemical assays, thus heralding the coming of the "Microfluidics Renaissance."[35] Motivated initially by the shortcomings in existing assay techniques, researchers soon discovered that miniaturization had the added benefit of reducing reagent and power required per assay. Additionally, work commenced in applying these novel silicon devices in fields outside of chemistry, such as molecular and cell biology.

However, despite the increased popularity, this remained a niche product of the microfabrication community, as the art of patterning delicate systems out of silicon remained out of reach for all but the experts in the field. All of this changed in 1998, when researchers from the lab of George Whitesides at Harvard University developed methods for building microfluidic devices using elastomeric polymers, dramatically increasing the ease of manufacturing and opening the door to researchers from all areas of biology, chemistry, and physics.[36] Thus commenced an era of enormous expansion for microfluidics, one that that continues to this day.

Figure 2.1.2 Microfluidics Renaissance
Methods developed in the labs of George Whitesides and others in the late 1990s, such as the seven-channel laminar flowstream pictured on the cover of a 1999 issue of *Science*, heralded the modern age of microfluidics. From[37]. Reprinted with permission from AAAS.

2.1.2 Current Status

Since the initial wave of excitement in the 1990s, the nascent field of microfluidics has grown exponentially, with work shifting away from silicon-based microcomponents and towards the design and fabrication of analogs to, and improvements upon, existing macroscale technologies, primarily for biomedical and biochemical applications such as genomics, diagnostics, and detection, though they do find uses in other fields as well.[38]

While a massive library of devices has been developed over the past several years, they all share some common characteristics.[39] At the broadest level, all microfluidic devices focus on manipulating fluids using micron-sized components such as channels, valves, and actuators, and

all manipulations rely to at least a certain degree on a few physical fluidic phenomena characteristic of this particular size scale:

- Fluid flow follows a laminar profile
- Diffusion is the dominant mixing method due to small length scales
- Forces negligible at macroscale, e.g. fluidic resistance and surface tension, become significant

Beyond these general commonalities lies a host of variety. The initial quest for a lab-on-a-chip, i.e. a device incorporating miniaturized versions of all common laboratory instruments, all on one handheld platform, yielded a tremendous volume of results, devices for every step of a typical assay.[40] These devices can perform everything from sample prep to injection, mixing, and separating.[41]–[45] For particle suspensions, they can perform focusing, sorting, trapping, and culturing.[46]–[48] For a clinician, they can perform everything from routine diagnostics to DNA testing to PCR.[49]–[51]

In addition to serving as small versions of existing laboratory technologies, microfluidics have also found use in addressing entirely new obstacles unsolved by previous technologies. Compared to older methods, microfluidic devices are significantly more portable and less reliant on laboratory infrastructure, allowing them to perform in remote locations, a particularly relevant concern in the developing world.[52] Additionally, cost per assay is a high priority in these environments, a concern easily addressed by microfluidic devices built around highly disposable materials such as paper and wax.[53]

For the biomedical research community, microfluidic devices have shown great promise in conducting assays not previously possible, while consuming less reagent and sample than their larger counterparts. For cell biology, microfluidics have proven ideal for the construction of

physiologically relevant three-dimensional *in vitro* models unachievable using traditional methods such as 96-well plates. For example, microfluidic models exist for studying the mechanism of breast cancer metastasis[54] and for the mechanism of axon growth and regeneration.[55]

However, despite this progress, target end-users still see microfluidics as anything from exotic tools with niche applications to gimmicky novelty items. Their skepticism is not without merit, as discussed below.

2.2 *Microfluidics Fabrication, Manufacturing, and Integration*

For the past decade, engineers have focused on exploring novel technologies made possible by microfabrication and fluidics at low Reynolds numbers; this tied in with the tempo of academia, still the driving force behind microfluidics research, which tends to focus on short-term goals and milestones.[56] While this trend has at the expense of longer-term goals such as manufacturability, component standardization, device integration, and user friendliness.

Today, however, the question is no longer whether or not we can build and/or miniaturize a certain device; the answer is an unequivocal yes. As discussed previously, microscale analogs to various lab technologies already exist, and new applications and markets have been identified. Instead, the real conundrum is the matter of where microfluidics can prove themselves most useful in advancing healthcare and biomedical research.

From a more practical standpoint, after the tremendous amount of resources invested in microfluidics prototyping since the late 1990s, the day has finally come when engineers can no longer devise a novelty technology and then shelve it immediately after publication. Instead, engineers must deliver on the claims made over the past several years, justifying the tremendous

resources invested in this field since the 1990s. Finally, if nothing else, there exists a strong financial incentive for the microfluidics community to gain mainstream acceptance.[57]

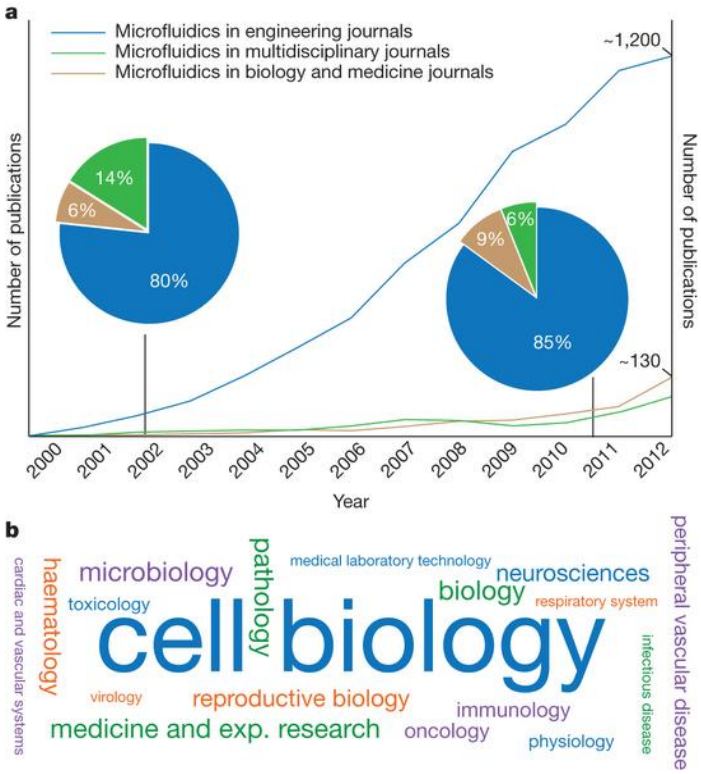

Figure 2.2.1 Trends in microfluidics research, 2000-2012
The field of microfluidics has experienced explosive growth since the turn of the twenty-first century. However, its presence in fields outside of engineering itself have stagnated, signaling the technology's inability to establish itself in mainstream research labs. Reprinted by permission from Macmillan Publishers Ltd: [39], copyright 2014.

A major obstacle, perhaps the main obstacle, towards mainstream adaptation of microfluidics lies in the poor usability and manufacturability of the current generation of devices. Current protocols were designed for engineers to rapidly test the wave of novel ideas emerging in the community, but little consideration was given to actual manufacturability. Additionally, user friendliness was de-prioritized, as often it is simply easier in the short-term for the engineer to struggle with a poorly integrated system than to streamline all the components. However, the

community is finally and rapidly evolving beyond that first stage, and microfluidic technologies are on the cusp of a revolution in device design and manufacturing.

2.2.1 Fabrication and Manufacturing

Despite their great variety, for most of their recent history, microfluidic devices have shared very similar fabrication techniques. Initial devices, borne of the semiconductor industry, were fabricated primarily from glass and silicon as both a matter of convenience in that these materials were standards for electronics and practicality in that early microfluidics projects focused on electronic applications.

However, as the field grew, silicon and glass proved non-ideal for most applications. They are brittle, costly to build, difficult to bond together to form fluidic channels, and posed a significant barrier to entry for various communities, such as cell biology and medical diagnostics, that would have otherwise pursued the topic. The search for alternative materials eventually led to the adaptation of soft polymers, favored for their durability and cost; popular early materials included polyurethanes, polyimides, polymethylmethacrylates, and various resins. In 1998, one material in particular, polydimethylsiloxane (PDMS), came to the forefront.[58] A silicone rubber originally used as a surfactant and hydraulic fluid, among other industrial applications, PDMS proved ideal for rapid prototyping for microfluidics. The material is optically transparent, durable, and can be formed into structures as small as a single digit number of microns, well beyond the practical requirements for microfluidics. Additionally, it is possible to perform various surface treatments on the material, such as adding antibody coatings, as well as adjusting its hydrophilicity and hydrophobicity.

Most importantly, PDMS revolutionized the process of soft lithography, greatly reducing the need for a cleanroom and dedicated fabrication staff. Briefly, the process is as follows: a negative of the desired microchannel geometry is fabricated on a hard substrate such as acrylic or silicon using one or more of several possible techniques, such as micromachining, photolithography, and/or wet or dry etching. Wet PDMS is primed by stirring in its curing agent to for m a thermoset polymer; a viscous fluid, this is poured over the mold and allowed to cure, a process that occurs over a period of one to twenty-four hours, depending on temperature. Upon setting, the PDMS component can be gently delaminated and its microchannels sealed and used.

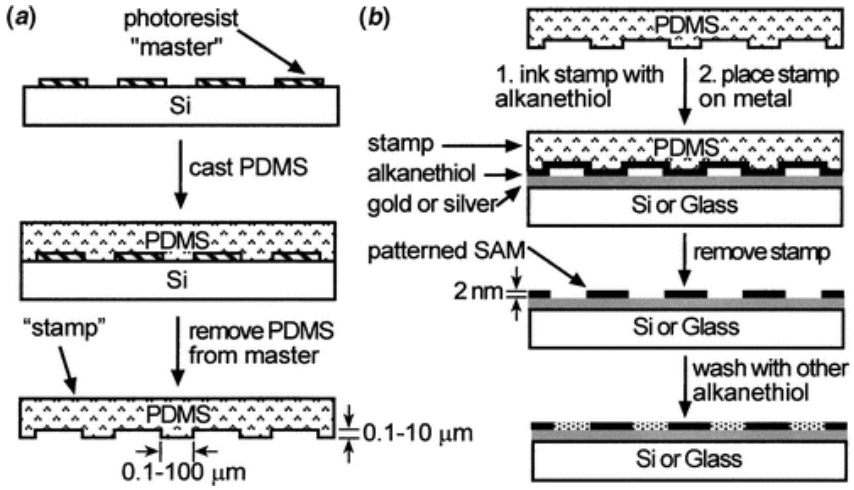

Figure 2.2.2 Soft lithography process
The so-called Microfluidics Renaissance culminated in the introduction of various soft lithography methods for rapid prototyping. The development of these protocols lithography heralded the dawn of a new era in bioMEMS. Reprinted with permission from [59].

Despite its pioneering role and continued widespread use in rapid prototyping, PDMS displays several drawbacks preventing it from rising beyond the proof-of-concept stage. Most glaringly, as a soft thermoset polymer with a relatively long cure time, it is incompatible with

large-scale manufacturing procedures such as hot embossing, injecting molding, or machining.[39]

The microfluidics community has thus begun a new search, this time for materials retraining all of the advantages of polydimethylsiloxane but without the biochemical and manufacturing concerns. The search intuitively begins with polystyrene, the staple polymer of the biology community for the past five decades.[60] Some inertia initially existed over the adaptation of a thermoplastic material that required hot embossing and injecting molding vice soft lithography, but protocols now exist to address these concerns.[61]–[64] In fact, over the past several years, the material has gained some traction in the microfluidics community: advantages include its high manufacturability relative to PDMS and compatibility with standardized protocols in molecular and cell biology.[65], [66] Other commonly used thermoplastic materials, such as PMMA, polycarbonate, polyurethane, and cyclic olefin polymers, share the same manufacturing benefits of polystyrene, though they do lack an established place in the bioscience community.[67]–[71]

Paper microfluidics have enjoyed a steady rise in popularity since its introduction about ten years ago.[72] Pioneered in the Whitesides lab as a new class of "extremely low-cost microfluidics," paper microfluidics and their cloth cousin[73] improve upon traditional microfluidics in that they require very little external instrumentation to either fabricate or operate: fabricators define channel geometry by selectively soaking a hydrophobic material such as wax[74] into the paper substrate, and users need only physically apply their fluidic samples to the defined inlets, after which capillary action takes over to drive the fluid through the channels.[53] Additionally, their significantly reduced cost compared to traditional microfluidics means greater disposability, and their nearly two-dimensional form factor enables a user to carry

significantly more devices to the point-of-care.[75] Finally, there already exists a very mature field of paper-based colorimetric assays which can be incorporated onto a paper-based microfluidic platform.[76]

2.2.2 Integration

The quest for novel materials and manufacturing methods, though vital steps, are merely stepping stones towards a more overarching obstacle: integration. In the context of microfluidic devices, full integration means that a patient, researcher, or healthcare professional can enter an input, namely a biological sample, and have the platform output a result, e.g. the desired information contained in the fluid, if the device's mission is diagnostic, or a product chemical in the case of a chemistry platform.[57] Up to this point, have paid little attention to developing the integration technologies required to drive microfluidics into the mainstream.[77] As microfluidic devices approach their era of commercialization, however, integration has finally risen to the forefront; no longer can a prototype pass for a finalized product.[78] More and more, a design engineer must consider the final device when beginning development of a new concept instead of diving headlong into a novel micro-component that might not work in conjunction with any other.[56], [77]

The exponential rise in the development of novel microfluidic technologies for biomedical applications came at the expense of its predecessor field, that of miniaturizing seemingly mundane devices for supporting roles within existing electronic devices. The field has now come full-circle, and the need for these supporting components has returned, this time for use in microfluidic devices themselves; indeed, omitting this and requiring that a user performs one of the steps of an assay off-chip renders the lab-on-a-chip a misnomer. Examples of necessary

components include miniaturized valves, interconnects, signal generators, power sources, mixers, optics, and the substrate onto which these components are mounted.[79]

However, an entire line of auxiliary devices means little given the current lack of standardization within the microfluidics community. Because researchers have focused on developing and presenting individual components in isolation, it remains a challenge to link multiple components of interest into one seamless system. Solving this will require an interdisciplinary effort on the parts of everyone from the electronics engineers to integrate various onboard IC to polymer chemists who must decide on an ideal substrate material to mechanical engineers dedicated to optimizing fluidic interconnects, a deceptively complex task; everyone will have to work cooperatively to ensure component compatibility. Finally, design considerations must be made towards minimizing or eliminating user input as the sample passes between components, to minimize the chance of user error.[39], [56], [79]

Finally, and arguably most importantly, integration refers not only to devices but to the people behind them. The microfluidics community has grown just as rapidly as the field itself, but the ever-expanding population of researchers has not collaborated efficiently,[78] a hindering development magnified by the inherently interdisciplinary nature of the community. For example, the first microfluidics inventors of the modern era were often chemists forced to build for themselves the exotic devices they needed for their experiments. Their methods, e.g. soft lithography, served this original mission well, but were not necessarily designed for applications beyond that. On the other hand, the microelectronics industry does indeed have in its toolbox a host of methods that do scale for mass production. However, these ideas are entering the microfluidics community only now, over a decade after the excitement generated by those early results and the visions of Manz, Beebe, and other leading researchers.

Significant efforts are underway to move the community beyond this hurdle though.[78] For example, the Micro/nano Fluidics Fundamentals Focus (MF3) group, an organized based at the University of California, Irvine, seeks to unite academic researchers with industry developers to accelerate the transition of a novelty technology into a commercialized product. Additionally, companies such as Microfluidic ChipShop GmbH, an MF3 partner, have taken it upon themselves to apply their fabrication expertise to providing microfluidics engineers with a "toolbox" of standardized components, with an eye towards ease of integration of independently designed devices.[80]

2.3 *Microfluidic Particle Detection and Sorting*

Microfluidic technologies have proven particularly ideal for particle detection and sorting.[81]–[86] Aside from the usual advantages of low reagent and power consumption, microscale technologies are able to probe particles using parameters previously inaccessible by methods such as FACS, such as deformability or dielectric constant. They do this using methods ranging from simple microscale-exclusive hydrodynamics to highly sophisticated actuators fabricated using techniques from the semiconductor industry. An exhaustive review of microfluidic sorting technologies is beyond the scope of this introduction. However, a brief sampling across the spectrum of currently available microfluidic technologies is included to provide the reader with a sufficient impression of the state of the art.

2.3.1 Passive Microfluidic Particle Detection and Sorting Technologies

Passive microfluidic particle sorters depend on channel geometry and fluidic properties unique to the micron scale. Most such devices sort particles based on size, though a few have been able to do so based on other mechanical properties, such as deformability.

The simplest passive sorter is based on filtration. Microfilters come in several variants. The most basic type consists of a membrane with pores of a fixed diameter, or an array of posts spaced a fixed distance apart, arranged normal to the direction of fluid flow. As the particle suspension passes through the membrane or array, those too large to pass are trapped in the gaps, perfectly analogous to a sieve or a strainer in the macro world.[87]–[89]

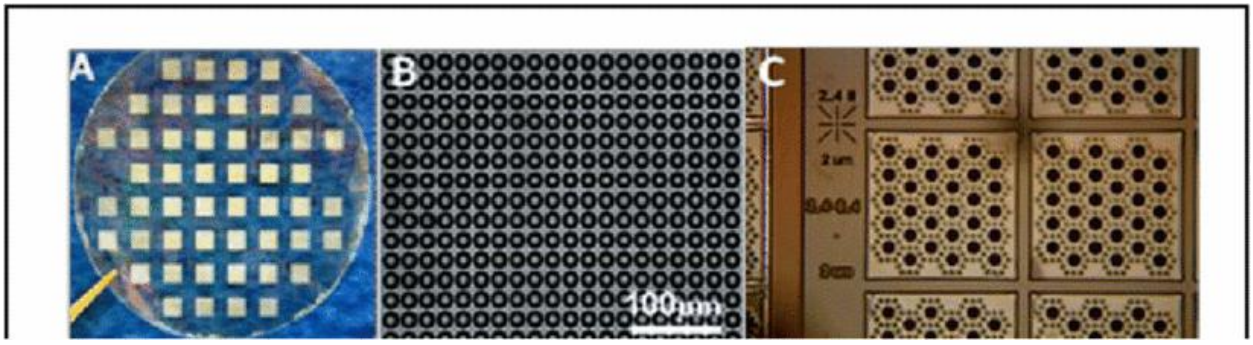

Figure 2.3.1 Microfluidic membrane filter
A: 2-D microfilter wafer. **B:** Close-up view 2-D microfilter with circular pores. **C:** 3-D microfilter for live cell capture. © 2013 IEEE.

However, while simple, this sort of device presents a major drawback in that as more and more particles are trapped in the gaps or pores, the device becomes clogged; flow must be reversed to dislodge and collect the trapped particles. Microfluidic crossflow is one method devised to counter this obstacle.[90], [91] Crossflow systems are designed such that the direction of fluid flow does not run orthogonal into the filter. As a result, particles too large to fit through

the filter slide along the filter are not pressed against the pores, while particles small enough to fit through the pores do so and are removed from suspension. The end result is a suspension containing only the particles unable to fit through the mores.

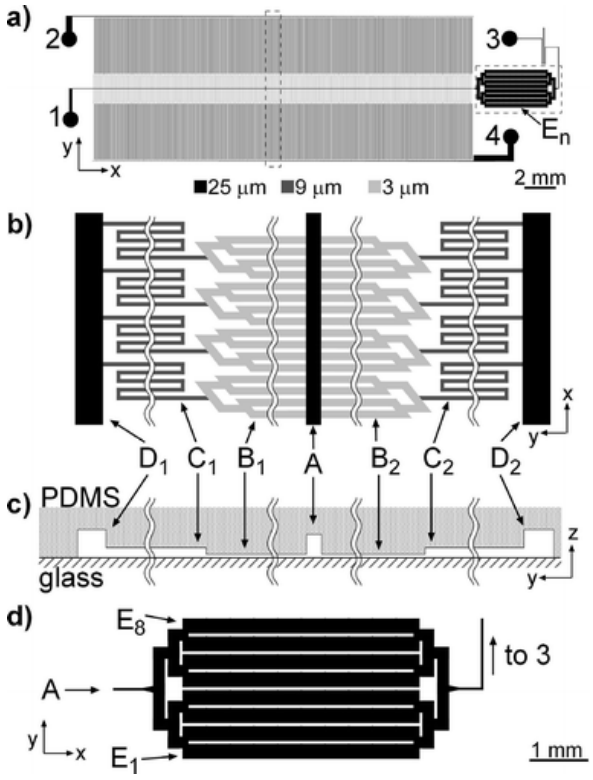

Figure 2.3.2 Microfluidic crossflow filter
A: Drawing of the microfluidic device. Ports labeled 1−4 are blood inlet, perfusion inlet, WBC outlet, and RBC outlet, respectively. **B:** Blowup of a fragment of the separation network outlined with dotted line in **A** turned counterclockwise by 90° with respect to **A**. **C:** Cross-sectional view of channels in the separation network. Dimensions are not to scale. **D:** Blowup of E channels outlined with dotted line in **A**. Channel depths, 25, 9, and 3μm, are gray scale coded in **A**, **B**, and **D**. Reprinted with permission from [92]. Copyright 2007 American Chemical Society.

The simplest passive particle deflector to take advantage of fluidic properties exclusive to the micro world is the pinched flow filter (PFF).[93] The PFF is rooted in a previously developed microfluidic technology, the hydrodynamic focuser, a process comparable to existing bulk focusers such as the fluidic sheath found in flow cytometry systems.[94], [95] Briefly,

hydrodynamic focusing takes advantage of the fact that in microfluidic devices, fluids flow exclusively in a laminar regime, hydrodynamic focusing functions by injecting the particle suspension of interest into a microfluidic channel in between two parallel streams of focusing fluid, usually consisting of the same buffer used in the particle suspension itself. Due to the laminar regime, there is minimal mixing between the particle suspension and the focusing buffer; instead, the particle suspension and the particles suspended within are pinched toward the microfluidic channel's centerline.[96] The amount and exact direction of pinching depends on the relative volumetric flow rates of the three fluids. For example, if all three fluid lines enter the channel at the same flow rate, each will occupy approximately one-third of the main flow channel's width. Alternatively, if one fluid line is significantly slower than the other two, it may be pinched down to a negligible volume. Finally, hydrodynamic focusing has been performed in three dimensions using multilayer microfluidic devices.[97]

PFF builds on hydrodynamic focusing by noting that particles in suspension are not point particles; rather they have a measurable radius, which can be used as a basis for separation. In a PFF system, two side-by-side inlets lead into a main microchannel; the particle suspension enters through one, which the focusing fluid enters through the other. The focusing fluid's volumetric flow rate is significantly greater than that of the particle suspension; as a result, the particle suspension is pinched against the microfluidic channel sidewall, and all suspended particles are pressed up against the sidewall itself, against which they slide and/or roll. However, while particles' centers of mass are theoretically points confined to a one-dimensional flowstream, the particles themselves are not, as they have non-zero radii. As a result, while all the flowstreams that together constitute the suspending medium can be pinched to near-zero width, the particles' centers of mass must maintain a distance of at least one radius length from the wall; under these

conditions they cannot remain in their original flowstreams. Indeed, if the suspending medium is pinched down to a width narrower than that of one particle radius, the particle will actually enter into a flowstream consisting exclusively of pinching buffer.[98]

In this lies the basis for size-based separation. In a mixed suspension of particles of varying diameter, smaller particles, i.e. those with smaller radii, are forced into flowstreams nearer the channel sidewall than those with larger radii. After all particles have been pinched against the channel wall, the channel is expanded to several times its original width, proportionally exaggerating the distance between flowstreams. Particles of different sizes, formerly separated only by their differences in radii, are now separated by several times that distance, and can be easily shunted into different outlets for recovery.

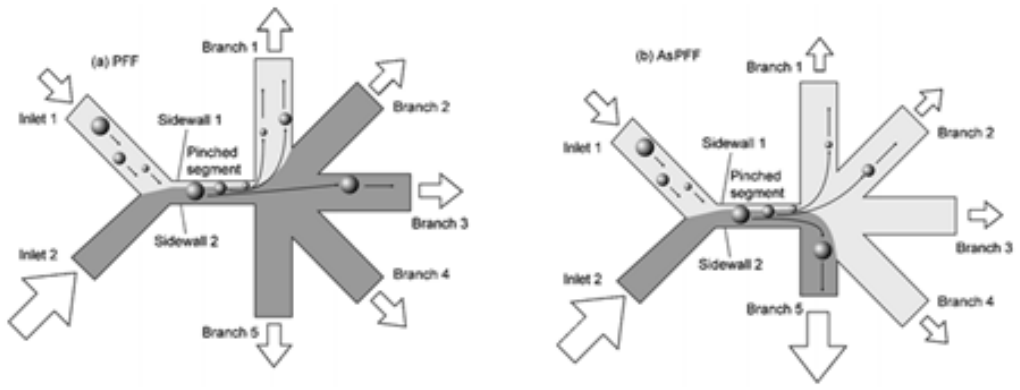

Figure 2.3.3 Pinch flow particle focusing
Schematic diagrams of particle separation: **A:** is PFF, and **B:** is As[ymmetric]PFF. Liquid containing particles is light-colored, and liquid without particles is dark-colored. The size of an arrow represents the flow rate. In PFF, identical branch channels are arranged, and liquid flow in the pinched segment is uniformly distributed. Therefore, Branch 4 and Branch 5 are never used, and the difference in effluent positions of particles is small. In AsPFF, one branch channel (drain channel) is designed to be short and/or broad, and liquid flow is asymmetrically distributed. So all the branch channels are effectively used, and the difference in effluent positions becomes large compared with PFF. Reproduced from [98] with permission of The Royal Society of Chemistry.

A more refined variant of PFF is a process known as deterministic lateral displacement, or DLD.[99], [100] Similar to its predecessor, a DLD device performs size-based separation based on a particle's inability to follow its original fluidic streamline due to its non-zero radius. However, instead of pinching the particles against a channel sidewall, particles are instead flowed through an array of carefully positioned obstacles, comparable to those in a filter-based sorter, only in a DLD device, all gaps are large enough for all particles to pass through. Separation occurs when a particle's streamline touches against an obstacle, while the particle collides into that same obstacle with its center of mass a full radius length away and forced into a new streamline. This process is repeated over a large number of iterations, with the particle being gently deflected to a new streamline with each encounter with an obstacle; the exact geometry of the obstacle array is calibrated such that the effects of each iteration are cumulative.

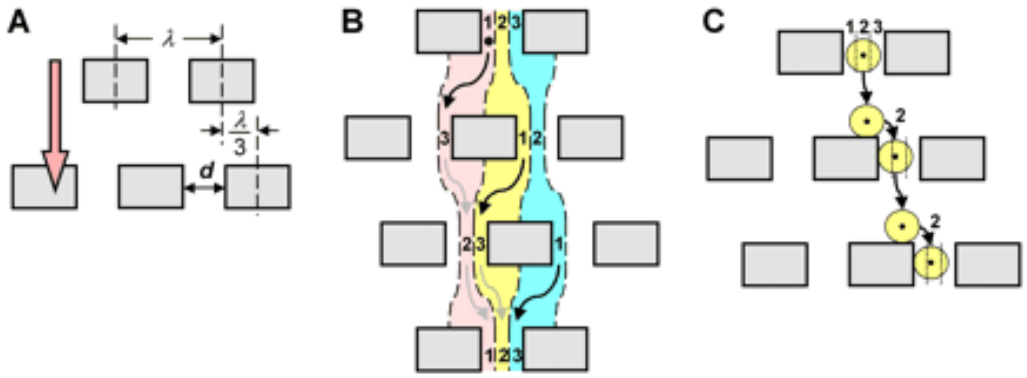

Figure 2.3.4 First deterministic lateral displacement sorter
A: Geometric parameters defining the obstacle matrix. A fluid flow is applied in the vertical direction (orange arrow). **B:** Three fluid streams (red, yellow, and blue) in a gap do not mix as they flow through the matrix. Lane 1 at the first obstacle row becomes lane 3 at the second row, lane 3 becomes lane 2 at the third row, and so on. Small particles following streamlines will thus stay in the same lane. **C:** A particle with a radius that is larger than lane 1 follows a streamline passing through the particle's center (black dot), moving toward lane 1. The particle is physically displaced as it enters the next gap. Black dotted lines mark the lanes. From [99]. Reprinted with permission from AAAS.

One version of DLD uses very high volumetric flow rates to sort particles based on deformability instead of size.[101] The high flow rate causes particles collide especially violently with the obstacles, causing them to deform and even flatten against the obstacle walls. Between two particles of identical radius, the more deformable of the pair can flatten more dramatically, allowing its center of mass to more closely approach the obstacle wall compared to its more rigid counterpart, and thus experience a lesser amount of displacement. This has found applications in separating diseased erythrocytes (red blood cells) from their more rigid healthy counterparts.

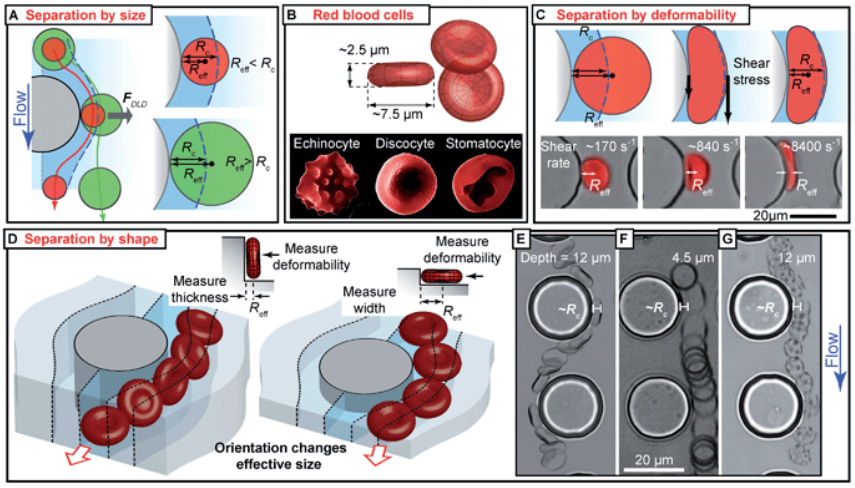

Figure 2.3.5 Deformation-based DLD sorter
Mechanisms of separation by DLD. **A:** Particles with $R_{eff} < R_c$ follow the flow direction and those with $R_{eff} > R_c$ are displaced at an angle to the flow direction. For hard spheres, R_{eff} is equal to the radius. **B:** Red blood cells are normally disc-shaped but they can adopt other shapes when exposed to different chemicals. **C:** Shear forces deform particles changing R_{eff}, and measuring the change in R_{eff} as a function of applied shear rate is equivalent to measuring the deformability of the particle. **D:** R_{eff} depends on the orientation of the particle. Controlling orientation and measuring R_{eff} gives information about shape. It is also possible to measure deformability in different directions. **E:** In a deep device RBCs rotate such that R_{eff} ($<R_c$) is equal to half the thickness. **F:** Confinement in a shallow device means that the cell radius defines R_{eff} ($>R_c$). **G:** An echinocyte with $R_{eff} > R_c$. Reproduced from [101] with permission of The Royal Society of Chemistry.

A method exists for using very high volumetric flow rates but in the absence of any channel features.[84], [102] Termed inertial lifting, or inertial migration, this process relies on unique fluidic properties that arise as Reynolds numbers approach 1, unusual for microfluidic flow. Under these circumstances, the parabolic flow profile of the fluid is sufficiently steep that particles in suspension experience a shear-induced lift force which drives it from regions of high flow towards regions of lower flow, i.e. towards the channel edges, where, in accordance with the no-slip condition, fluid flow rate approaches zero. This is opposed by a lesser wall-induced force, generated by the particles' asymmetric wakes. The equilibrium position for a particle is thus along streamlines near, but not touching, the walls; the net effect scales linearly with particle volume.[84]

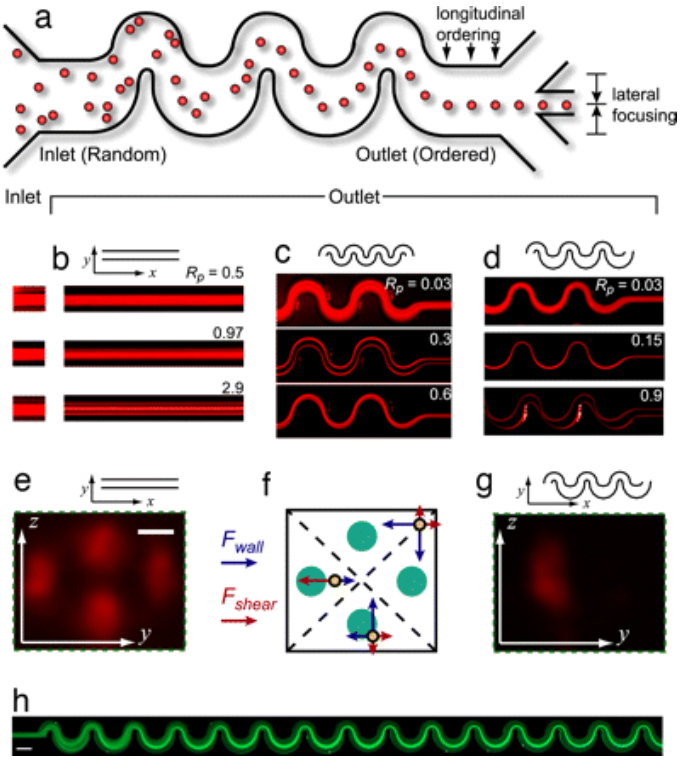

Figure 2.3.6 Inertial lifting for particle sorting
Inertial self-ordering. **A:** Schematic drawing of the inertial ordering process. After flowing through a channel of a particular symmetry, precise ordering of initially scattered particles is observed both longitudinally along the direction of flow and laterally across the channel. **B:** Top-down views of fluorescent streak images of flowing 9-µm-diameter particles in a square channel (50µm) filled with water (density ρ = 1.00 g/ml and dynamic viscosity µ = 10^{-3} Pa·s). Flow is from left to right. The inlet region is shown at the left, where the particles are initially uniformly distributed within the fluid. Longer images show the outlet 3 cm downstream for the channel Reynolds number R_c = 15, 30, or 90 (particle Reynolds number R_p = 0.48, 0.97, or 2.9). Focusing of particles into four single streamlines is observed. From above this appears as three lines with double the intensity in the middle streak–line. **C:** For a symmetric curving channel the symmetry of the system reduces focusing to two streams. Above a critical Dean number (*De*) focusing is perturbed. **D:** For an asymmetric curving system, focusing down to a single stream is favored. Focusing is again more complex as *De* increases. **E:** A confocal cross-section of the rectangular channel shown in *b* shows focusing of particles to the four channel faces. (Scale bar, 10µm.) **F:** Schematic diagram showing the force balance between the shear-gradient (F_{shear}, red arrows) and wall-induced lift (F_{wall}, blue arrows) for particles in three positions. **G:** Confocal cross-section for an asymmetric channel. **H:** Starting at the inlet on the left, a random inlet distribution of fluorescent microparticles is focused to a tight streamline on the right after a short distance. (Scale bar, 160µm.) Reprinted from [102]. Copyright 2007 PNAS.

2.3.2 Active Microfluidic Particle Sorting and Detection Technologies

Active microfluidic particle sorters include one or more miniaturized actuators that exert forces on suspended particles beyond those naturally occurring due to the hydrodynamics of the micro world. Some such technologies are miniaturized analogs of existing, bulk-scale technologies, while others are novel phenomena exclusive to the micro world.

Though designed for protein separation and somewhat outside the scope of processes for sorting microparticles, electrophoresis and blotting deserve brief mention given their obvious candidacy for miniaturization: a ubiquitous process in molecular biology that dates back to the dawn of the field itself, electrophoresis and blotting nonetheless remain cumbersome and time- and resource-intensive., but miniaturization simplifies the process and can even provide a degree of resolution beyond the capabilities of the bulk process.[103], [104] These devices generally consist of a microchannel full of polyacrylamide gel, the same material used in the bulk technology, and a tool for applying direct current along the channel length.[105] Gel and signal properties can be configured based on the desired sorting parameters.[106]

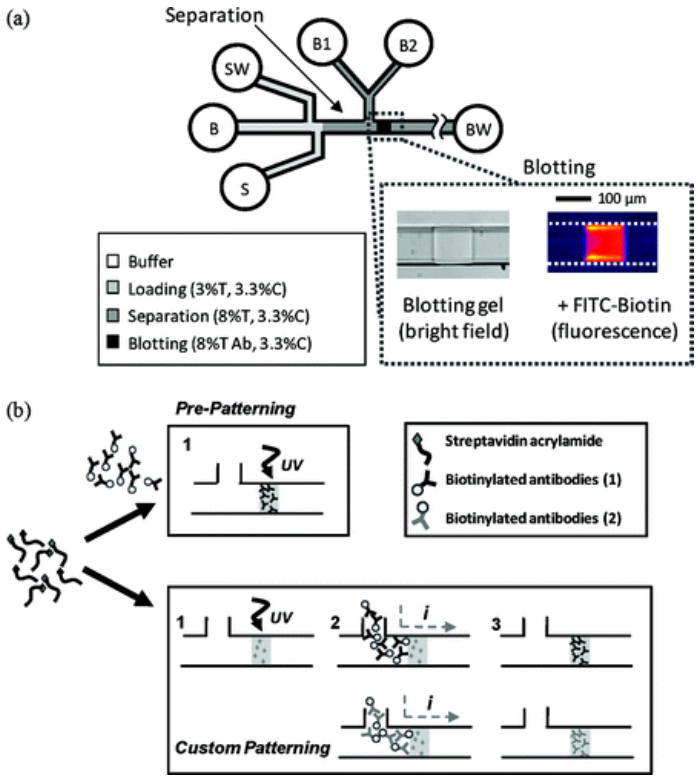

Figure 2.3.7 Microfluidic electrophoresis sorting
Fabrication of microfluidic native PAGE in situ immunoblotting device: **A:** schematic of chip layout (not to scale). Fluid reservoirs are labeled according to contents: S, sample; B, buffer; SW, sample waste; BW, buffer waste. Polyacrylamide gel composition is indicated by grayscale (% T and % C are percentage of total acrylamide and cross-linker, respectively). The inset images show a 10× view of a streptavidin functionalized blotting membrane photopatterned within the channel. **B:** Schematic depicting fabrication steps for blotting membrane: one-step prepatterning strategy and two-step custom patterning strategy. In the custom patterning strategy, loading of the biotinylated antibody is via applied electric current (indicated by i).Reprinted with permission from[107]. Copyright 2009 American Chemical Society.

Magnetic sorters are another technology based on a large existing device. Pioneered in the early 1990s by Miltenyi [12] and dubbed MACS, for magnetically-activated cell sorting, the original device was as crude as flowing cells coated with antigen-specific superparamagnetic beads and flowed through a column of magnetized steel wool. Microfluidic analogs have since driven this relatively primitive technology to interesting new heights, and currently, MACS-based microfluidics systems are available in both label-based and label-free formats. The label-

free method primarily consists of a strategically-positioned magnetic source, often placed alongside a microfluidic channel.[108] As particles flow through the channel, variations in their electronic properties yield different lateral forces in the same magnetic field, and the stream breaks up into several streams as a result. The label-based method is a microscale analog of the bead-coupling technology referenced previously. Briefly, magnetic particles selective conjugated to the target cell via a surface receptor.[109] Upon experiencing the external magnetic field, the beads experience a particularly strong magnetic force and will drag the conjugated cell along, like tugboats in a harbor. In both cases, sorted streams are shunted into different outlets for recovery.

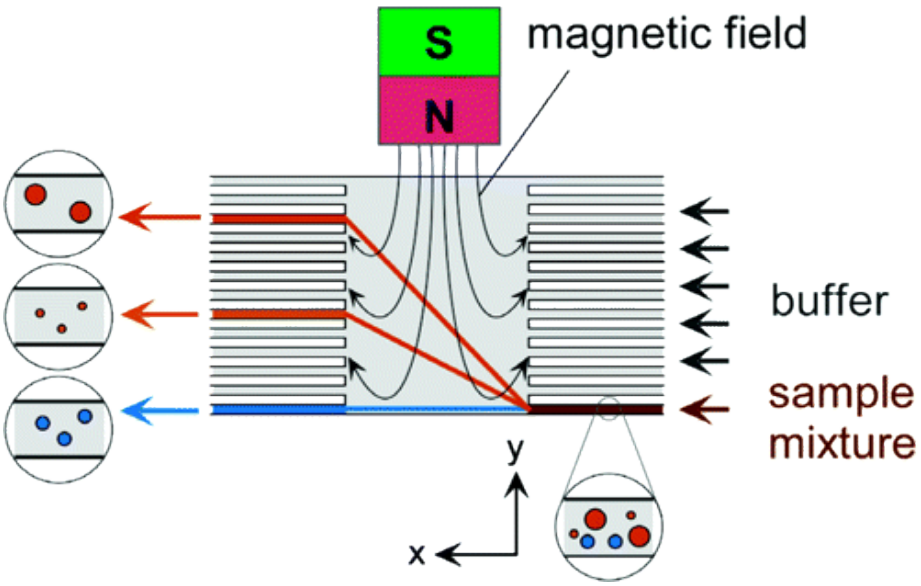

Figure 2.3.8 Free-flow magnetophoresis particle sorting
Concept of free-flow magnetophoresis. Magnetic particles are pumped into a laminar flow chamber; a magnetic field is applied perpendicular to the direction of flow. Particles deviate from the direction of laminar flow according to their size and magnetic susceptibility and are thus separated from each other and from nonmagnetic material. Reprinted with permission from [110]. Copyright 2004 American Chemical Society.

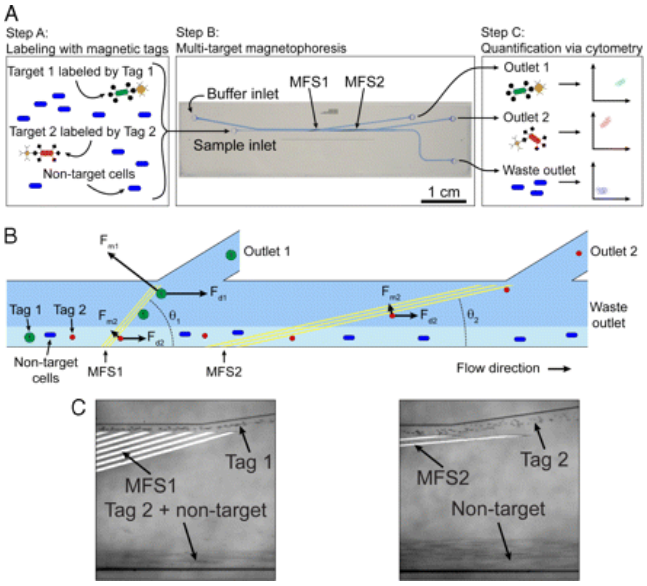

Figure 2.3.9 Magnetophoresis particle sorting
MT-MACS separation architecture. **A:** (Step A) The sample contains an excess of nontarget cells and 2 different target cells (target 1 and target 2) that are labeled with 2 different magnetic tags (tag 1 and tag 2) by specific surface markers. (Step B) The sample is continuously pumped into the device where the 2 target cell types are sorted into spatially-segregated independent outlets. Separation occurs in 2 regions of high magnetic field gradient generated by the microfabricated ferromagnetic strip (MFS) 1 and MFS 2. (Step C) After sorting, the eluted fractions from each outlet are analyzed via flow cytometry. **B:** A free-body diagram showing the balance of forces at the MFS structures. At MFS 1 ($\theta_1 = 15°$), tag 1-labeled target 1 cells are deflected and elute through outlet 1 because $F_{m1} > F_{d1} \sin(\theta_1)$. This is not the case for tag 2-labeled target 2 cells, which are instead deflected at MFS 2 ($\theta_2 = 5°$) because $F_{m2} > F_{d2} \sin(\theta_2)$, and elute through outlet 2. Nontarget cells are not deflected by either MFS and elute through the waste outlet. **C:** Optical micrographs (magnification = 100×) of the tags being separated at the 2 MFS structures at a total flow rate of 47 mL/h (sample = 5 mL/h, buffer = 42 mL/h). (*Left*) Tag 1 is deflected by the steep angled MFS 1. (*Right*) Tag 2 is deflected by MFS 2. Reprinted from [111]. Copyright 2007 PNAS.

Sound-based particle sorting is one example of a microfluidic-exclusive technology. While the technology, dubbed acoustophoresis, is available in many variations, but the general operating principle is that a standing acoustic field (SAW) propagated through a particle suspension is able to exert a force on the particles that scales in accordance with field geometry, acoustic energy density, channel geometry, particle size, and particle and medium density and compressibility.[112]–[114]

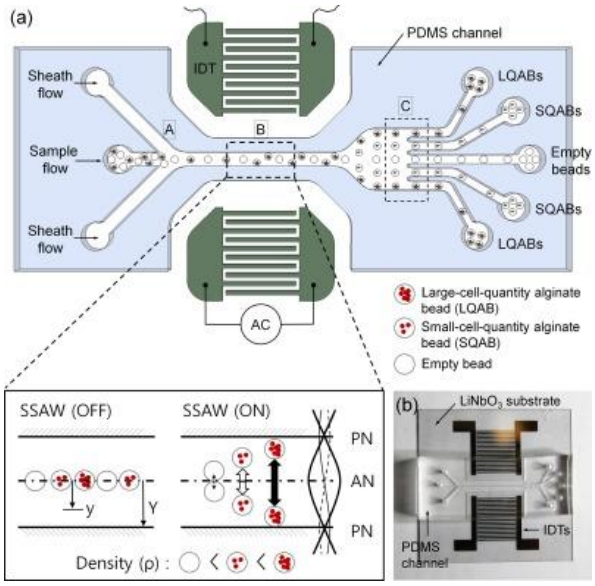

Figure 2.3.10 Acoustic particle sorting
A: Schematic illustration of the working principle of the SSAW for density-based alginate bead separation. **B:**Photograph of the device consisting of a PDMS microchannel and patterned IDTs on a piezoelectric LiNbO3 wafer. Reprinted with permission from [113]. Copyright 2012, AIP Publishing LLC.

Optical sorting systems are another microfluidic-exclusive technology. Based primarily on the concept of optical tweezing, these systems sort particles based on momentum changes that occur as a particle scatters incoming photons emanating from a laser beam.[115] The radiation pressure forces from the beam can sufficiently push hold the particle in a fluidic medium. In microfluidics, the force generated by these beams can yield significant effects, e.g. by shoving particles into different laminar flowstreams. Trapping efficiency is a function of laser wavelength and intensity, as well as the geometry of the optical trap, and can reach 1 pN/mW for 10μm cells.[116]

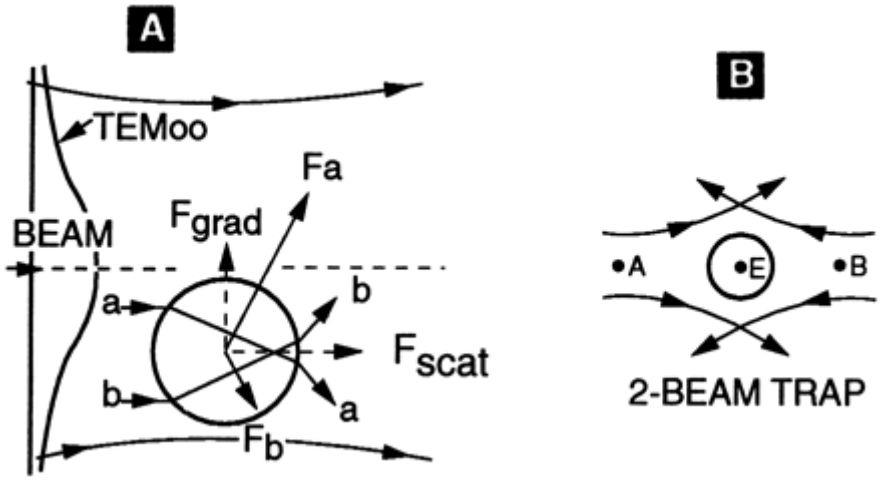

Figure 2.3.11 Optical switching mechanism
A: Origin of F_{scat} and F_{grad} for high index sphere displaced from TEM_{00} beam axis. **B:** Geometry of 2-beam trap. Reprinted from [117]. Copyright 1997 PNAS.

2.3.2.1 Dielectrophoretic Particle Sorting

Dielectrophoresis (DEP) deserves a special mention due to the tremendous amount of interest shown towards it by engineers and researchers in the past decade. A detailed presentation on dielectrophoresis theory is beyond the scope of this paper; instead, a brief synopsis is presented to cover the use of this phenomenon for microparticle separation. When exposed to a non-uniform AC electric field, microscale particles such as polystyrene beads or mammalian cells can polarize and experience translational forces despite their lack of permanent charge.[118]–[120], as the pole nearer the field maxima experiences an force stronger than that felt by its opposing pole towards the field minima. The direction of this force depends on the particle's polarizability relative to that of the medium: if the particle is more polarizable it will migrate up the field gradient (positive dielectrophoresis, or pDEP), while if it is less polarizable it will migrate down (negative dielectrophoresis, or nDEP).[121], [122] The basis of dielectrophoretic detection and sorting, then, lies in tuning the frequency and voltage of the applied signal as well as the conductivity of the buffer such that at a certain configuration, each particle type in a given

suspension experiences a DEP force sufficiently different from that experienced by particles of every other type.[123], [124] Because the DEP force depends on various factors, many of which are intrinsic to the particle, including the particle size, polarizability, and speed of polarization alignment, DEP is a useful tool for probing differences among particles with different dielectric properties, primarily through physical sorting based on the forces associated with DEP.[125]–[129]

For homogeneous spherical particles, the dielectric force is governed by:

$$\vec{F}_{DEP} = 2\pi r^3 \varepsilon_m Re(CM) \vec{\nabla} \left|\vec{E}\right|^2 \quad (1)$$

where *r* is the particle radius, ε_m is the permittivity of the media, *Re(CM)* is the real component of the Clausius-Mosotti relation, and $\vec{\nabla}\left|\vec{E}\right|^2$ is the gradient of the square of the electric field. The Clausius-Mosotti relation is expressed as the following:

$$\frac{\varepsilon_p^* - \varepsilon_m^*}{\varepsilon_p^* + 2\varepsilon_m^*} \quad (2)$$

where

$$\varepsilon^* = \varepsilon - \frac{\sigma}{i\omega} \quad (3)$$

and summarizes the relationship between the polarizabilities of the dielectric particles and the suspending medium.[130] The real component of the Clausius-Mosotti factor ranges from $-\frac{1}{2}$ for particles much less polarizable than the medium to +1 for the opposite case. Thus, while particle size and strength of the electric field as well as the steepness of the gradient contribute towards the magnitude of the dielectrophoretic force, it is the particles' electronic properties that ultimately determines the direction of the force.[128]

Finally, at the microfluidic scale, resisting this dielectrophoresis force is a substantial drag force governed by Stokes's Law; particles reach terminal velocity when these two forces balanced, which for spherical particles is expressed as:

$$v = \frac{\vec{F}_{DEP}}{6\pi\eta r} = \frac{2\pi r^2 \varepsilon_m Re(CM)\vec{\nabla}|\vec{E}|^2}{6\pi\eta r} \quad (4)$$

where η is the viscosity of the suspending medium.[128] Thus, lateral DEP separation functions primarily due to different particles arriving at different lateral terminal velocities: as particles travel downstream in the direction of flow, they shift laterally at different speeds, and find themselves in varying flowstreams leading up to the device exit. Assuming all particles started along the same flowstream, particles are thus grouped into flowstreams based on their physical and electronic properties, and can thus be shunted into different outlets as sorted batches.

2.3.3 Microfluidic Particle Detection and Sorting, In Brief

As shown, a large variety of techniques for microfluidic particle detection and sorting have appeared since the "Microfluidics Renaissance" of the mid 1990s to include both passive sorters that function based solely on hydrodynamic properties at low Reynolds numbers and active sorters that apply external fields to the particles in question. A primary advantage of passive sorters lies in their simplicity, durability, and cost. However, this simplicity is reflected in their performance relative to active sorters: passive sorters are typically just size-based sorters, and can only perform at relatively low flow rates. Active sorters are generally more difficult and expensive to construct and cumbersome to use, but can probe for parameters beyond a particle's geometry and mechanical properties. Additionally, within each of the two categories, each subtype of sorter has its own advantages and disadvantages. Finally, improved techniques in component integration are enabling the use of multiple sorters on a single platform. As such,

there is no “best” method; instead, it is left to the engineer to weigh the costs and benefits of each sorter or combination of sorters when building a microfluidic device.[131]

2.4 *Summary*

The last decade has seen an explosive growth in the development of microfluidic technologies for biomedical applications. Of particular importance is the developing of microfluidic devices for rare particle detection, sorting, counting, and separation, an area in which microfluidic devices have proven especially capable compared to existing bulk technologies. In fact, in addition to performing assays analogous to those previously performed by bulk devices, microfluidics have found applications in whole new roles, ones in which bulk devices have failed to perform despite decades of refinement. These systems vary widely in both form and function, and range from cheap and disposable tools that separate particles solely using fluidic properties unique to the microworld to elaborate devices incorporating electronic components fabricated using high-end cleanroom methods.

However, despite the wealth of innovation in microscale particle sorting and detection strategies, microfludic devices have not gained acceptance in biomedical laboratories and health clinics, partially due to underdevelopment in device manufacturability and integration on the engineering and user ends, respectively. As the field comes of age, efforts should shift from the invention of exotic but inapplicable miniaturized technologies that exist for the sake of novelty, and towards the miniaturization and standardization of all components, including less exciting but equally vital components such as fluidic interconnects and onboard power sources. Designers will also have to develop these devices in the context of a totally integrated system, and not as an

isolated tool. Overcoming these hurdles is crucial towards the development of a true lab-on-a-chip device, and for their widespread adaptation in the biomedical community.

Chapter 3: Microfluidic DEP Sorter Using Gel Vertical Electrodes

3.1 *Overview*

We report the development and results of a two-step method for sorting cells and small particles in a microfluidic device. This approach uses a single microfluidic channel that has (1) a microfabricated sieve which efficiently focuses particles into a thin stream, followed by (2) a dielectrophoresis (DEP) section consisting of electrodes along the channel walls for efficient continuous sorting based on dielectric properties of the particles. For our demonstration, the device was constructed of polydimethylsiloxane (PDMS), bonded to a glass surface, and conductive agarose gel electrodes. Gold traces were used to make electrical connections to the conductive gel. The device had several novel features that aided performance of the sorting. These included a sieving structure that performed continuous displacement of particles into a single stream within the microfluidic channel (improving the performance of downstream DEP, and avoiding the need for additional focusing flow inlets), and DEP electrodes that were the full height of the microfluidic walls ("vertical electrodes"), allowing for improved formation and control of electric field gradients in the microfluidic device. The device was used to sort polymer particles and HeLa cells, demonstrating that this unique combination provides improved capability for continuous DEP sorting of particles in a microfluidic device. This chapter reprinted with permission from [132]. Copyright 2014, AIP Publishing LLC.

3.1.1 Three-Dimensional Electrodes

Traditionally, the electric field gradient necessary for DEP is formed in a microchannel using two-dimensional electrodes strategically patterned on the device substrate.[133] The field tends to be strongest at the edges of these planar electrodes, and weaker in between them. Additionally,

electric field strength dissipates as the field lines extend away from the electrodes and disperse over a larger volume.[134] Together, this forms the gradient for exerting the DEP force on passing particles.

Recently, interest has grown in more precisely refining and optimizing all three dimensions of these field gradients.[135]–[143] Vertical electrodes are one such development in this technology.[134], [144] By expanding on various photolithographic techniques, these electrodes are cast into the walls of microfluidic channels and project vertically-uniform electric fields spanning the microchannel when an electric potential is applied. Vertical electrode devices avoid the two main complications associated with most DEP devices constructed with planar electrodes. Planar electrodes tend to separate particles either by repelling them away from, or trapping them to, the electrodes, making retrieval of sorted particle batches a challenge, necessitating either that the user collect fractions from the outlet[145] or that the device be switched on and off to collect particles caught at the electrodes' edges.[146] Second, in devices utilizing planar electrodes, the electric field gradient can dissipate dramatically as the field lines move away from the electrodes such that particles entering the device near the channel ceiling experience a negligible DEP force.[147] With vertical electrodes spanning the height of the device, one dimension is invariant, effectively creating a continuously operable two-dimensional particle separation profile, eliminating any dead zones and streamlining the particle sorting and retrieval processes.[148]

3.1.2 Micropillar Focusing

Efficient sorting of particles by lateral dielectrophoresis mandates that each particle passes through the DEP section of the device along the same flowline. Because the field gradient is strongest along one channel sidewall and weakest along the other, were particles to enter the

device randomly distributed across the width of the channel, those nearest the strong side might experience a disproportionately large force while those who happen to flow through the weak side might experience little or no DEP force at all. To alleviate this, in the device presented, particles are continuously focused into a narrow stream using two rows of microposts. In this filter-like system, particles above a pre-set diameter are gently swept toward a consolidated flowline until, immediately prior to entering the DEP sorting region, the particles are arranged in a narrow band and consequently experience essentially identical exposure to the electric field gradient and the resultant DEP force is exclusively the result of the particle's physical properties.

However, under the low Reynolds number conditions found in microfluidic devices, particles are difficult to rearrange or shift into different flow lines.[38] Hydrodynamic focusing is often used to generate a narrow stream of particles, such as in a flow cytometer. In such a strategy, separate streams of fluid (sheath flow) are brought in to pinch a main flow stream, resulting in a narrow band of flow.[94], [149] However, this requires the use of a separate flow, and carefully controlled flow rates, adding significant complexity to the system. Several techniques for creating a narrow stream of particles in a microfluidic device have been described including taking advantage of laminar flow properties[38], [93], simultaneously exposing particles to multiple forces, e.g. gravity in field-flow fractionation[123], [150]–[152], or a second electric field gradient such as in earlier 3-D electrode devices[148], thereby forcing the particles to settle into equilibrium streamlines. In the presented device, we have demonstrated efficient passive focusing via an elegant, continuous-flow micropillar system. This focusing apparatus forces incoming particles to enter the DEP device along a narrow stream approximately one particle diameter wide using only laminar flow principles and particle size as drivers for the focusing.

The method works as follows: rows of pillars spanning height of the channel are cast into the inlet channel of the device, spaced several microns apart. Exact sizes for the pillars and gaps can be designed for specific particle suspensions. The row of pillars is angled relative to the direction of fluid flow such that it disrupts but does not impede the movement of particles. Theoretically, row angle can range from 0^o, i.e. parallel to flow, in which case it exerts no effect, up to 90^o, in which case it would act as a traditional size-based filter, completely immobilizing all incoming particles above a certain diameter. In actuality, the angle is very near parallel with fluid flow: in this configuration, buffer and particles below the size threshold pass through the gaps between posts while particles too big to fit through the gaps are nonetheless able to continue along the direction of fluid flow, skimming along the row of pillars. By carefully tuning row angle and gap size, as well as the position of the micropillar row within the microfluidic channel, it is thus possible to gently guide larger particles into a tight stream for collection or further processing downstream. Additionally, the synchronous use of two or more such micropillar rows can effectively direct particles into a flow stream located at any position across the width of the channel and to repeatedly redirect a particle line in the same device. A limited number of variations to this technology has seen application in redirecting particles into different laminar flowstreams in general as well as in shuttling them back and forth through various reagents for strategically applying various coatings in a layer by layer process.[153]–[155] Our use of this focusing step significantly improves the DEP separation process.

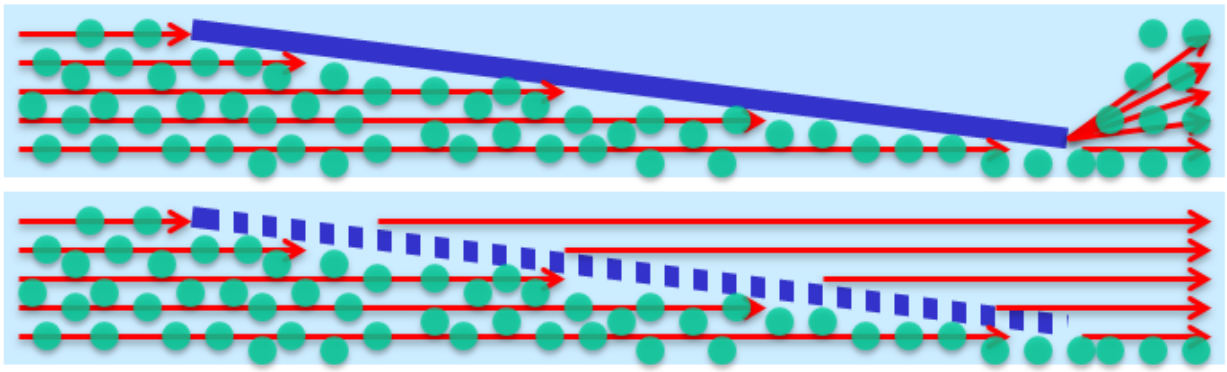

Figure 3.1.1 Micropillar deflection principle
Top: Redirection methods that work at the macroscale, such as physical obstructions, are ineffective at low Reynolds numbers, as particles cannot change flowstreams easily. **Bottom:** Micropillars are one method for bypassing these constraints by deliberately preventing particles from following its original flowstream.

3.1.3 Gel Vertical Electrodes

Photolithographic techniques for the fabrication of microfluidic devices that include vertical electrodes can be challenging. Proposed alternatives include DEP devices employing various forms of insulating barriers to sculpt the electric field. These DEP devices are known as liquid dielectrophoresis (lDEP), insulator-based dielectrophoresis (iDEP), or contactless dielectrophoresis (cDEP) devices.[126], [156]–[162] These devices generally consist of two-dimensional electrodes that inject field lines into the channels. As the field lines expand and develop in the device, they are sculpted using insulating features cast in the channels; the fields are thus forced to expand and contract in specific positions, yielding a precisely-shaped gradients typically aligned orthogonal to the direction of flow to yield lateral DEP sorting.[158], [163], [164]

The gel electrodes presented here are a fusion of microfabricated vertical electrode DEP and iDEP. Using a conductive liquid that cools into a semisolid, it is possible to take advantage of laminar flow techniques to direct the hot material in liquid form into a microfluidic device and to

deposit the hot liquid into strategically placed segments, which rapidly cools into a durable gel structure that resists deformation and flow. Thus, a solid conductive material can be precisely patterned in the device without the use of any difficult cleanroom fabrication techniques.

Finally, the electrodes in the insulator-based DEP devices are by definition separate from the medium; because voltage dissipates as electric field lines travel through the various elements of the device towards to particles of interest, this necessitates the use of large voltage differences across the planar electrodes in order to generate a sufficient field gradient for particle sorting. Conductive materials such as saline gels effectively transfer field lines towards the particles with minimal voltage drops in the electrodes themselves, thus reducing the power required to perform a similar particle separation. Thus, the design presented herein provides additional advantages over previously proposed iDEP designs to improve lateral DEP sorting.[165], [166]

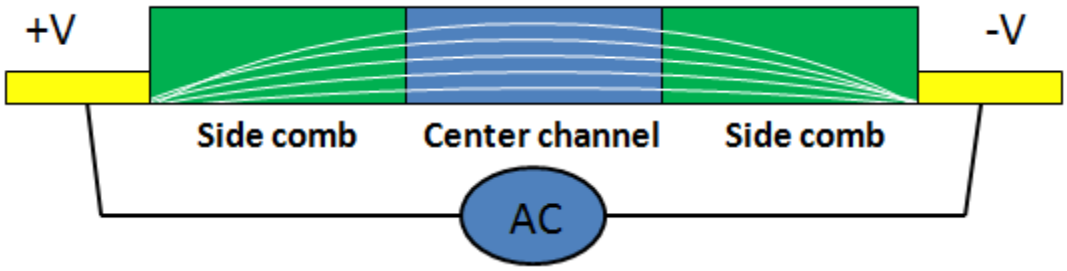

Figure 3.1.2 Development of vertically uniform electric field
Cross-sectional view of main flow channel (blue) and orthogonal side channels (green). Electric field lines emanate from planarized electrodes (gold) and develop in the side channels. When they reach the main flow channel, they are approximately uniform along the z-axis.

3.2 *Methods*

The device combines both passive focusing and active dielectrophoretic sorting. As shown, it consists of an inlet, a focuser that serves to concentrate all incoming particles into a tight stream,

an electronic component that sorts particles by type, and a trifurcation that separates the particles into sorted batches for retrieval. The device is cast in polydimethylsiloxane (PDMS) (Ellsworth Adhesives, Germantown, WI) and aligned over planar Au/Ti electrodes, which are in turn wired to an external electronic AC generator. The PDMS channels are sealed to the electrodes via an acrylic manifold; the bulk particle suspension is connected to the device via this manifold, and is itself driven by an external syringe pump.

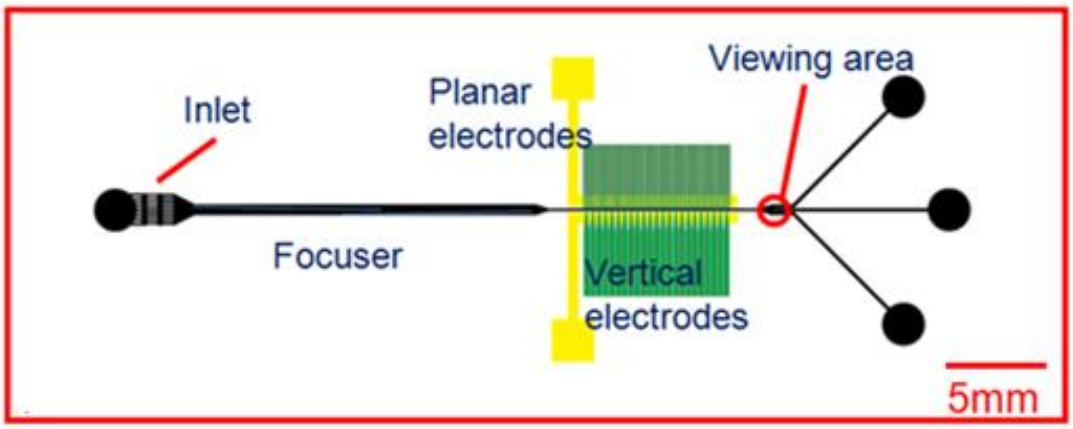

Figure 3.2.1 Device schematic
Device schematic, to scale. Particles enter through the inlet into the PDMS microchannel (black). Particles pass through focusing region and are focused into a tight stream at the centerline of the flow channel before entering the DEP sorting region. AC potential applied through the planar electrodes is transferred by the vertical gel electrodes (green) into the main channel. Signals deflect particles, which then exit through one of three outlets. Particles that experience nDEP exit through the lowermost channel while particles that experience pDEP deflection exit through the uppermost. Separation depends on calibrating the signal such that particles of different type exit through different channels.

3.2.1 Numerical Simulations

Device geometry was guided using coupled physics simulations that combined the results of finite element modeling of fluids and electric fields, with transport simulations of particles subject to forces that result from flow and DEP. All geometries for the simulations were prepared

using SolidWorks (Dassault Systèmes, Vélizy, France), then exported to the appropriate numerical package for calculations. The simulations consisted of three steps. First the electric field was numerically calculated in 2D using COMSOL's finite element solver, using the Laplace equation with Dirichlet-conditions on the electrode edges and homogeneous Neumann-conditions on the outer boundary. Second, the flow of the water was numerically calculated in 2D using COMSOL's finite element solver, using the Navier-Stokes equation for incompressible fluid, and non-slip conditions at the boundary and fully developed flow at the inlet and outlet. Third, custom transport code was written in Python to calculate forces on small particles using (a) known DEP force equations (see above), and (b) drag forces using Stokes's law, and transport them through the system. The real component of the Clausius-Mossotti factor was calculated in the code using known conductivities and dielectric values for the particles' and buffer. The transport algorithm used both the COMSOL fluid flow results and COMSOL electric field results to determine the forces on the particles at each time step. In addition, the transport algorithm checked to ensure that particles could not pass into regions that were geometrically impossible, such as through the small openings of the sieve (if they were too large). 2D modeling assumes a high aspect ratio channel and underestimates spread caused by particles flowing near the top and bottom of the channel. DEP and Stokes forces were calculated using materials properties for particles of various size and material, from 6μm erythrocytes and 20μm tumor cells to 15μm polystyrene spheres.

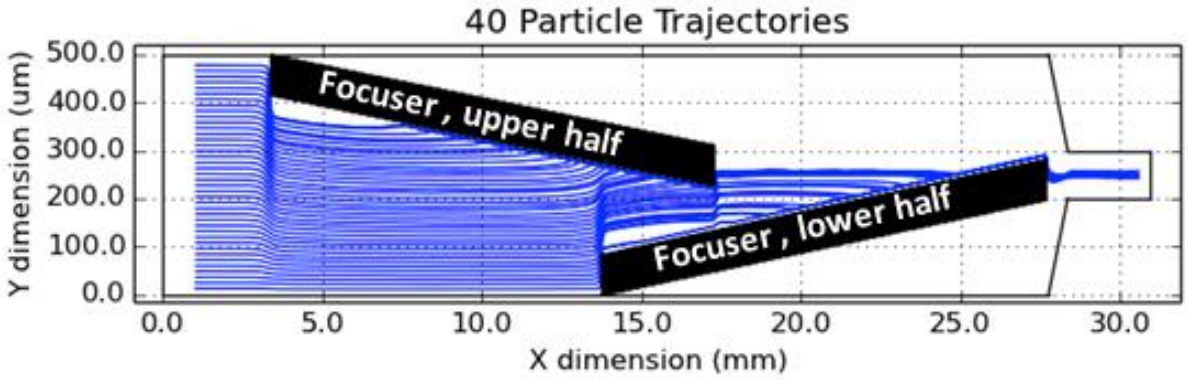

Figure 3.2.2 Simulated particle focusing
Simulated trajectories (blue) for 40 individual 10 µm particles distributed across width of inlet as they flow through two angled rows of pillars (black). Device length is compressed to facilitate imaging.

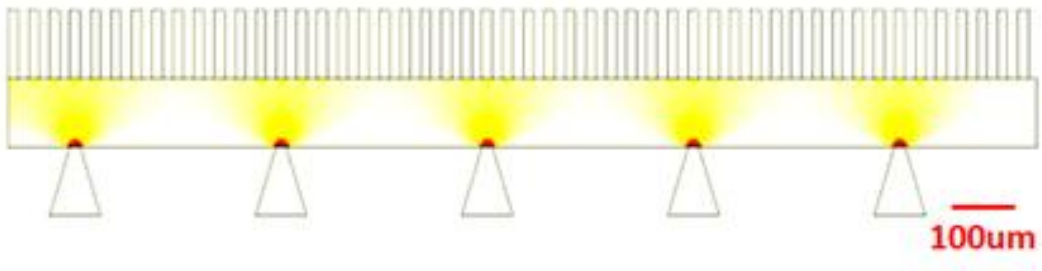

Figure 3.2.3 Simulated electric field gradient geometry
Numerical simulation of non-uniform electric field across width of DEP sorter. Planar electrodes are located along top and bottom edges of schematic. Asymmetric distribution creates field gradient spanning width of channel (denoted in red to yellow color map of electric field). For viewing convenience, only five electric field gradient repeating units are pictured; actual device contains 23 such repeating units. All features drawn to scale.

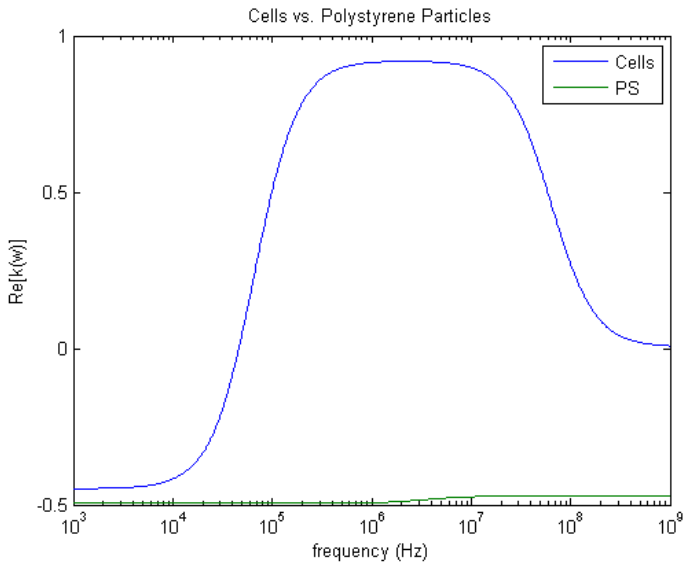

Figure 3.2.4 C-M factors for PS beads vs. HeLas
The real component of the Clausius-Mossotti relation for both mammalian cells and polystyrene beads in low-conductivity buffer was plotted in MATLB using values derived from the literature. Real components were exported and applied to the Python algorithm to determine the exact DEP force experienced by a particle under a certain signal. A cell's combination of an insulator bilayer over a conductive cytoplasm yields a curve that spans the entire theoretical range of real C-M values, while polystyrene's low conductivity and permittivity keep it near -0.5.

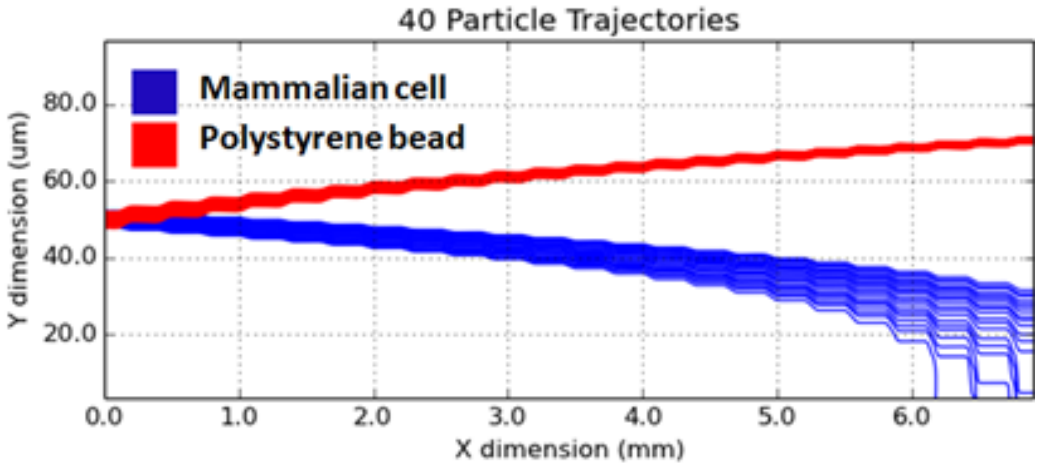

Figure 3.2.5 Simulated DEP separation
Calculated trajectories for low dielectric constant polystyrene particles (red) and high dielectric constant mammalian cells (blue) in low conductivity buffer passing through entire length of DEP sorter at 3 MHz and 50 Vpp and 1µL/min. Schematic is compressed along x axis for visualization. Cells are attracted to the field maxima and trend towards lower edge of device while polystyrene attracted to toward the field minima and trend toward the upper edge of the device.

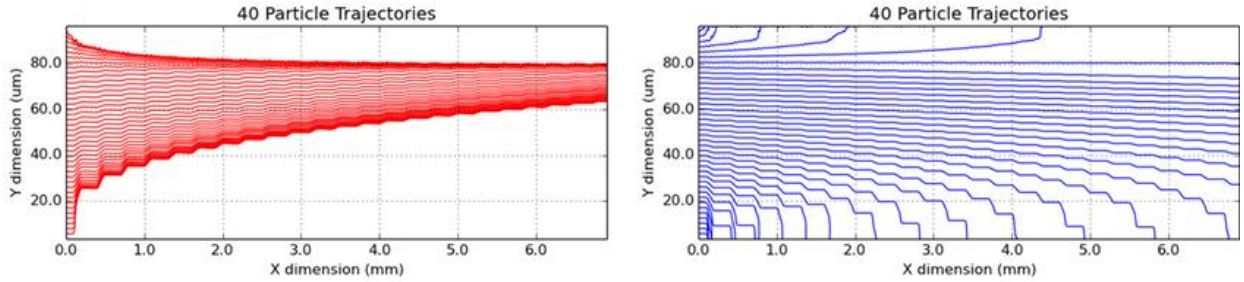

Figure 3.2.6 Simulated DEP separation of unfocused particles
Numerical simulations of particle distributions for polystyrene particles (red) and mammalian cells (blue) passing through the DEP sorter at 3 MHz, 50Vpp, and 1µL/min unfocused, illustrating the benefit of an upstream pre-focuser in a DEP system.

3.2.2 Continuous Particle Focusing

Based on numerical simulations of resulting particle trajectories, and the focuser geometry was designed such that suspending media and particles under 10µm in diameter were able to slip between individual pillars, maintaining their original streamlines, and consequently, due to laminar flow, their positions relative to channel width. Particles exceeding this clearance size, however, were pushed along the length of the row of pillars and settled into a single streamline by the time they exited the focuser.

The resultant pillars were 10µm wide, 80µm high, spaced 10µm apart, and spanned the entire height of the channel. The pillars were arranged in two rows, offset $\pm 0.5^{o}$ from the horizontal. This angle was chosen based on its ability to focus particles into a stream in as short a distance as possible while at the same limiting resistance to flow and not impeding particles as they shift towards the same streamline. Pillar rows at sharper angles tended to clog more easily and resulted in poorer focusing performance. A steeper angle would theoretically focus the particles over a shorter length of inlet, but in practice traps particles and creates increased resistance to flow, instead of allowing them to gently roll along the length of the rows of pillars towards a

single streamline, while a shallower angle, which would theoretically minimize clogging, yields too long a footprint, exceeding the length of the entire inlet. Each of the two rows of pillars was set to terminate such that the final focused stream of particles would be positioned directly along the main flow channel's centerline.

To quantify pre-focuser efficacy, a mockup device was fabricated consisting of a straight channel with the pre-focuser positioned at the center. Viewing areas exist at positions of particle entry into and exit from the focuser. Particles are flowed into the focuser at various flow rates. Imaging was performed using an LSM780 set at 2 fps and run for 500 cycles. All frames were stacked and flattened using ImageJ; the width of the total particle distribution pre- and post-focusing was then measured digitally. The focuser was tested using 20µm diameter particles, the largest that can pass through the device without confounding phenomena such as clogging and snagging to channel surfaces. The width of the total particle distribution for 20µm particles was measured before and after passing through the focuser. A comparable result was obtained using 10µm particles, the smallest focusable size with this geometry of pillar line.

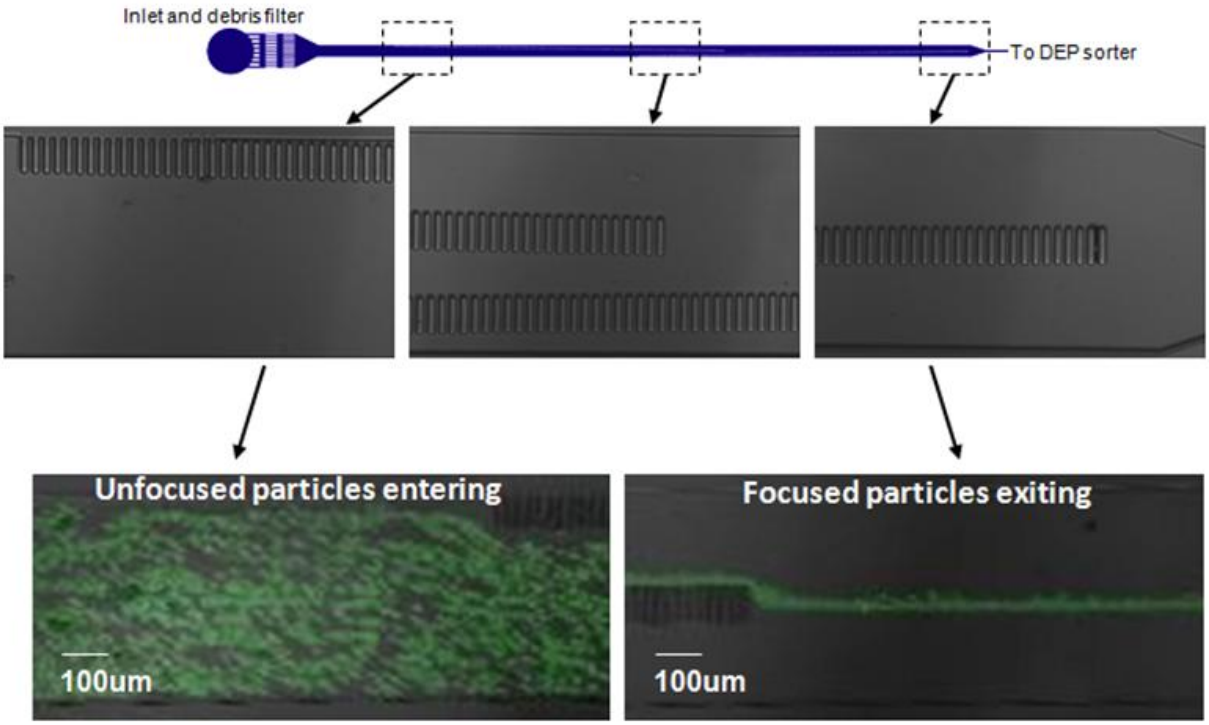

Figure 3.2.7 Particle focuser validation
Top and middle rows: Entire length of passive focuser, to scale, zoomed in at start, middle, and end. Gaps between pillars allow buffer to pass through but particles are redirected towards the centerline. **Bottom row:** Fluorescent polystyrene beads are shown entering the focuser randomly distributed across the entirety of the channel width and exiting in a focused stream at the channel center.

3.2.3 Liquid Electrodes

The fabrication of the gel electrodes is a multistep process. A pair of planar Au/Ti traces each 1cm x 100µm, spaced 300µm apart, were patterned onto a 1" x 3" glass side using photolithographic technique; wires were then soldered to these electrodes using lead free solder allowing them to interface with the external function generator. Subsequently, the PDMS channels are aligned over these planar electrodes such that the main flow channel runs between the two parallel planar electrodes, separated from each by 100µm of clearance, while the orthogonal side channels extending from the main flow channel sit directly on top of the planar electrodes.

To form the vertical electrodes that inject the electric field gradient into the main flow channel, the device is filled with a heated agarose 0.5% w/v saline solution at 30mS/cm. While the solution remains liquid, fresh saline is pumped into the device at 300µL/min, clearing all accessible sections of the channel of agarose solution. Due to laminar flow, however, the agarose saline mixture in the side channels are unaffected by this sudden influx of fresh saline and remain filled with agarose solution, which solidifies into a conductive gel as it cools below 65°C.

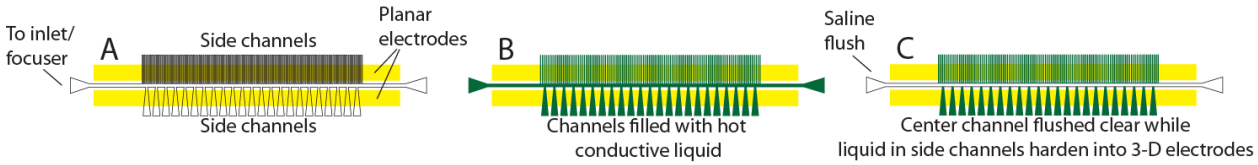

Figure 3.2.8 Gel electrode loading protocol
A: The device (gray) is aligned over electrodes (gold); **B:** The device is filled with hot conductive agarose gel solution (green). **C:** Saline is then flushed through channel, clearing conductive liquid from the main channel but ignoring electrode sites due to laminar flow principles. After cooling and gel formation, the saline in the central channel is removed and particle suspension of interest put through the device.

The gel included fluorescein for visibility under 488nm excitation. Small dead zones in the gel electrodes may occur when the saline is used to flush the main region; however regions are shallow and the change to the fluidic channel and overall flow is minimal. We observed typically less than 5% change to the channel widths, with no loss of laminar flow and no trapping of particles in the dead regions.

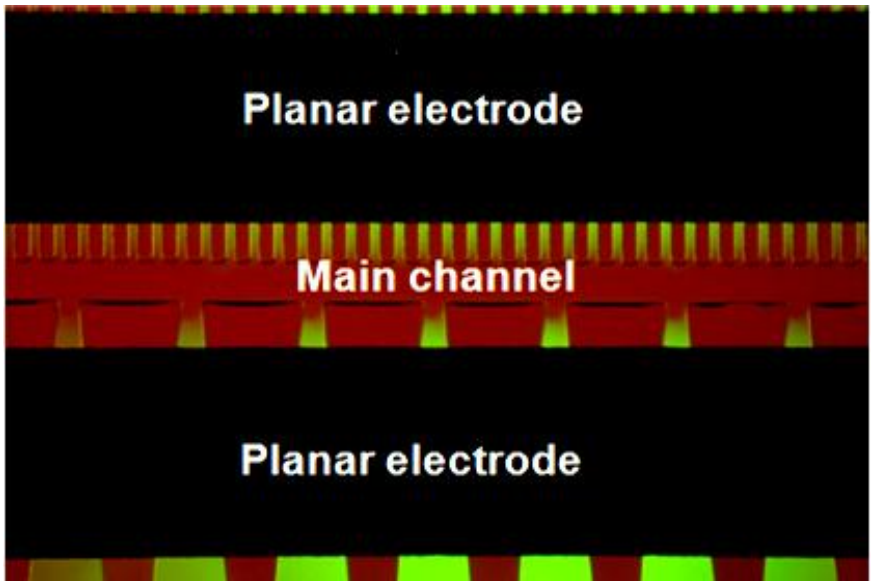

Figure 3.2.9 Electrode visualization
Overlay of brightfield and fluorescent image of assembled device; gel electrodes (fluorescent green) are visualized using fluorescein additive.

3.2.4 DEP Separation

This device uses a consistent frequency for all electrode pairs and generates field lines extending from one edge of the channel to the opposite; the electric field gradient is shaped entirely by strategic asymmetric positioning of the vertical electrodes. In contrast, most iDEP devices consist of symmetrically-distributed side channels, each side connected to its own function generator with electric field lines that terminate in the same edge from which they originate [134], [144], [167] and by adjusting the relative difference in signal amplitude between each side, particles are shifted across the width of the channel. The positions of our electrodes on each side of the channel were guided by drawing a schematic in COMSOL and numerically simulating the shape of the resultant fluid flow field and electric field gradient. The resulting field information and device geometry were then imported into a program written in Python to predict particle trajectories using governing equations for dielectrophoresis and laminar flow as

described above. Based on this, the specific shape and distribution of side channels as well as the strength of the signals used to energize them were derived. In the final design, electrodes on the upper (low E-field strength) edge of the device were 30µm wide and 30µm apart, while those on the lower (high E-field strength) edge of the device were 60µm wide and 240µm apart.

According to the numerical simulations, low dielectric constant particles, e.g. polystyrene particles, and higher dielectric constant particles, e.g. mammalian cells, in low conductivity buffer experience significantly different DEP forces at frequencies in the megahertz range, with cells experiencing a strong pDEP force while the polystyrene particles experience the opposite, yielding DEP-based separation. Theoretical trajectories for these two particle types flowing through the device at 1µL/min are shown; the simulated device is set at 3MHz and $50V_{pp}$ Polystyrene beads were modeled as perfect spheres with poor conductivity and permittivity (diameter = 15µm, σ_p = 0.1µS/cm, ε_p = 2.6), while cells were modeled as perfectly spherical cytosols with physiological conductivity and permittivity (diameter = 15µm, σ_{cyt} = 15mS/cm, ε_{cyt} = 80) enclosed in a thin insulating membrane of low conductivity and permittivity (thickness = 9nm, σ_{mem} = 1.6µS/cm, ε_{mem} = 20). All particles are modeled in low-conductivity media (σ_m = 150µS/cm, ε_m =78). Electronic properties for particles and media were derived from literature.[168]–[173] Under these conditions, at 3MHz, the CM factor for the polystyrene approaches -0.5, while the CM factor for the cells approaches +1.

3.3 *Results and Discussion*

Validation was performed by running mixed particle suspensions through the device and demonstrating that by carefully tuning the voltage and frequency of the applied signal, the device

can perform DEP-based particle separation. Both size- and dielectric constant-based sorting was performed.

3.3.1 Size-Based Particle Sorting

An initial run of the device was performed using, for simplicity, only polystyrene beads suspended in deionized water. Because of their identical composition, all particles in suspension were expected to display the same C-M curve. Thus, sorting would depend exclusive only on particle size, with DEP force scaling by volume and the resisting Stokes drag scaling by cross-sectional area.

Given that for any frequency, the mixed particles would move in the same direction, and that the field gradient across the main channel was strictly unidirectional, with the maxima located along the bottom edge and the minima along the top edge, validation was conducted by focusing all the particles against one edge of the sorter instead of along the centerline. According to the numerical simulations, for the entire range of interest, i.e. 50kHz to 3MHz range, polystyrene particles in low-conductivity buffer would experience nDEP. Thus, to perform the validation, all particles were focused along the bottom edge of the microchannel, the top of the field gradient, and the resultant nDEP force was observed.

The asymmetric focuser was adapted from the symmetric design, retaining all critical features, including angle and post geometry. Instead two half-rows facing each other, however, it consists solely of one full row, angled at -0.5^{o} from the median and spanning the entire width of the prefocuser section. In lieu of running the full numerical simulation package, the asymmetric focuser was quickly evaluated by confirming its flow field distribution in COMSOL and then simply running particles through a rapidly fabricated sample.

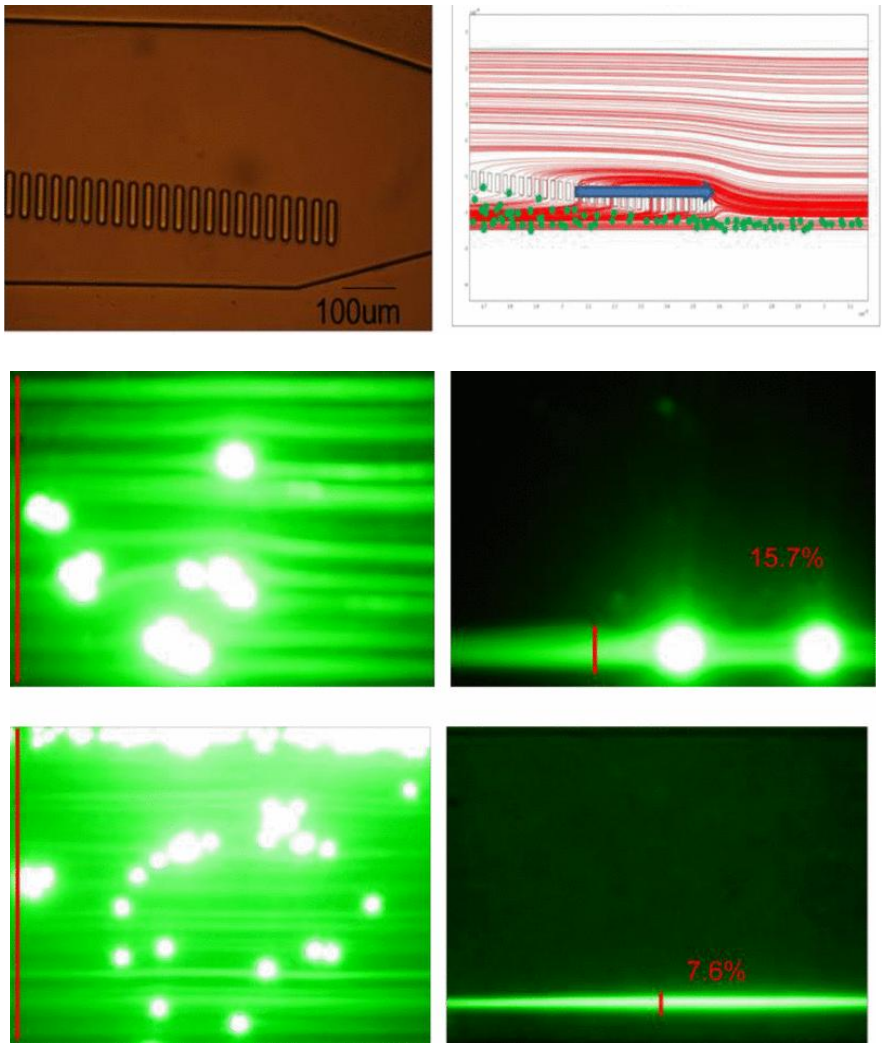

Figure 3.3.1 Asymmetric focuser initial validation
Top left: Focuser geometry. Features are identical to the symmetric design, only the row of pillars leads to bottom edge of device instead of centerline. **Top right:** Fluid flow simulation in COMSOL. Particles added manually to illustrate their positions along flow lines. **Middle row:** 25µm particles before and after passing through focuser. **Bottom row:** 10µm particles before and after passing through focuser. **Middle and bottom rows:** Marked width of focused beam relative to width of unfocused particle distribution.

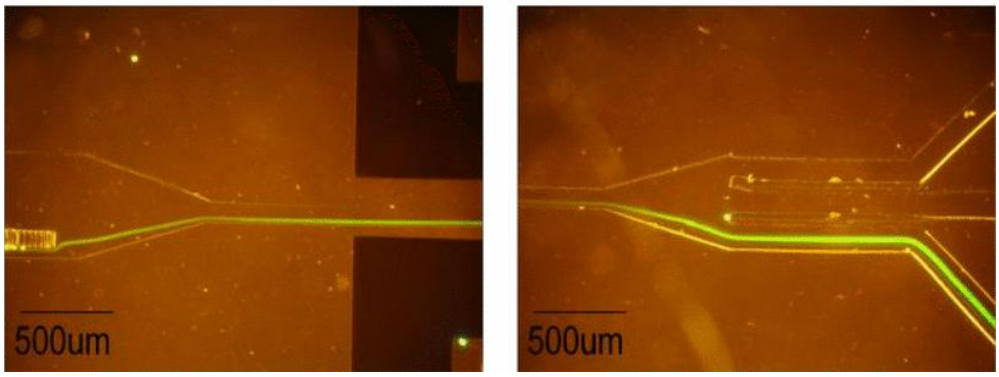

Figure 3.3.2 Asymmetric focuser integrated onto DEP sorter
Left: 10 second time lapse depicting 20um fluorescent particles entering DEP region in focused stream. **Right:** Particles maintain stream and exit device through lowermost outlet.

The preliminary size-only-based separation was performed using fluorescent particles of 15µm (yellow) and 20µm (green) diameter (Polysciences, Warrington, PA, USA) suspended in deionized water (σ_m= 40µS/cm, ε_m = 80). Size-based nDEP sorting is primarily a function of selecting for an appropriate combination of frequency, voltage, and flow rate that allows for the two particle types to, in the channel length available, migrate to flowstreams that eventuate into two different outlet channels. For the presented device, which features three outlets, particles deflecting different thirds of the channel width would yield such an outcome. Keeping flow rate and frequency at 1µL/min and 50kHz, respectively, voltage was gently tuned from 0V to 30V_{PP}, and variations in deflection between larger and smaller particles observed. As expected, while both particle sizes eventually deflected all the way from one side of the channel to the other, the larger particles experienced a slightly larger net force.

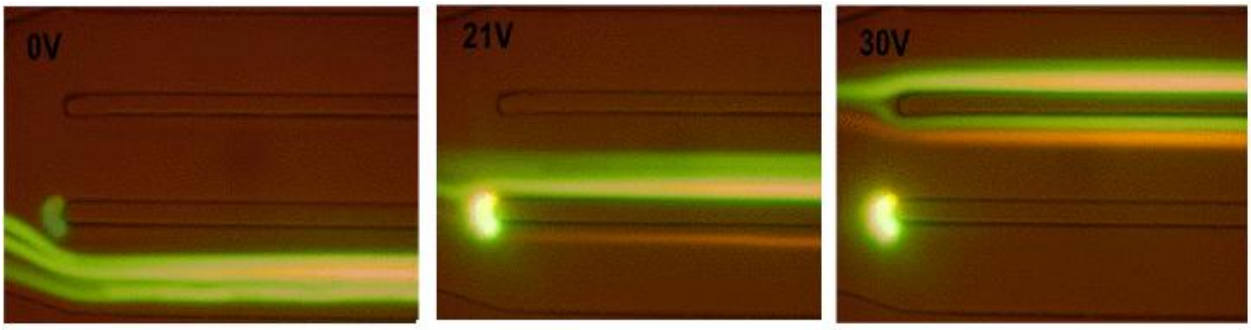

Figure 3.3.3 Size-based particle sorting
Imaging at outlet: **Left:** Deactivated device. **Middle:** Device at 21Vpp. Sorting observed between lower and center outlets. **Right:** At 30Vpp, analogous sorting between center and upper outlets. Yellow = 15µm diameter, green = 20µm diameter.

3.3.2 Cell vs. Non-Cell Particle Sorting

As a subsequent proof of principle for application of this device to eukaryotic cells and to demonstrate the device's ability to sort cells from a heterogeneous mixture, we employed HeLa cells (ATCC CCL-2, Manassas, VA) and polystyrene beads. A suspension of freshly detached HeLa cells labeled with CFSE (50µM in PBS, Sigma-Aldrich, St. Louis, MO) in low-conductivity buffer consisting of 8.5% sucrose (wt/vol), 0.3% dextrose (wt/vol), and 0.725% RPMI (vol/vol)) (150µS/cm, pH = 7.38) at a concentration of $1x10^6$ cells /ml was prepared. 15µm polystyrene fluorescent beads (FluoSphere 580/605, Life Technologies, Eugene, OR) were then added to this mixture to a resulting concentration of $2x10^5$ particles/ml. This permitted visualization of both beads and cells using standard fluorescent video microscopy.

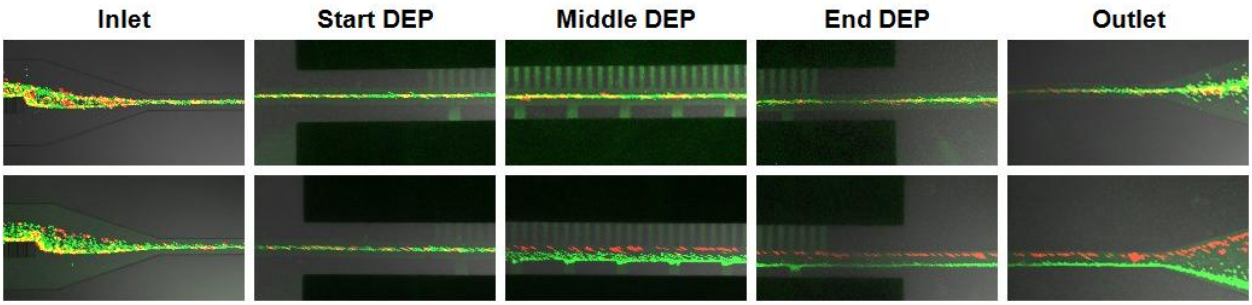

Figure 3.3.4 Particle separation in DEP sorter
Top row: Five-image sequence of mixed particle suspension (red 15 µm polystyrene beads and green HeLa cells) exiting the focuser, entering the DEP region, halfway through the DEP region, exiting the DEP region, and exiting the channel in deactivated device. Second row: Same sequence, device energized at 3MHz.

To quantify separation efficiency, video footage of particles exiting the device at the channel trifurcation was collected using the LSM780 (Carl Zeiss Microscopy, Thornwood, NY) at 2fps for 100s and particles were counted as they passed through one of the three exits. As the particle mixture enters the device, it is initially focused into a stream located at the center of the flow channel; 82% of polystyrene particles and 93% of cells were focused into the center outlet, with the balance scattered into the two other channels, yielding no separation. Upon the application of a low frequency signal of 30kHz and $30V_{pp}$, strong nDEP is experienced by the polystyrene beads, which are completely deflected into the top channel. HeLa cells display a more mixed response: the stream of cells broadens, and while most cells exit primarily through the center outlet, some are observed exiting through one of the two side outlets as well.

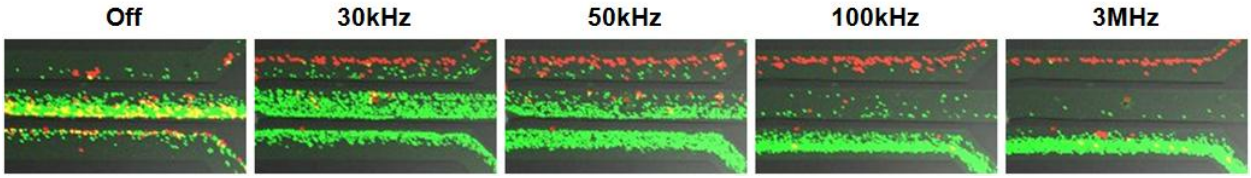

Figure 3.3.5 Particle separation as a function of frequency
Particle distribution (red 15µm polystyrene beads and green HeLa cells) imaged at trifurcated device outlet. Initially, nearly all particles are focused into the center channel. Upon activating the function generator at 30 kHz, polystyrene particles immediately deflect into upper channel (nDEP) while cell stream broadens into the upper and lower channels. As frequency is further increased, polystyrene particles remain in the upper channel while HeLa cells gradually transition towards the lower channel (pDEP).

As the frequency is increased, the polystyrene particles continue to exit through the top channel while the live cells transition gradually towards pDEP; at 3MHz and $50V_{pp}$, near-total separation is observed with over 97% of HeLa cells and over 94% of polystyrene particles deflected into the bottom (pDEP) and top (nDEP) outlets, respectively. Trace amounts of each particle type passed through the center channel.

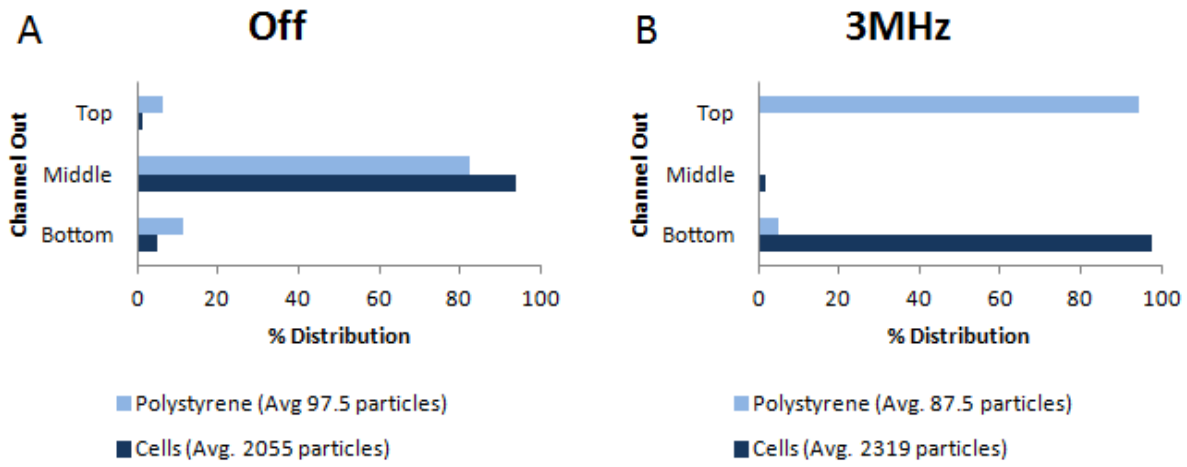

Figure 3.3.6 Quantification of sorting
Particles were counted as they exited the device through one of three outlets: undeflected particles exited through the center outlet, particles experiencing an nDEP force exited through the top, and particles experiencing a pDEP force exited through the bottom. Flow rate was 1 µL/min. Panel **A:** Particle distribution in deactivated device. **B:** Particle distribution under 50Vpp, 3 MHz signal.

3.4 *Conclusions*

The microfluidic device presented addresses several critical issues in DEP particle sorting, namely, the decreased DEP sorting efficiency without pre-focusing of the particle stream, the dead zones commonly found in microfluidic electric field gradients, and the capacity to easily fabricate vertical 3-D electrodes using historically 2-D photolithographic methods. The design improves upon earlier liquid dielectrophoresis methods by allowing for the formation of higher conductivity 3-D gel electrodes within the device using only the properties of the laminar flow found at low Reynolds numbers. These three-dimensional electrodes were fabricated by strategically flowing a thermosensitive conductive liquid into the device and then selectively removing material from the main channel prior to device cooling, leaving 3-D structures shaped to generate vertical uniform and lateral non-uniform field gradients.

Initial work shows that the device can deflect particles across a wide range of frequencies and differentiate between particles of low and higher dielectric constant with high accuracy. Future work will focus on applying this sorting technology towards distinguishing subsets of live eukaryotic cells and for isolation of low population cell subsets from a larger heterogeneous mixture, e.g. hematologic cellular subsets (leukocytes) or circulating tumor cells from whole blood. This work provides an avenue to explore sorting based on detecting subtle differences in seemingly homogeneous cell populations, such as progenitor or stem cells from single tissue population, e.g. epithelium from a specific organ. Finally, future studies will be performed in buffers more conductive than the low-conductivity DEP buffer presented here; of special interest is the device's ability to sort particles at physiological conductivity, which would simplify the sample prep process and allow the device to sort using both nDEP and pDEP, across a wide range of frequencies.

Chapter 4: Lab-on-PCB Device Using Alloy Vertical Electrodes

4.1 *Overview*

Presented is a microfluidic lab-on-PCB device containing alloy vertical electrodes for sorting microparticles using dielectrophoresis (DEP). The device consists of a continuous hydrodynamic prefocuser and an electronic particle sorter. Lining the two sidewalls of the electronic sorting region are regularly spaced rectangular metal electrodes reaching from the floor to the ceiling of the flow channel that bridge electric field lines laterally across the channel. The size and distribution of these vertical electrodes are arranged asymmetrically such that the resultant electric field forms sharp electric field gradients across the channel; specific geometries were optimized using finite element methods. Particles entering the device are initially focused into a single stream as they pass through the prefocuser. Subsequently, they are exposed to the lateral electric field gradient and separate into separate streams based on size and dielectric properties. Validation was performed by dielectrophoretically separating live cells from dead cells. Unlike the first generation of microfluidic devices, the system presented can be integrated with various external sensors and actuators using commercially available components towards a true lab-on-PCB system.

4.2 *Manufacturability of Microfluidic Devices*

As discussed in Chapter 2, despite tremendous advances in the miniaturized particle sorting technologies themselves, device packaging has not developed at a comparable pace, limiting the adoption of these technologies.[175] Devices still almost universally consist of channels cast onto a polymer, often PDMS, and mounted onto a brittle substrate such as glass or silicon. To incorporate electronic components, conductive Au/Ti or ITO traces are often

photolithographically patterned onto the substrate itself to carry current from external sources into the microfluidic channels; this method of fabricating electrodes can be prohibitively expensive, owing to labor, equipment, and material costs, as well as the significant amount of Au/Ti wasted to produce simple traces. These methods, while sufficient for device prototyping and concept proving, run counter to the lab-on-a-chip mission of microfluidic devices, and present scaling and cost concerns that hinder acceptance of microfluidic devices within the clinician and laboratory researcher communities. Printed circuit boards are an effective means of addressing these ongoing difficulties of standardization, implementation, durability, and cost.

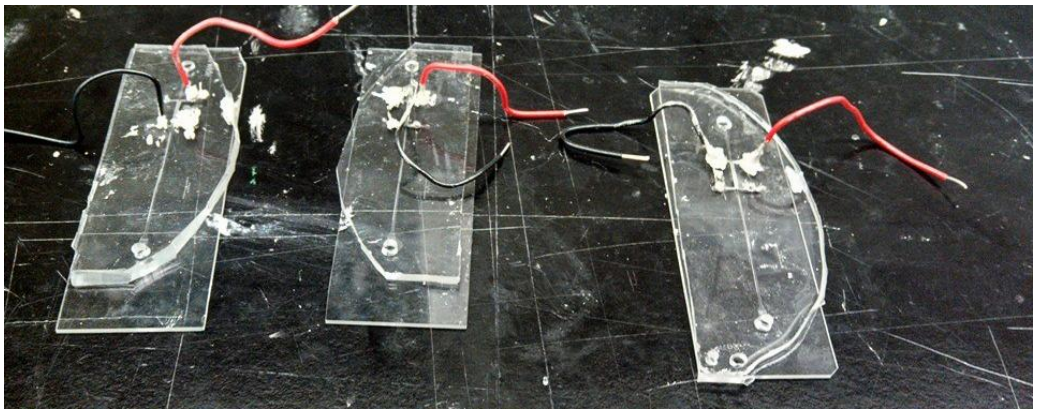

Figure 4.2.1 Early prototype of alloy electrode device
Initial attempt at fabricating metal vertical electrodes using only conventional fabrication techniques. PDMS components were not permanently bonded to glass substrates, to allow for their reuse in the likely event of a failure in the alloy-filling step. Additionally, glass slides were not patterned with costly conductive pads, which would be permanently fouled if the alloy did not fill properly. As a result, wire attachments for interfacing with external components were too tenuously connected for practical use, and PDMS delamination occurred frequently.

First and foremost, PCBs are a cheap and easy method for mass-producing complicated metal traces from a simple CAD drawing, eliminating the need for wet etching processes and time-intensive fabrication. Additionally, the boards themselves are tougher than brittle materials such as glass, and are a promising method for translating microfluidic devices from an engineering lab

into real-world environments such as a wet bench or patient bedside. This is especially advantageous given that a primary mission of microfluidics is specifically to extend the capacities of a traditional clinic or lab into rough locations inaccessible by traditional laboratory technologies. Finally, PCBs are a convenient platform for attaching mechanical components such as manifolds and fluidic lines, as well as existing standardized electronics, such as on-board switches, relays, and interconnects. One can envision a system in which all of the necessary electrical components for operating a microfluidic device (e.g. function generator, amplifier, logic elements) could be incorporated directly onto the PCB. Indeed there have been efforts to design PCB accompaniments to microfluidic devices[176], but work to integrate PCB functionality directly onto the microfluidic device has been very limited.[177]

To demonstrate, a PCB-based microfluidic device was prepared for sorting particles using dielectrophoresis, a mechanism that has found widespread use in the microfluidics community. This PCB enabled a facile and robust connection of the alloy electrodes to external prototyping wires used to deliver the electrical actuation signal.

Figure 4.2.2 Initial prototyping work towards lab-on-PCB
Skeptical project collaborator Melinda G. Simon, PhD, takes a first attempt at a soon-to-be routine soldering job. Note the unnecessary use of examination gloves, a leftover habit from a history of cell culture and performing rapid prototyping using PDMS.

4.3 *Methods*

The presented device consists of an inlet, a hydrodynamic prefocuser, an electronic sorter, and three outlets for recovering sorted particles. Device channels were first cast in PDMS from a silicon wafer master patterned using DRIE. Once the DRIE master has been fabricated, all other steps of the fabrication including vertical electrode fabrication, can be completed outside of the cleanroom environment. The electronic sorting component consists of two side channels, each parallel to the main channel and separated from the main channel by a line of evenly spaced pickets. At each end, the main channel branches into three inlets/outlets. The inlet trifurcation

serves as an injection point for the particle suspension and the focusing buffer, while the outlet trifurcation allows the user to divide the sorted particles into three batches for recovery.

The device is connected to an external amplifier and function generator. Fluid flow is driven using two syringe pumps (Harvard Apparatus, Holliston, MA, USA). Visualization is performed using inverted fluorescent microscopy (Olympus Corp., Tokyo, JP) and digital imaging (Nikon Corp., Tokyo, JP). Videos were recorded using a commercial SLR camera (Canon 5D Mark II, Canon Inc., Tokyo, JP), mounted to the microscope, and analyzed in ImageJ.

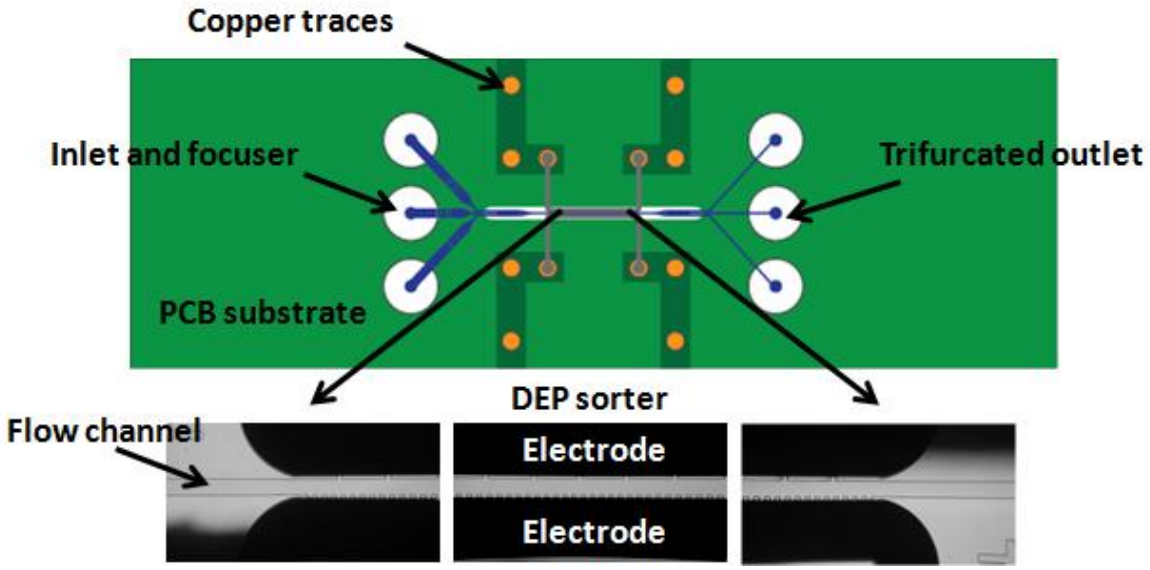

Figure 4.3.1 Device schematic of PCB-based DEP sorter
Top: Device schematic, to scale. The device consists of a hydrodynamic flow prefocuser which directs all incoming particles into a single line, and an electronic component, which injects an electric field gradient into the channel and sorts the stream of particles based on their size and dielectric properties. **Bottom:** Electrodes are formed by flowing alloy into side channels parallel to main channel. Gaps in the walls between the main channel and the side channels expose the electrodes to the main channel.

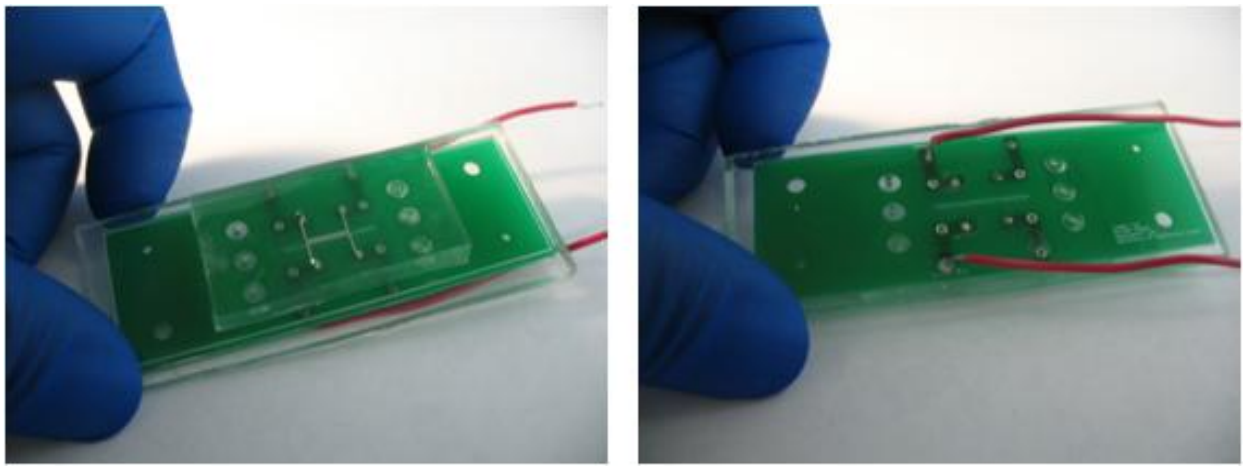

Figure 4.3.2 Assembled PCB-based DEP sorter
Left: Top surface of device. Visible are the pair of vertical electrodes in the center of the device, as well as the topmost block of PDMS containing the microchannels. **Right:** Bottom surface of device. Visible are some of the vias and copper traces used to connect the electrodes with external instrumentation such as oscilloscopes, power supplies, and signal generators.

4.3.1 Numerical Methods

Channel geometry was optimized by analyzing models built using COMSOL Multiphysics and a custom Python package. The device was drawn in COMSOL and used to generate flow- and electric-field data. The data was exported and imported to a Python program in which governing equations for collision detection, fluid flow, and dielectrophoresis were incorporated. Subsequently, simulated particles of various sizes and dielectric constants were flowed into the virtual device and particle trajectories were recorded. The geometries of the pickets and the focuser, as well as the voltage and frequency of the applied electronic signal, were adjusted until separation was achievable for various types and mixtures of particles.

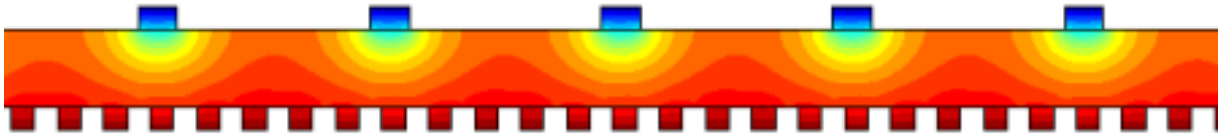

Figure 4.3.3 Simulated electric field gradient in DEP sorting region
The electric field gradients generated by the alloy vertical electrodes were simulated in COMSOL. As shown, the fields are strongest at the top edge of the device and weakest at the bottom edge. Particles undergoing pDEP would thus tend to trend towards the top, while those undergoing nDEP would tend to trend towards the bottom.

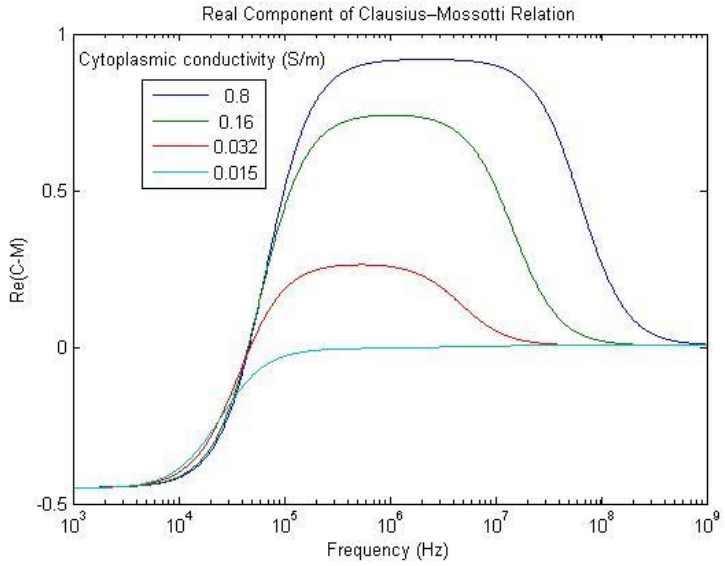

Figure 4.3.4 Theoretical C-M curves for mammalian cells
The real component of the C-M curves for cells of varying health were simulated in MATLAB by varying cytoplasmic conductivity, based on the fact that as cells die, their membranes porate, allowing their cytoplasms to gradually match the conductivity of the surrounding media.

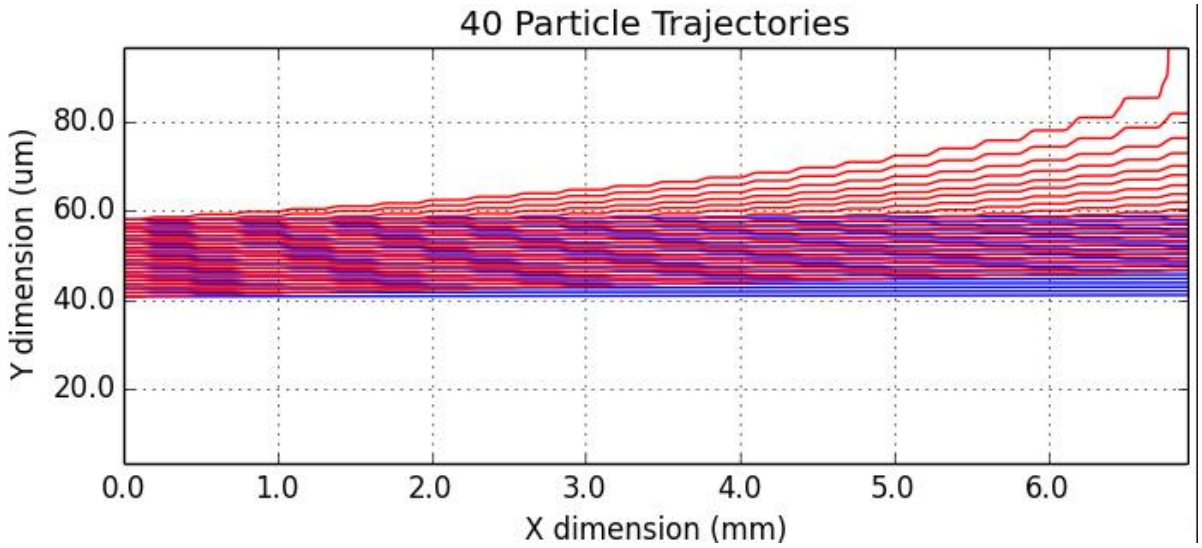

Figure 4.3.5 Simulated particle trajectories
The custom Python program incorporating governing equations for laminar flow, particle collision, and dielectrophoresis was used to calculate the trajectories of 40 particles, starting from 40 different positions across the middle fifth of the width of the channel (Y dimension). The X dimension corresponds to the distance traveled along the DEP sorting region of the microfluidic device by each particle. In this simulation, particles entering at the 50µm streamline or above in the Y dimension are deflected to a higher Y dimension (i.e. the left side of the microfluidic channel) as they traverse the length of the sorting region.

4.3.2 Implementation of Printed Circuit Boards

To facilitate electrical and fluidic connections to the device, a 1”x3” printed circuit board containing all necessary electrical leads and fluidic ports was designed in EagleCAD (CadSoft Computer, Ft. Lauderdale, FL, USA) and custom printed (Smart-Prototyping, Kowloon, HK). A bespoke protocol was used to bond the PDMS channels to the PCB. Briefly, a layer of PDMS approximately 5mm thick was applied to the surface of the PCB, providing a smooth surface to facilitate a strong bond between the board and the PDMS film, preventing delamination. Subsequently, the PDMS slab containing the patterned microchannels was covalently sealed channel-side-down against the PDMS film using plasma treatment.

4.3.3 Metal Vertical Electrode Fabrication

The microfabrication of vertical electrodes is a challenge, generally requiring a series of photolithographic steps and, in the case of electroplating, fine electrical current control to fabricate these three-dimensional structures and then to seal the device.[134]

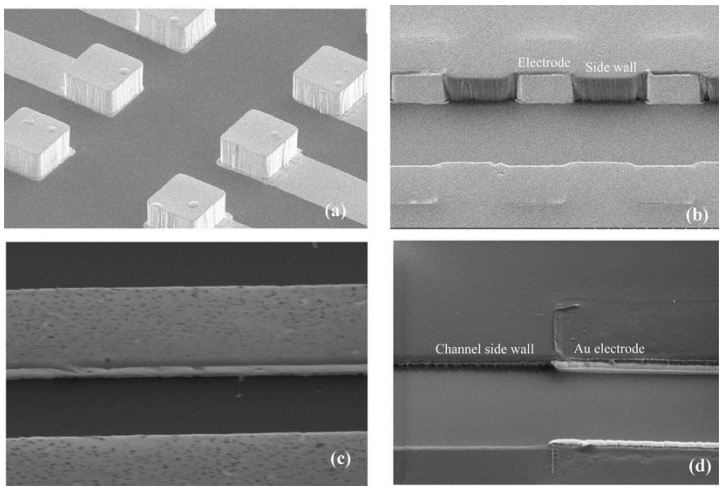

Figure 4.3.6 Example of electroplated vertical electrodes
SEM pictures of the electrodes. **A:** Electroplated Au electrode array before channel layer is coated. **B:** Electrode arrays embedded in the side wall of channel. **C:** Au electrodes for MHD before coating of channel. **D:** Close-up view of the electrodes and SU-8 wall inside channel. Reprinted with permission from [134] © 2007 IEEE.

While various methods have been proposed to circumvent these difficulties, and have been successful at performing DEP separations, metal electrodes of an optimized size and shape remain the most effective method of injecting electric fields of a specific shape and strength, with minimal voltage loss, into a microfluidic device.[178] Presented is a novel method for combining the convenience of liquid electrode fabrication with the performance of their metal counterparts. In addition, this method allows for out-of-cleanroom fabrication of these vertical electrodes, thus significantly decreasing the time and cost required for their fabrication. Using a

low-melting-point indium-based alloy and exploiting the increased importance of surface tension forces at the microscale, three-dimensional electrodes can be rapidly and reliably formed in 5 minutes using only a hotplate. Combined with a PCB platform, this demonstrates that a geometrically-complex microfluidic device can be fabricated for little cost, with minimal cleanroom dependence, and ready for integration with standardized auxiliary micropumps and electronics for introduction to a non-engineering audience of clinicians and biological researchers.

To form the vertical electrodes themselves, devices were placed on a hotplate, heated to 90^{o}C , and an low-melt-point alloy of 51% indium, 32.5% bismuth, and 16.5% tin (Indium Corporation, Clinton, NY) was gently flowed into the side channels using hydraulic pressure through vias in the PCB aligned over the inlets and outlets of the side channels. The alloy's high viscosity forces it to flow laminarly through the side channels while the high surface tension owing to the small radius of curvature between pickets prevents the alloy from entering the main fluidic channel.[178] After the alloy is in place, the device is cooled and the alloy solidified. Finally, wires are soldered to the vias on the back side of the PCB for connection to external electronics.

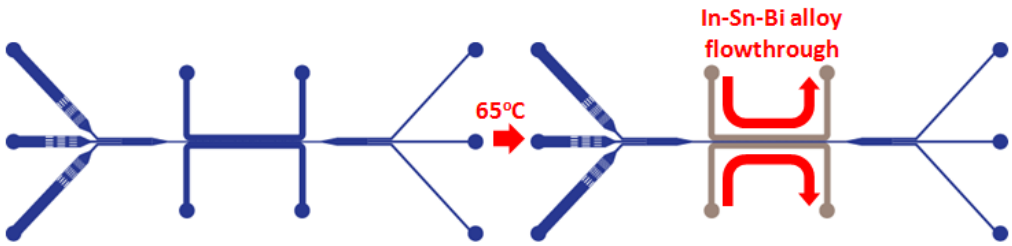

Figure 4.3.7 Electrode loading protocol, top view
Left: Parallel to the main flow channel are two U-shaped side channels separated from the main channel by pillars. Two alloy inlets are bored in the PDMS. **Right:** The alloy enters through the inlet and travels the length of the U shape. Surface tension keeps it from leaking into the main flow channel, thinly visible in blue.

Figure 4.3.8 Electrode loading protocol, side view
A: Side channels are initially empty. **B:** To load the electrodes, a wire of In-Sn-Bi is inserted into the side channel inlet. **C:** As it contacts the warm PDMS-PCB substrate, it melts and flows through the channel. The solid wire above it acts as a piston, driving the melted alloy through the channel with a hydraulic force. **D:** After the entire side channel has been loaded with melted alloy, the device is removed from heat and the alloy allowed to solidify. Excess material is removed.

Unlike vertical electrode fabrication using electroplating, fabrication using the alloy material imposed additional constraints on the optimal electrode design. Models showed that the electric field gradient was maximized in designs where the difference in size in electrodes on either side of the channel was greatest, however the maximum usable electrode size was ultimately constrained by the upper limit on the radius of curvature which would retain alloy in the alloy channel by surface tension. In practice, electrode fabrication was most robust when the gaps between pickets were 50µm or lower. This limitation could potentially be improved by decreasing the channel height, thus decreasing the radius of curvature in the perpendicular direction and increasing the overall surface tension at this location; however our design required a channel height of 50µm in order to prevent cell clogging and ensure a long device lifetime.

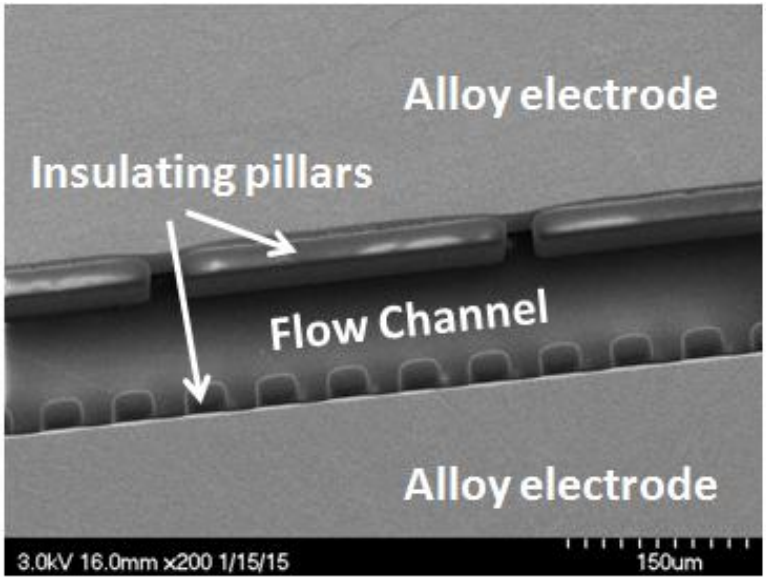

Figure 4.3.9 SEM of vertical electrodes
Depicted is a section of the 50μm tall main flow channel and the asymmetrically distributed PDMS pillars that form the channel's sidewalls. The top edge of the channel is formed by large sections of PDMS, with sparsely distributed gaps, while the bottom edge contains an even distribution of PDMS and gaps.

To address possible toxicity issues regarding the use of the alloy electrodes in cell sorting applications, HeLas in cell media were spiked with varying amounts of alloy and cultured for up to thirty-six hours. Cell survival was checked every four hours by staining with trypan blue, a live-dead dye and compared to the negative and positive controls. Positive controls were killed by exposure to 70% ethanol for one minute. As shown, even after thirty-six hours, there is no noticeable difference between the exposed cells and the negative.

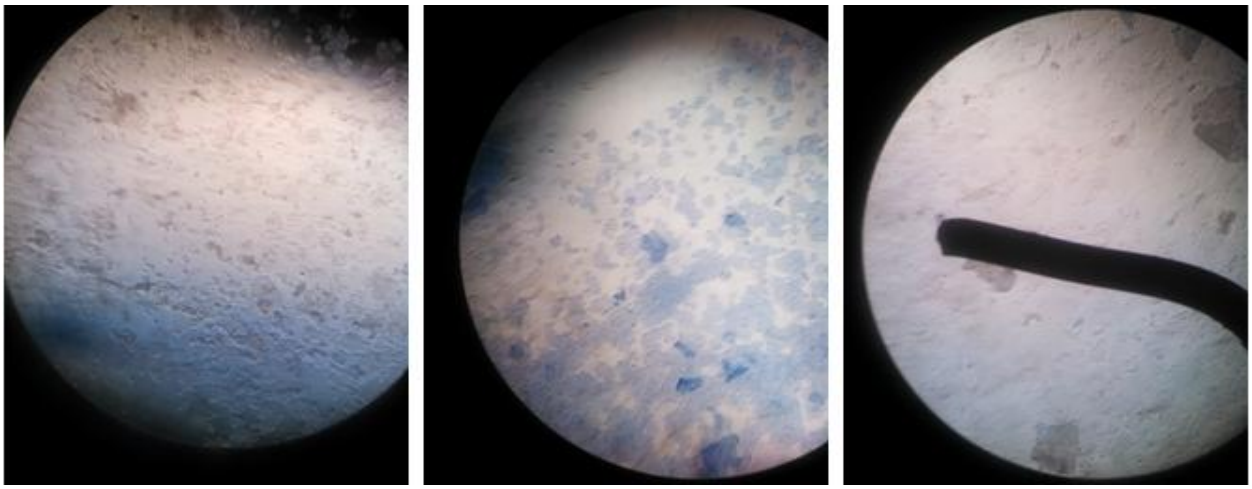

Figure 4.3.10 Biocompatibility assay
Samples of the alloy were cultured with HeLa in cell media for up to 36 hours. No obvious toxicity was noted. **Left:** Negative control. **Middle:** Positive control. **Right:** Positive.

Additionally, it was demonstrated that a the alloy can be electroplated with a thin film of gold using a standardized protocol after installation in the microchannel, rendering it nontoxic to cells.[179] Special care must be taken to ensure that plating temperature does not exceed 65^{o}C, to prevent the destruction of the electrodes.

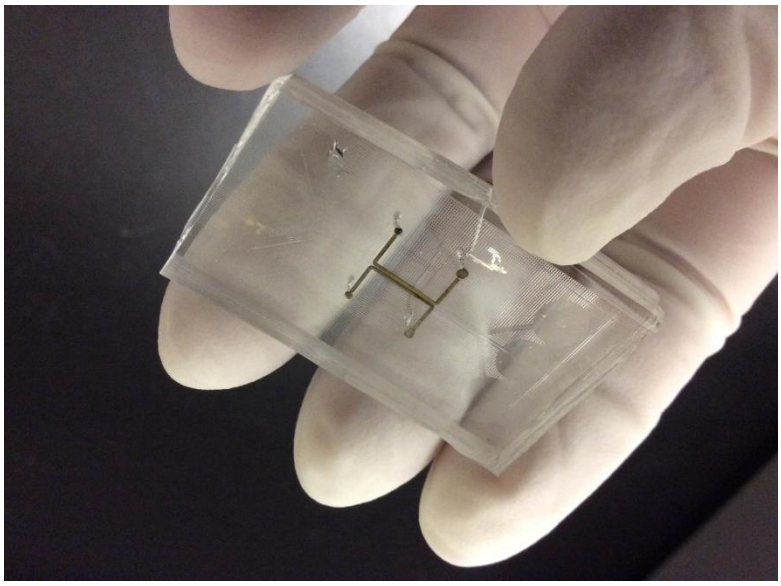

Figure 4.3.11 Gold plated electrodes
A PDMS component whose loaded electrodes have been plated in gold. Gold plating addresses any potential biocompatibility concerns that might arise in cell sorting applications.

4.3.4 Hydrodynamic Focusing

All particles must enter the device along the same flowstream if they are to experience identical electric field conditions for dielectrophoretic sorting; to do otherwise introduces confounding situations, such as certain particles eluding DEP sorting completely by entering along a flowstream that only passes through weak field gradients. For this reason, the particle stream is focused into a tight band at the center of the main channel using a hydrodynamic focuser. Briefly, this is an established technology that takes advantage of the fact that under laminar flow conditions, such as those found in a microfluidic device, if multiple fluid streams converge into one, each will flow parallel to the others, with no convective mixing. The percent width of each stream after convergence is proportional to its volumetric flow rate relative to the combined volumetric flow rate of all streams. In the presented device, particles are flowed into the main channel through a central inlet, while pure DEP buffer is flowed into the main channel

through two side inlets. When the flow rate of pure DEP buffer into the main channel through these two side channels exceeds that of the particle suspension itself, the particle suspension is forced into a thin stream so narrow that particles enter the DEP sorting region approximately single-file.

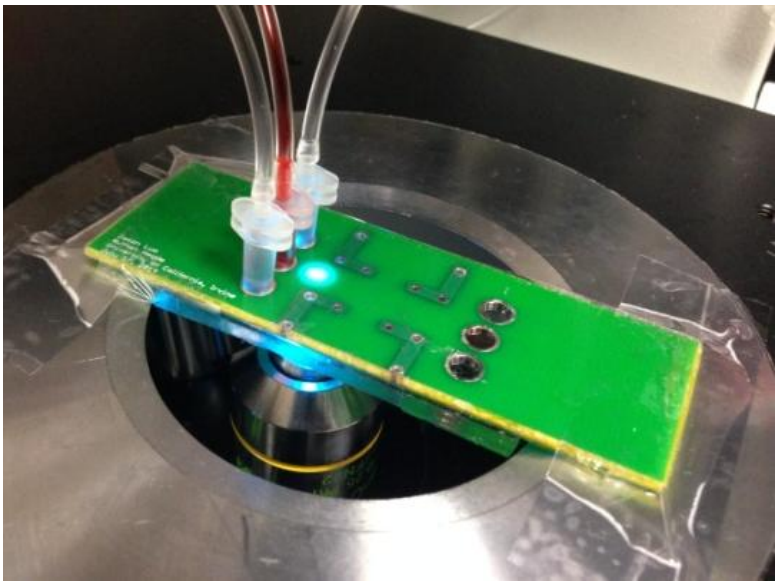

Figure 4.3.12 Hydrodynamic focuser lines
Particles were hydrodynamically focused using a three-line system at the inlet. The particle suspension (red) enters through the center line, while the focusing fluid (clear) enters through the two side inlets. Relative flow rates of all three lines were adjusted to maximize the compression of the particle suspension without encountering unwanted effects such the focusing fluid contaminating the centerline reservoir.

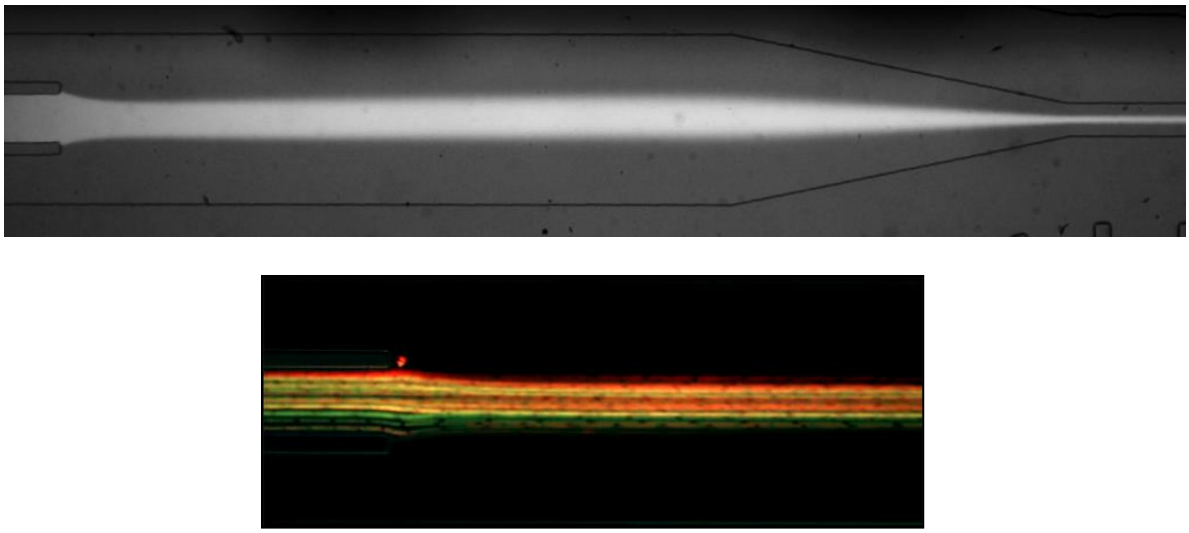

Figure 4.3.13 Hydrodynamically focused fluids at device inlet
Top: Three lines of PBS are seen entering the inlet. The central line has been stained with fluorescein for visibility. By entering the central fluid at 0.8µL/min and the pinching fluids at 2.6µL/min, an approximately 75% reduction in stream width is observed. **Bottom:** The fluorescein-stained PBS replaced with a live-dead suspension of HeLa cells. Stream compression is comparable to that of the PBS trial.

4.4 *Results and Discussion*

Freshly detached HeLa cells in PBS were separated into two aliquots at a concentration of 1E6/ml each. One batch was stained with carboxyfluorescein succinimidyl ester (CFSE) (Sigma-Aldrich, St. Louis, MO) at 50µM for 30 minutes at room temperature; in live cells, CFSE is activated to fluoresce green at an excitation wavelength 488nm, whereas in dead cells, no fluorescence occurs. The other batch was heat-killed via immersion in a 57^{o}C bath for 30 minutes.[180] Subsequently, these cells were stained with propidium iodide (PI) at 1% (wt/vol). In live cells, PI is unable to penetrate the cell membrane and no staining results, but dead cells' membranes are porated, granting the dye entry. Upon binding to the dead cells' exposed nuceic acids, PI fluoresces under an excitation wavelength of 561nm. Finally, both aliquots are recombined at a 1:1 ratio in a low-conductivity DEP buffer consisting of 8.5% sucrose (wt/vol),

0.3% dextrose (wt/vol), and 0.725% RPMI (vol/vol)); final conductivity and pH are 100µS/cm and 7.38, respectively. Final concentration of each cell type is 1E6/ml. As shown in the CM factor plot for our system, the high conductivity of cell media (RPMI) results in a CM factor that is negative at every frequency. While cell separation is possible using negative DEP, lowering the medium conductivity to 100µS/cm enables cells to experience positive or negative DEP, depending on the frequency of actuation used, which enhances the separation power of the technique. Since the low conductivity buffer is osmotically-balanced with the cells, it provides a harmless medium to accomplish this separation technique.[15]

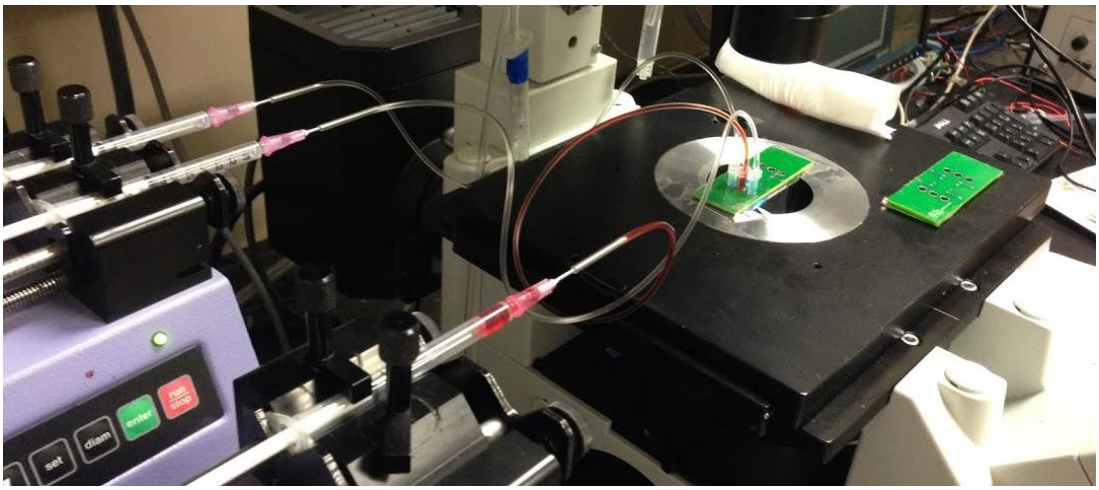

Figure 4.4.1 Device setup for validation
Apparatus for validation. Three lines (left) deliver a pinched stream of cells into the device. Electronics for DEP signal generation (upper right corner) are shown detached.

The prepared cell suspension was flowed into the device through the central inlet at a rate of 0.8µL/min, while DEP buffer was flowed through the hydrodynamic focuser at 2.6µL/min. In the deactivated device, all particles flow through the device without experiencing any lateral deflection and exit through the center outlet. When the device is activated at 1MHz and 40V_{pp}, however, live cells are deflected towards the top edge of the device and are sorted into the upper

outlet, while dead cells experience no net dielectrophoretic force and exist through the center outlet. To quantify sorting efficacy, particles exiting each channel were tallied for both the activated and deactivated device, and the two results were compared.

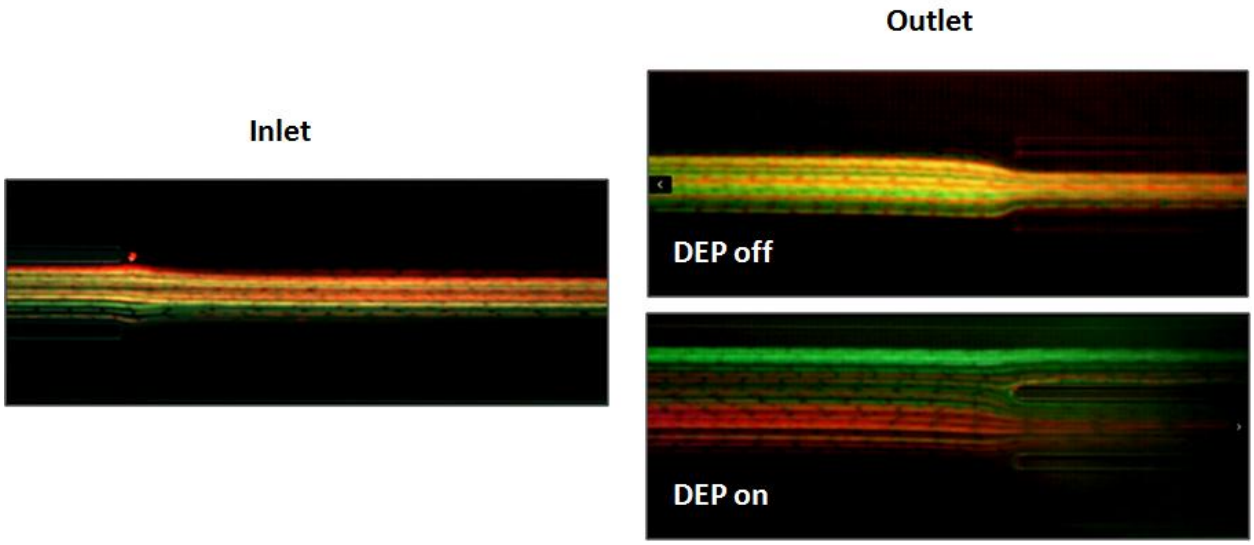

Figure 4.4.2 Live-dead separation, visualization
Live-dead assay, showing live cells stained with CFSE dye (green) and dead cells stained with propidium iodide (red). Images of particle traces from a video were stacked to show the trajectories of many particles. **Left:** At the inlet of the device, all of the cells (both live and dead) are focused in the middle of the three channels by hydrodynamic flow focusing. **Right, above:** With no applied electric field, all cells, both live and dead, exit through the center outlet. **Right, below:** However, at 1MHz and $50V_{pp}$, live cells, with their conductive cytosols and intact membranes, can form strong dipoles compared to those of the suspending media and experience pDEP, deflecting towards the upper edge of the flow channel and exiting through the upper outlet, indicated by the stream of green cells in the top channel. Dead cells experience no net DEP force and continue to exit the device through the center outlet, indicated by the stream of red cells in the middle channel.

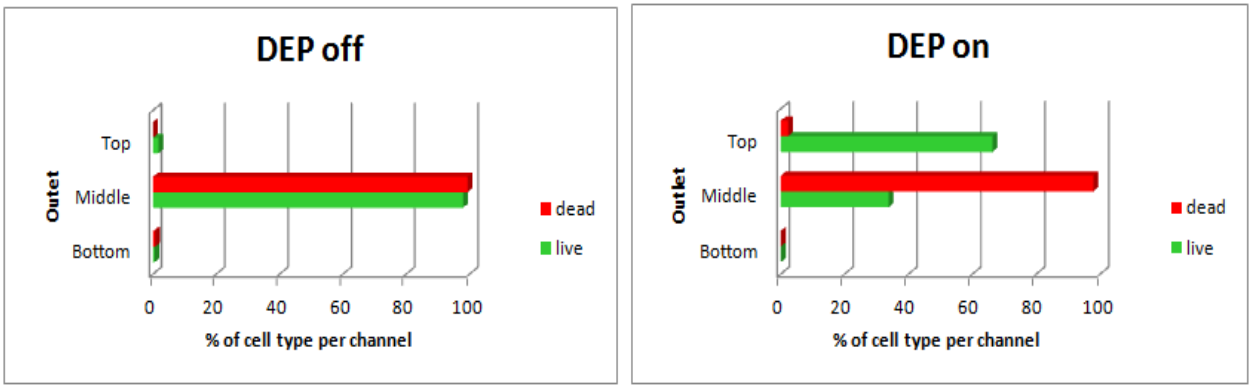

Figure 4.4.3 Live-dead separation, quantification
Particle distribution across the channel width is measured using video footage as they exit the device through one of three outlets. Percent distribution for each outlet is shown.

As shown, nearly all dead cells were isolated into the center outlet. The live cells, however, did not sort into as tight a stream, and while most were observed to experience pDEP and deflect into the upper channel, some did not experience as strong a dielectrophoresis force and remained mixed into the dead batch. This could be the result of a few factors. First, owing to the steepness of the electric field gradients in the device, over time, some live cells can become dielectrophoretically trapped at the sites of field maxima, physically blocking succeeding cells from deflecting sufficiently into new flowstreams. These trapped cells can, through their own dielectric properties, also alter the shape of the electric fields generated by the device such that succeeding cells do not experience as strong a gradient. Finally, it is possible that the seemingly live cells that remain mixed with the dead cells are simply less healthy than the rest of their live cohort, and are unable to polarize sufficiently defect away from the dead cells. In the final scenario, no correction is necessary as there is actually no error in DEP sorting. In all other scenarios, it is a commonly-used rectification in microfludic particle sorting to pass the contents of the center outlet through the device a second time to account for any straggling live cells. Finally, it goes without saying that the provided demonstration is only one example of particle

separation. End users should adjust the device's flow rate, voltage, and frequency to optimize the deflection of any particle they wish to enrich/separate.

4.5 *Conclusions*

The device presented addresses various obstacles in DEP cell sorting. Most importantly, vertically uniform electrical fields are generated by vertical electrodes, enabling continuous separation of cells and particles by balancing DEP force with fluid flow to steer different populations of cells or particles to different outlets. A pre-focusing region in the device ensures that particles and cells enter the separation zone in single-file, and thus experience an identical DEP force.

Additionally, the device is unique in its ability to integrate seamlessly with existing electronic components. Microfluidic cell sorters have experienced significant developments in the past decade, but there has been limited interest in the actual integration of these new technologies into real-world devices for portable point-of-care diagnostics. Importantly, the vertical electrodes can be fabricated quickly and out of the cleanroom, while the PCB substrate enables inexpensive and readily-available substrates to produce these devices. By building this device on a standardized electronics platform, it is a significantly simpler task to integrate miniaturized external components such as pumps, valves, and switches, as well as electrical components such as an amplifier and signal generator towards the development of a true lab-on-chip.

Chapter 5: Switchable Pick-and-Place Vertical Electrodes

5.1 *Overview*

Presented is an externally-controlled lab-on-PCB device for dielectrophoretic particle sorting. The heart of the device consists of an electronic sorting space whose inner walls are lined with three-dimensional vertical electrodes that project electric field lines into the space. As particles flow through the space, they are dielectrophoretically affected by the electric field and, depending on their size, conductivity, and polarizability, are deflected in a certain direction. By selectively activating and deactivating individual electrodes using an external controller, it is possible to sculpt the net electric field, and consequently, the field gradient in the space. This is in contrast to traditional DEP-based sorters, whose electric field gradients are predetermined by the devices' fixed electrode geometry, and cannot be modified by the user. Additionally, unlike the first generation of microfluidic devices, the system presented can be integrated with various external sensors and actuators using commercially available components towards a true lab-on-PCB system.

5.2 *Surface-Mount Technologies*

As addressed in Chapter 4, the microfluidics community can no longer build novelty items for the sake of novelty itself; rather, it faces the difficult question of what role the technology will take in the years to come, and must start taking steps in that direction. Currently, the community is trending towards extreme simplicity: the argument goes that rather than investing significant resources towards complicated systems that might compete with high-end technologies such as FACS, efforts should lean towards the opposite end of the spectrum, namely, devices that trade sensitivity and speed for reduced cost and power consumption and

increased durability and portability.[175] This forfeits in a way the original mission of a lab-on-a-chip: deliberately simple devices, e.g. home pregnancy tests, have their role, but ultimately, the biomedical community wants a device that integrates every step of their assay, from reagent input to data output, not one that crudely conducts one step of the assay, however cheaply or easily.[77], [181] Transitioning to a PCB-based paradigm is a first step towards reviving the original μTAS mission, but only a first step: a rectangle of plastic and copper cannot perform many assays, after all. The next step requires that we actually use the PCB as a starting point towards finally integrating on-chip all the tools required to perform the assay.

Surface-mount technologies (SMTs), a staple of the microelectronics industry, dovetails perfectly into this role. SMTs refer to, as the name suggests, methods and components for fabricating circuits by directly mounting components onto a printed circuit board. Developed in the 1960s to facilitate the integration of certain electronic components onto the glass substrates of the time, SMTs came to the forefront of the microelectronics industry in the 1980s, when engineers reached the limits of shrinking through-hole-based technologies, the predecessor to SMTs. At the broadest level, SMTs would bring to microfluidics the same manufacturing advantages they did to electronics thirty years ago, dramatically reducing the footprint, weight, volume, and cost of the attached components.[182]

Specific to microfluidics, SMT-based methods would enable an engineer to overcome various obstacles in device design and manufacturing specific to the field. For example, a major reason behind the poor reception microfluidics have received in the mainstream community is the difficulty in integrating auxiliary components. SMTs provide a deceptively powerful solution to this problem: a lab-on-PCB equipped with standardized SMT sockets, ports, and other interconnects facilitates the integration of components depending on the user's needs.[183]

SMTs provide capabilities beyond simple modularity, too. As shown in microelectronics, SMTs allow a user to bundle large amounts of small delicate components into one durable package, which in turn can easily be mounted onto a PCB.[182] For microfluidics, this means that miniaturized auxiliary tools, such as pumps and electronics, which already exist in some form or another, can be easily integrated onto a chip in a standardized manner. In addition to the increased convenience and manufacturability this confers, it would also improve the portability of any microfluidic device, crucial for the point-of-care mission.[184]

Finally, SMTs provide some possible solutions to the various manufacturability concerns in microfluidics.[185] For example, microfluidics are generally assembled monolithically, i.e. fabrication begins with a single substrate, e.g. a 1”x3” sheet of Au/Ti-coated glass, and additional components and materials are added and subtracted irreversibly with each step. This was suitable for early devices, which consisted of little more than patterned silicon, and, later, patterned elastomer, but as devices grew more elaborate to include more and more steps, device yields under this paradigm dropped exponentially. This remains a tolerable, albeit inefficient, method for rapid prototyping, but cannot be scaled in a cost-effective manner for large-scale production.

SMT-based pick and place methods, on the other hand, bypass this constraint. Each component of a device can be manufactured in a batch, each of which can be checked for quality using standard statistical methods. Using this method, the overall failure rate is limited to that of the most bothersome component; the errors do not propagate during the assembly process.

Additionally, for microfluidic devices, monolithic fabrication places unnecessary constraints on fabrication: for example, vertical electrodes are rarely incorporated despite their advantages

because with existing techniques, engineers cannot fabricate them until after the microfluidic channel has been sealed, a microscale version of the impossible-bottle problem.

Under an SMT paradigm, however, this frustrating situation can be avoided. By treating the bulk of the polymer body, with major features patterned onto it, as a substrate the way a PCB is treated, it naturally follows that components such as electrodes and pumps and perhaps, thanks to advances in polymer printing technologies, even passive units such as microposts [186], could be fabricated separately and then mechanically placed onto the polymer body. Self-assembly methods could also be incorporated to facilitate this process and increase the tolerances of such a process.[187] By building components individually and assembling the device as a final step, the engineer to bypass these fluidic constraints, opening the door to microfluidic components previously thought too impractical, if not nearly physically impossible.

5.3 *Methods*

As a proof of concept, three-dimensional microelectrodes were fabricated using various techniques adapted from photolithography and installed into a microfluidic device using pick-and-place methods.

5.3.1 Device Overview

The device builds on the lab-on-PCB technologies presented in Chapter 4. Briefly, a 1”x3” printed circuit board substrate was patterned with all necessary vias, ports, and electrical interconnects. The surface of the PCB was planarized with a layer of PDMS approximately 1mm thick, and appropriate vias were drilled using a biopsy punch to facilitate the fluidics and electronics. The actual microfluidic component, a long microchannel with a circular central

sorting region, are patterned in PDMS using soft lithography and aligned over the PCB. Embedded in this component in their specially grooves are six independent electrodes that converge at a circular sorting region at the center of the microchannel. the electrodes are Each electrode is independent of the other five and can send a signal, serve as a ground, or float itself out of the circuit. By selectively activating, grounding, and deactivating individual electrodes, the user can modify the net electric field located in circular chamber, and thus the resultant DEP force on any particles in the chamber as well.

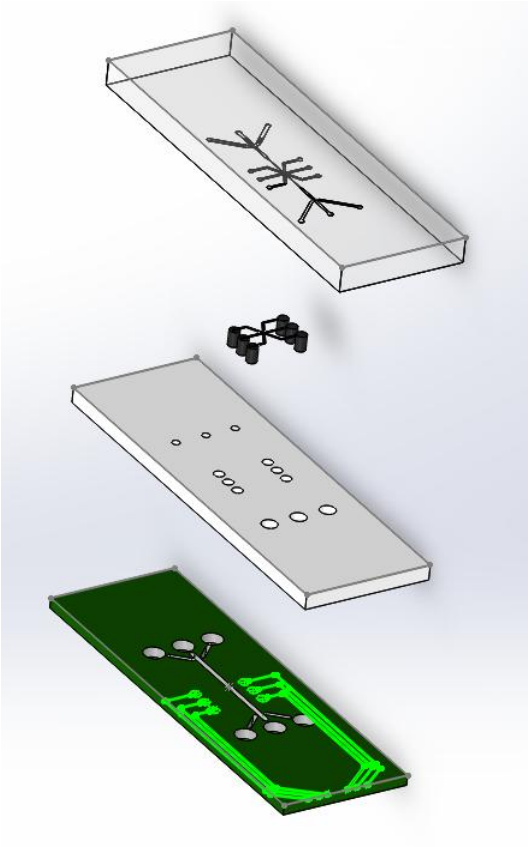

Figure 5.3.1 Device layers
The device starts with a PCB substrate (dark green), which includes all required vias, copper pads, and electrical traces (light green). On top of the PCB is a planarizing layer of PDMS, which includes all necessary vias and ports. Above that are the actual microchannels, patterned in PDMS using soft lithography. Electrodes are fabricated using a custom process and installed onto the microchannel layer separately. A low melting point solder was used to bridge the electrodes to the copper traces.

5.3.2 Numerical Methods

The Python-based DEP module used to generate particle trajectories in Chapters 3 and 4 was modified to perform analogous analyses with this device. To reiterate, the main flow channel and circular sorting chamber was drawn to scale in COMSOL, as were the positions of the six vertical electrodes. In COMSOL, the fluidic flow field in the chamber was generated. Finally, the net electric field in the sorting chamber was generated by setting the electrodes to signal, ground, or float, and to the appropriate voltage. The field data were then imported into Python along with the physical properties of the particles and the media, and the governing equations for dielectrophoresis were then applied to generate the predicted trajectories.

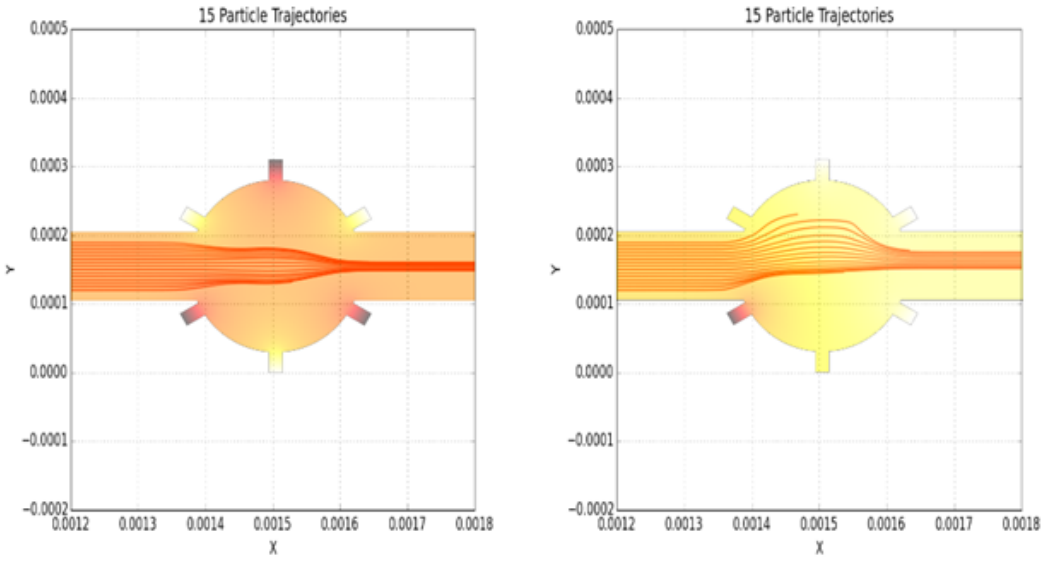

Figure 5.3.2 Simulated particle trajectories
Particle trajectories for various electrode switching configurations were simulated; two are depicted here. **Left:** Chamber as focuser. All electrodes are activated; every other electrode is set to signal while the rest are set to ground. **Right:** Chamber as deflector. One electrode is set to signal while the rest are set to ground.

5.3.3 Device Geometry

The finalized device design, based on the results from the simulations, is pictured below, with the electrodes in gray and the channels in blue. The microfluidic channel begins with the hydrodynamic focuser developed in Chapter 4; however, a system such as a micropillar focuser can easily be integrated. The main flow channel is 100µm wide and leads into a circular sorting region 250µm in diameter. The main flow channel reverts back to its 100µm width following on the other side of the circular sorting region and trifurcates into three outlets downstream.

The electrodes themselves converge at a circular sorting region located at the center of the main flow channel to form six vertical electrodes that sit flush with the perimeter of the circle. The vertical electrodes are each 20µm wide, and spaced 60^{o} apart. Each electrode is connected via a copper trace patterned in the PCB to an external switch for independent actuation.

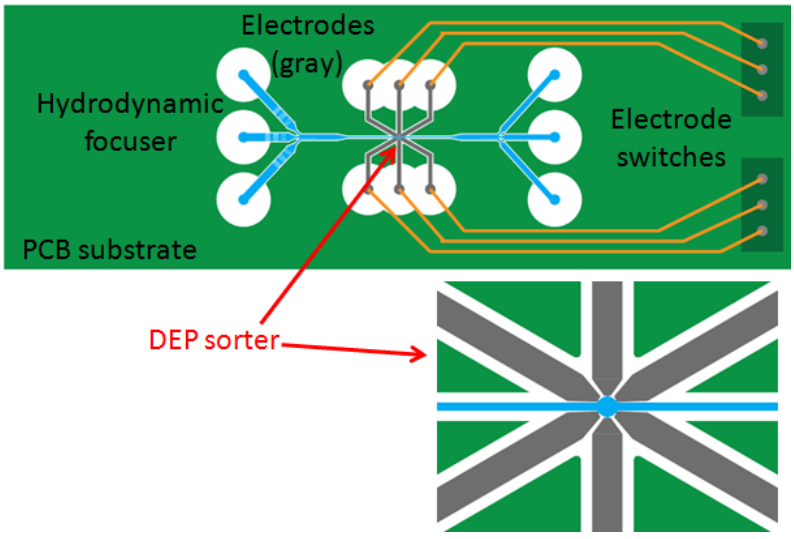

Figure 5.3.3 Device schematic
1"x3" PCB substrate (green) with microfluidic channels (blue) and electronics (gray). Electrodes converge at circular sorting region at the center of the main flow channel, and can be individually actuated to modify the shape of the net electric field in the sorting region. Electrodes are connected to off-board switches and electronics via traces patterned in the PCB (copper). All components are drawn to scale.

5.3.4 Electrode Fabrication

Three-dimensional microelectrodes were fabricated using a combination of techniques from photolithography, pick-and-place assembly, and microfluidics. Briefly, a 1”x3” glass substrate was covered with a 35µm thick film of adhesive-backed copper tape (3M, St. Paul, MN, USA). Subsequently, the tape was cleaned with acetone, isopropanol, and water, dried at 120^{o}C, and spin-coated with a 50µm thick layer of 1002F, a viscous negative photresist developed in-house. Next, openings are patterned in the 1002F using UV radiation, exposing areas of copper in the shape of the desired electrodes. The patterned sample is next immersed in a 40^{o}C bath of Techni Nickel HT-2 (Technic Inc., Cranston, RI, USA) opposite a nickel anode, and a DC current oscillating between 0-15mA is applied between the two for a period of five hours to isotropically electroplate nickel in the electrode-shaped openings up to 50µm. The copper tape, photoresist, and nickel electrodes are then delaminated from the glass as one unit, cleaned of all residual adhesive, and immersed in a mechanically agitated 60^{o}C bath of Copper Etchant BTP (Transene Company, Danvers, MA, USA) to selectively destroy the copper while preserving the nickel. Upon the removal of the copper, the film of 1002F is left, with the electrodes embedded within it.

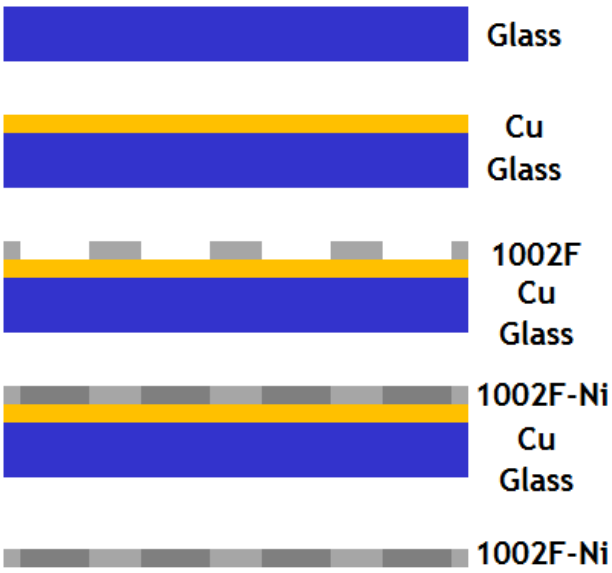

Figure 5.3.4 Electrode fabrication protocol
Copper tape mounted on a glass substrate is used as the base layer for the electroplating process. A film of 1002F photoresist is patterned on the copper, leaving pores in the shape of the desired electrodes. The entire complex is then immersed in nickel-plating solution at approximately 15mA for five hours to achieve the desired thickness. Finally, the copper substrate is destroyed using a wet etch process, leaving the electrodes and their photoresist carrier.

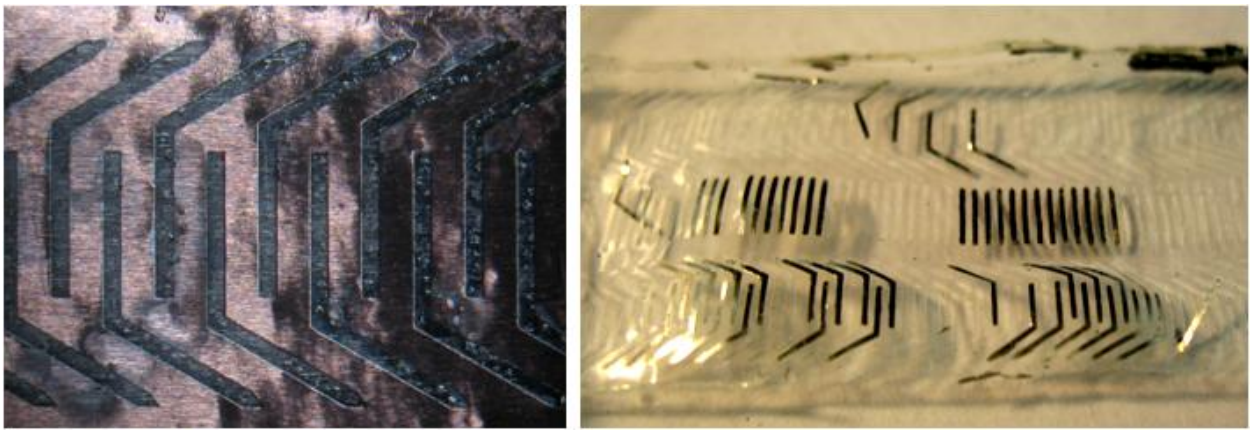

Figure 5.3.5 Electrodes
Left: Seed layer of nickel formed against a copper base. Areas free of nickel are covered with 1002F photoresist. **Right:** 1002F film and accompanying electrodes after release from copper. Film is partially depleted from use.

To address any concerns about biocompatibility between the nickel electrodes and the live mammalian cells flowing through the device, the fabricated electrodes were finished with a ten-minute immersion in Bright Electroless Gold solution (Transene Company, Danvers, MA, USA) at 85^{o}C for ten minutes. The final result is pictured below.

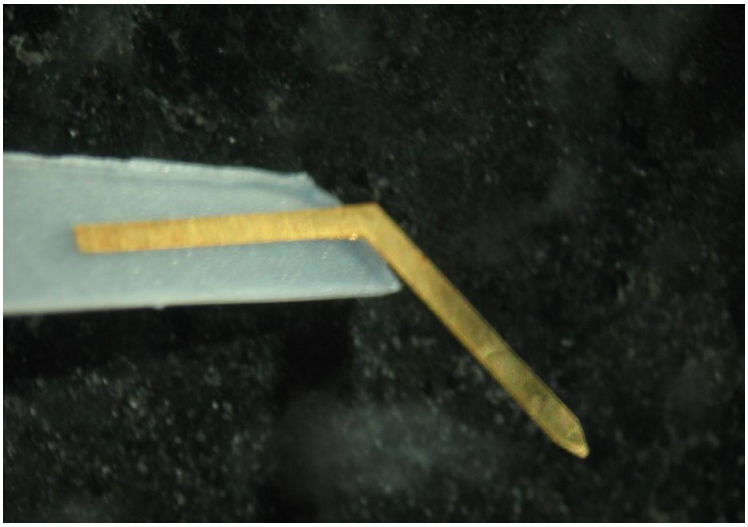

Figure 5.3.6 Completed electrode
Single electrode on electrostatic probe. Electrode has been plated in gold for biocompatibility purposes and released from 1002F carrier.

5.3.5 Pick-and-Place Assembly

These electrodes are patterned to fit snugly into microfluidic side channels that point into the circular deflection region in the main flow channel, and sit nearly flush against the inner wall of the deflection region. To physically place the electrodes, the patterned PDMS section was turned face-up under a stereomicroscope and needlepoint tweezer attachments were used to accurately slot them into position within the PDMS, guided by grooves patterned in the PDMS.

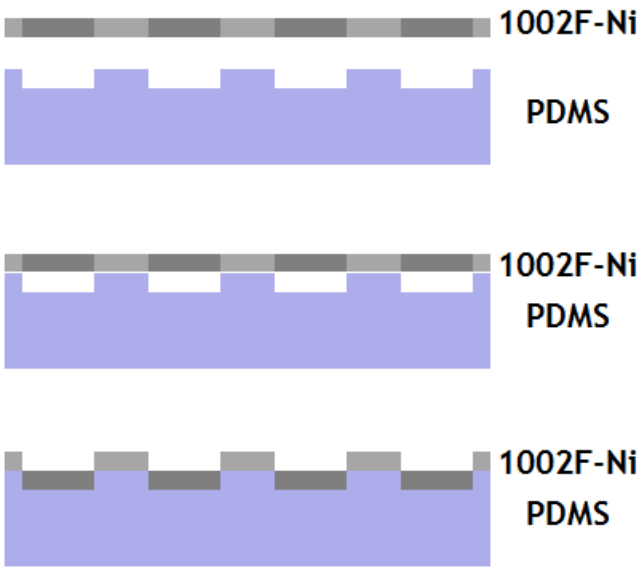

Figure 5.3.7 Transfer process
Electrodes embedded in photoresist film are aligned over their positions in the PDMS device; a small normal force is applied to transfer electrodes to their slots on the PDMS. Photoresist allows for the use of tools and methods such as micrometers, clamps, and patterned alignment markers, as well as for all embedded components to transfer to the target material per-aligned relative to each other.

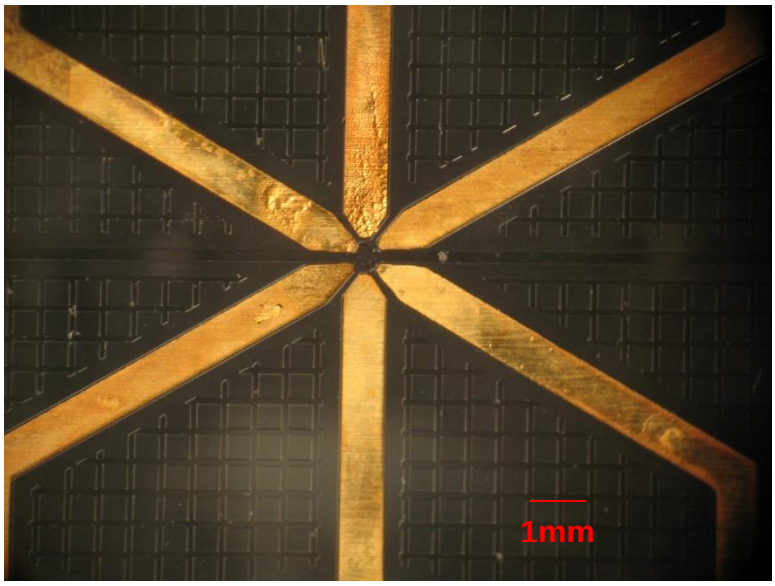

Figure 5.3.8 Placed electrodes
Six gold plated electrodes are shown in position on the PDMS component of the device.

5.3.6 External Interfacing

To facilitate external fluidic and electrical interconnects, 1”x3” printed circuit boards were drawn in EagleCAD and fabricated by a dedicated PCB manufacturer (NOA Labs, Kowloon, HK, PRC). The PCBs were planarized with a thin layer of PDMS and all necessary vias and ports were bored using biopsy punches. The prepared PCBs and the PDMS channels with embedded electrodes were plasma treated and then aligned and covalently bonded together.

Finally, to complete all electrical connections, the devices were heated up to 100^{o}C and an indium-bismuth-tin alloy (Indium Corporation, Clinton, NY, USA) was carefully applied to six separate vias on the PCB, connecting each electrode to a separate external switch which can apply a signal to the electrode, ground it, or float it. The signals themselves emanate from an external function generator and power amplifier.

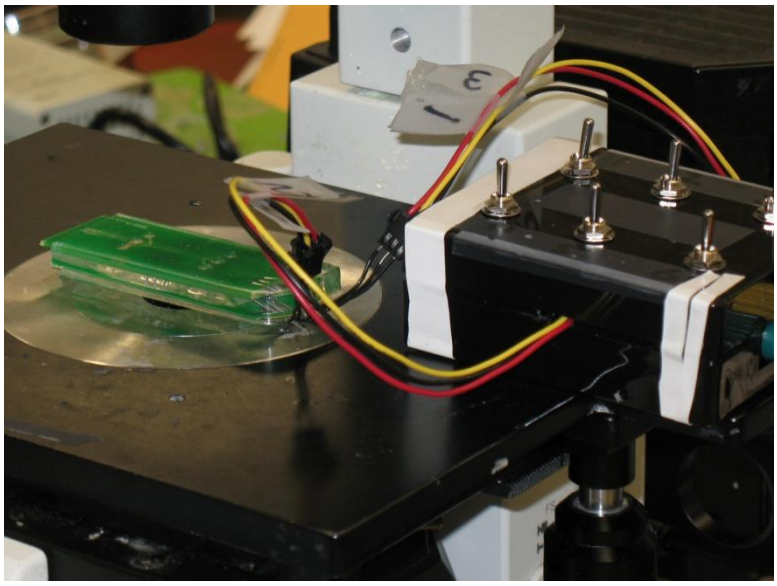

Figure 5.3.9 External interfacing
Electronic inputs are routed from an external signal generator and amplifier through a six-channel switchbox. Switching allows each electrode to deliver a signal or to ground or float itself.

5.4 *Results and Discussion*

A preliminary device was designed and built to demonstrate the fabrication processes developed; a completed device is depicted below. As shown, the device consists of a 100µm wide microchannel leading into a circular sorting region 250µm in diameter. Positioned around the perimeter of the sorting region are six microfabricated vertical electrodes arranged 60^{o} apart from one another; each can be actuated independently of the others. Exact electrode geometry and distribution was determined using numerical methods.

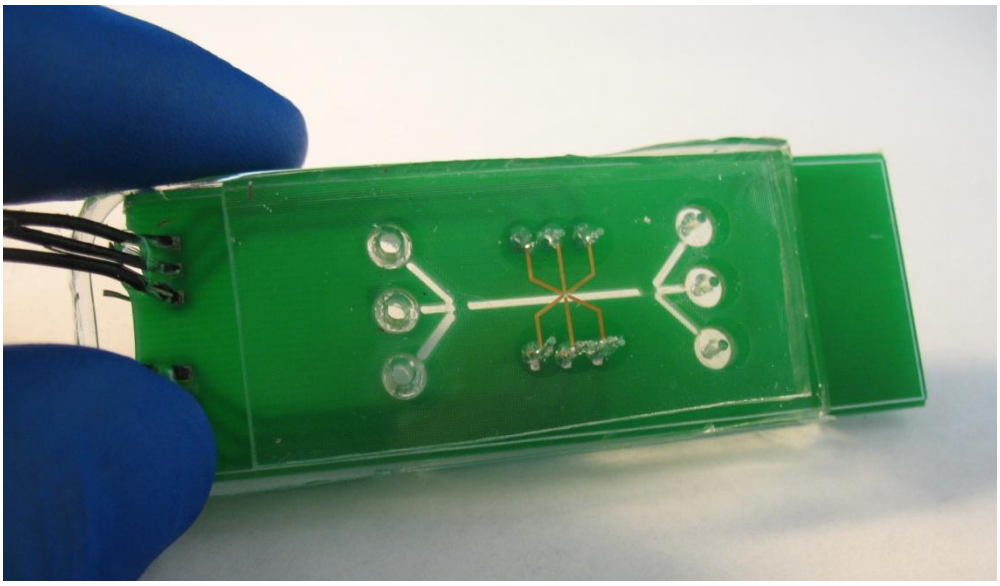

Figure 5.4.1 Completed device
A completed device is shown. Wires for external interface are to the left, in black. Traces are partially visible, leading external wiring to individual electrodes. Gold-plated electrodes converge at center of PDMS microchannel.

This device is unique among microfluidic DEP sorters in its ability to create a variety of electric field gradients. Most dielectrophoretic sorters can create one fixed field gradient geometry; the user can vary the amplitude only. As a result, the versatility of the device is limited to one function, e.g. particle trapping, deflecting, etc. Because all six electrodes in this device can be individually actuated or floated however, the net electric field in the sorting region is nearly endlessly modifiable.

Additionally, this device is unique in its fabrication process. Previous vertical electrode fabrication was constrained by various limitations: the devices either require significant electroplating, a difficult process further complicated by the fact that significant portions of the device, include the channels themselves, were made of silicon, a brittle material unsuited for use in most environments calling for microfluidics, or depended heavily on laminar flow principles, which limited the geometries of vertical electrodes to those depicted in Chapter 4. By fabricating

the electrodes separately from the main device, a wide variety of geometries became possible, free of the previous limitations.

5.5 *Conclusions*

A novel method is presented for the fabrication of three-dimensional metal electrodes inside a microfluidic device. Whereas previous work in three-dimensional electrode fabrication relied either on complicated microfabrication techniques or on fluidic properties unique to low Reynolds numbers, this process utilizes only methods

This work also demonstrates a novel method for microfluidic device fabrication. Microfluidic devices have historically been constructed in a monolithic process: each component or feature is carefully built on top of one another in a stepwise manner. As a result, as the number of steps increases, the cumulative failure rate rises exponentially, rendering the process more and more incompatible with large scale manufacture. By building components in batches and then assembling them together after each batch has passed quality assurance, however, the cumulative failure is merely that of the least successful batch individually; its troubles are not compounded against those of less failure-prone components.

Chapter 6: Conclusions

6.1 *Future Directions*

"Now this is not the end. It is not even the beginning of the end. But it is, perhaps, the end of the beginning."

-Sir Winston Leonard Spencer-Churchill

This work describes the progression of an electronic cell sorter from a traditional microfluidic device fabricated using non-ideal components all the way to a highly manufacturable device ready for incorporation with other microfluidic technologies. In the process, established methods from the electronics industry were effectively adapted or microfluidics, and significant improvements in device packaging were made over existing methods.

However, this only scratches the surface towards a lab-on-a-chip that will achieve a mainstream role in a biomedical laboratory. A completely integrated device must accept an input (biological or chemical sample) and seamlessly output a result (diagnosis, data about sample, etc.); this requires the development of all the auxiliary components leading both to and from the active analysis system. Interestingly enough, these components were themselves the focus of the initial wave of research into microfluidics, before the field shifted to development of the sorters themselves; by closing the circle and returning to this area, researchers would move the field into an ideal position for commercialization and mainstream adaptation. Some examples of the auxiliary components necessary are listed below.

6.1.1 Onboard Pumping

Crucial to the operation of microfluidic devices is the precise flow of fluids through them. Currently, this is performed using external mechanisms, namely syringe pumps, peristaltic pumps, or gravity. While sufficient for prototyping, it defeats the purpose of device miniaturization to require that a user carries a large heavy pump alongside the microfluidic device itself.

A logical solution is the addition of an onboard pump small enough to fit onto the handheld platform. Many such pumps are reported in the literature, and some such devices are already commercially available; it is a simple matter to extend traces on any PCB device to integrate them into the electronic system. Mechanically, as demonstrated previously, the use of a PCB platform facilitates the easy incorporation of interconnects to facilitate fluidic flow. The most obvious solution is the class of piezoelectric pumps developed specifically for microfluidic applications, though traditional gear-driven pumps are available as well. Alternative methods for driving fluids through microchannels include the use of less traditional techniques, such as capillary action and thermoconvection. Some examples are pictured below.

Figure 6.1.1 Piezoelectric pump
The depicted device is specifically designed from the ground up for microfluidics. Application-specific features include small form factor, lower power consumption, and high precision fluid delivery. Image courtesy of Dolomite Microfluidics.

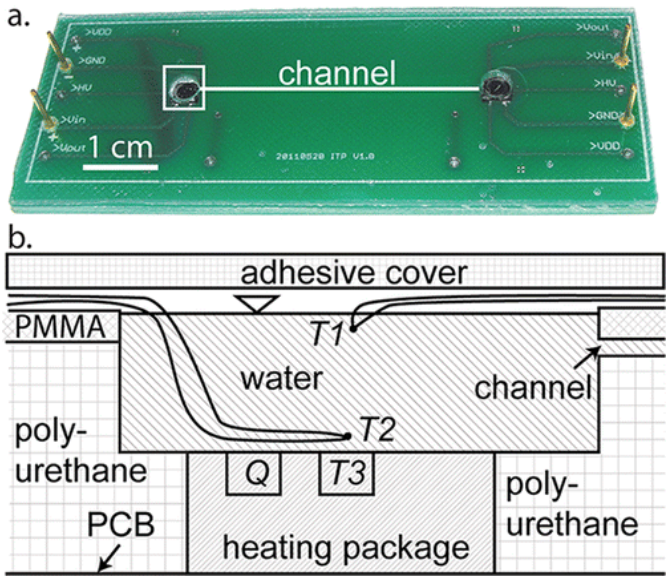

Figure 6.1.2 Thermoconvective pump
Hybrid PCB microfluidic device. **A:** (Green) PCB substrate with surface-mounted components and (clear) polymer microfluidic layers. The channel location is highlighted using a white line for clarity. Each end-channel reservoir is integrated with a thermistor temperature sensor and heater. **B:** Schematic of the cross section of the heated reservoir (outlined by the small white rectangle in part a). The thermistor (T3) and heaters lie within a 1 mm layer of thermal epoxy in the heating package. These are embedded in the 1 mm polyurethane planarization layer on the PCB substrate, above which is the polyurethane fluidic layer. The top layer of the device is 0.2 mm of stiff PMMA. Heat was applied at the embedded heater (Q). For temperature characterization, we instrumented the reservoirs with thermocouples T1 and T2, which measured temperature near the top and bottom of the liquid in the reservoir as shown. Reprinted with permission from [177]. Copyright 2011 American Chemical Society.

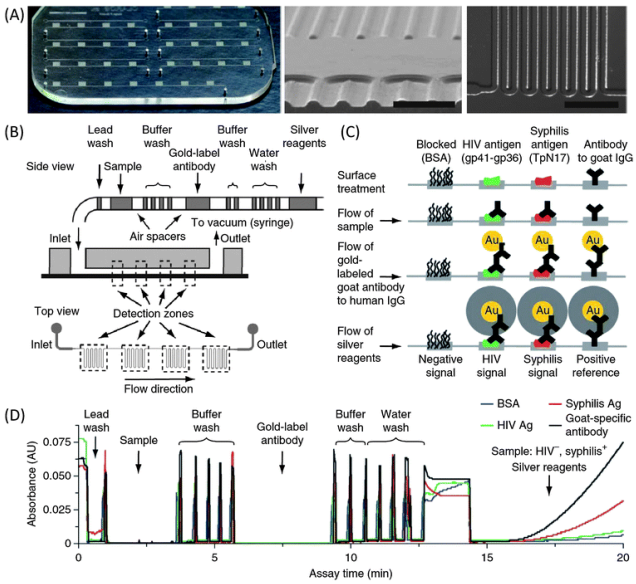

Figure 6.1.3 Preloaded fluidic system
A: Picture of microfluidic chip. Each chip can accommodate seven samples (one per channel), with molded holes for coupling of reagent-loaded tubes. **B:** Scanning electron microscope image of a cross-section of microchannels, made of injection-molded plastic. Scale bar, 500µm. **C:** Transmitted light micrograph of channel meanders. Scale bar, 1 mm. **D:** Schematic diagram of passive delivery of multiple reagents, which requires no moving parts on-chip. A preloaded sequence of reagents passes over a series of four detection zones, each characterized by dense meanders coated with capture proteins, before exiting the chip to a disposable syringe used to generate a vacuum for fluid actuation. **E:** Illustration of biochemical reactions in detection zones at different immunoassay steps. The reduction of silver ions on gold nanoparticle–conjugated antibodies yields signals that can be read with low-cost optics (for quantification) or examined by eye. **F:** Absorbance traces of a complete HIV-syphilis duplex test as reagent plugs pass through detection zones. High optical density (OD) is observed when air spacers pass through the detection zones, owing to increased refraction of light compared to in the liquid-filled channels. The train of reagents mimics the pipetting of reagents in and out of multiwell plates. This sample was evaluated (correctly against a reference standard) as HIV negative and syphilis positive. Ag, antigen. Reprinted by permission from Macmillan Publishers Ltd: [188], copyright 2011.

6.1.2 Miniaturizing Auxiliary Electronics

Analogous to the current obstacle with fluidics, microfluidic devices incorporating active sensors and actuators are currently heavily dependent on external electronics components such as signal generators, transmitters/receivers, power supplies, and optics. All of these are large bulky systems that cannot be removed from the laboratory; as such, miniaturizing them and developing

a standardized manner in which they are integrated onto a microfluidic platform is a top priority. Such electronics are already available and widely used in handheld devices such as cellular phones and tablet computers. Some examples are pictured below.

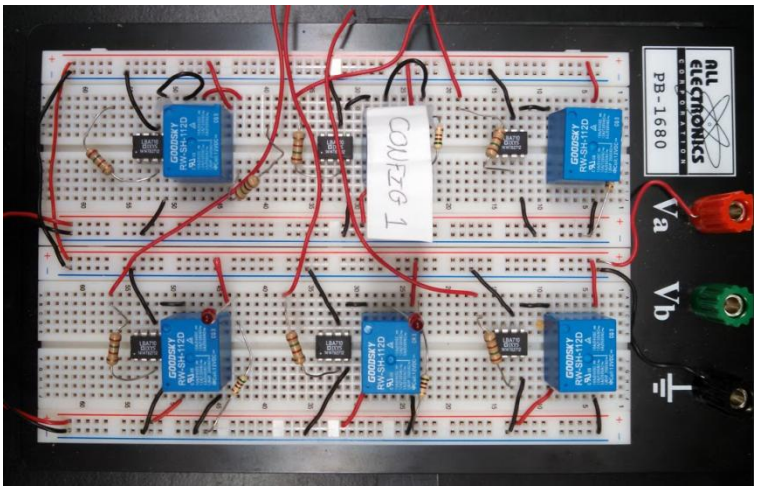

Figure 6.1.4 Electronic switching
Both mechanical and integrate switches have been developed for use in microfluidic devices. The switch pictured here consists of six mechanical relays controlled using a microcontroller and software interface. It is used to actuate vertical electrodes in the next iteration of the device presented in Chapter 5.

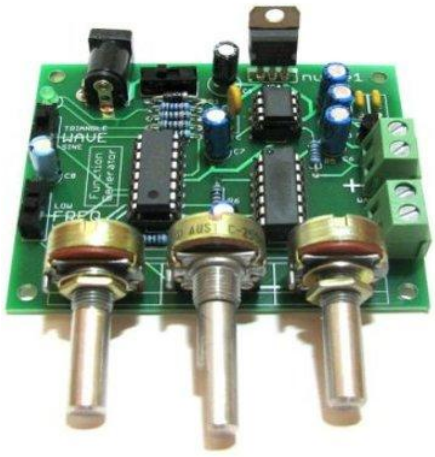

Figure 6.1.5 On-chip function generator
The advent of miniaturized signal generators allows engineers to bypass the cumbersome signal generators used in prototyping. Image courtesy of SparkFun Electronics.

6.1.3 Software Control

Microfluidic devices rarely include any sort of user interface at all, much less a dedicated GUI. Instead, users are required to manually operate each individual component of the experimental apparatus separately, all in parallel. Conventional tools such as LabVIEW can aid in this regard, but its applications are limited, and would not be appropriate in a situation in which all components are miniaturized and mounted onto a platform.

In conjunction with some of the miniaturized hardware mentioned above is the development of an Arduino-based program for use with integrated Arduino microcontrollers. Additionally, a Python-based package is in development to include generic microfluidics components, such as channels, valves, pumps, electrodes, and signal generators. The microfluidics engineer can thus easily assemble a GUI for the user, who in turn can intuitively and conveniently control all aspects of the device from a single interface.

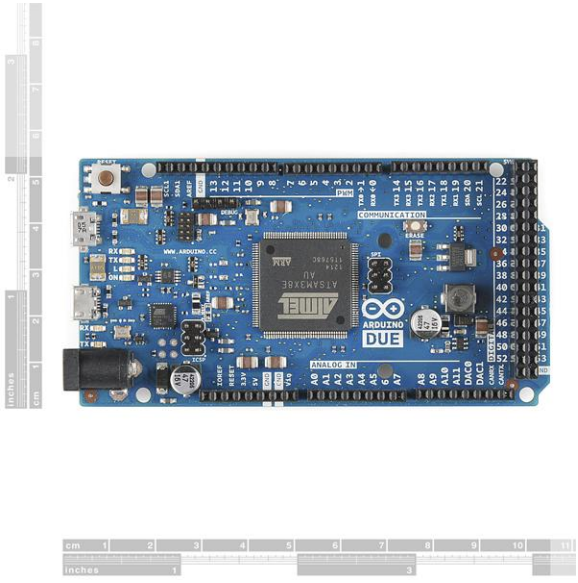

Figure 6.1.6 Miniaturized microcontroller
Off the shelf components such as Arduino-based microcontrollers enable engineers to overcome various issues regarding electronics integration in microfluidics. Image courtesy of SparkFun Electronics.

6.2 *Biomedical Applications of Interest*

This project was born of an initial interest in providing point-of-care diagnostic and analytical tools for clinicians and patients, as well as tools for routine cell biology assays popular along wet-bench researchers. However, it was soon discovered that devices fabricated using established microfluidics manufacturing techniques yielded devices that no end users would find practical or even operable. To that end, various methods were developed to improve the manufacturability and user-friendliness of microfluidics of all types. Listed below are some potential applications in which microfluidics might play a larger role after incorporating the methods developed in this project.

6.2.1 At-Home Complete Blood Counter

The spark for this project came when we learned that chemotherapy patients living in rural areas would often undergo an arduous commute to the nearest oncology clinic for a drug administration only to find themselves too immune deficient upon arrival to receive the prescribed course of treatment, at least without the use of IV antibiotics. If a patient could perform a complete blood count at home, the hypothesis became, much as a diabetic could collect a blood sugar reading with a simple finger prick, it would greatly simplify the process of monitoring the patient's immune health, and to more efficiently structure a chemotherapy regimen. The task seemed simple; after all, the literature included a large tome of methods for distinguishing one blood cell type from another using theoretically portable microfluidic devices. However, even as the device came together (Appendix A), it became obvious that a tremendous amount of development still stood between the crudely fabricated piece of glass and silicone before us and an actual device useful to the cancer patients who desperately needed the

technology. Now, several years of work later, that day has nearly arrived. By incorporating the fabrication methods developed in this work along with a few of the components described in Chapter 6.1, it would be possible to provide the end-user with all the tools required to perform a CBC, all in a convenient handheld package.

6.2.2 Rare Cell Detection

The at-home CBC system is a subset of a broader technology, the cell detector. In fact, rare cell detection may very well be the "killer app" that propels microfluidics into the mainstream. These devices have already demonstrated that, for certain cases, they can rival and even outperform FACS, the most venerated of particle sorters. However, unlike FACS, which carries with it over four decades of refinement, microfluidic cell detectors are, with few exception, are raw technologies with no development towards user friendliness or practicality. Additionally, while FACS systems are nearly entirely self-contained, microfluidic detectors tend to require costly and cumbersome pieces of laboratory equipment, such as pumps, power supplies, optical instrumentation, and a computer interface; the device can seem more like just one component of a large improvised apparatus than a self-contained analytical system. A standardized electronic base to modularly include common electronic and fluidic components as well as a slot for the active particle detection chip could simplify or solve this conundrum. The user would simply insert the chip of interest to complete the system. This approach saw widespread use in the 1980s and 1990s in another groundbreaking feat of miniaturization, that of bringing video arcade systems into the home via cartridge-based video game systems in which most of the components were installed in the system itself, with the balance selected, integrated, and programmed by the game engineer and included inside the video game cartridge.

6.2.3 Actively Controllable Particle Labeling

Particle labeling for applications such as immunoassays can be a time- and labor-intensive process. The ability to automatically and continuously move particles from one reagent to another would greatly simplify the process: the experimentalist would need only start the flow of the cell suspension, and the technology will do the rest. Microfluidic devices have already demonstrated some ability for this, such as a pillar system that can direct particles along a fixed path through multiple parallel streams of reagents, but a tool that can continuously identify each incoming particle and then not only direct it through the appropriate sequence of reagents but to keep the particle in a certain reagent for an appropriate time, e.g. however long it takes for a certain reaction to complete, would greatly remove the tedium from the task. This would require the integration of a few optical and electronic components, however, steps made relatively simple by the technologies presented in this work.

6.3 *Summary and Significance*

Microfluidic technology has grown over the past decade from crude channels for conducting simple chemistry experiments into a host of tools for biomedical science and clinical use. The ultimate challenge in the nascent field is to develop microscale analogs for every instrument in a conventional biomedical laboratory and integrate them all onto a single lab-on-a-chip. Their theoretical advantages over conventional biomedical lab instruments are tremendous: microfluidic devices consume less power, reagent volume, and potentially precious samples, carry significantly lower costs of entry, use, and maintenance, and can be used in remote environments independent of a fixed facility.

For these reasons, our group became interested in developing this technology for in-home medical diagnostics. However, in this endeavor, it was quickly discovered that despite the initial enthusiasm that propelled some rapid advances in microfluidics, to this day they rarely advance beyond the proof-of-concept stage and have not gained appreciable acceptance in the biomedical community.

A primary reason for this disappointing loss of momentum lies in the inattention to integration. Microfluidics engineers are primarily academics working under relatively small timescales and thus interested in short term goals; as a result, synergistic components are miniaturized and published individually. Unfortunately, this takes away from the time, energy, and material resources required to implement them onto a single platform. Instead, prototyping consists of running these designs independently, often tethered to ancillary bulk devices in the laboratory they were meant to replace.

This work demonstrates several steps towards overcoming this quagmire and restoring the course towards a true lab-on-a-chip. First, a device was fabricated combining multiple microfluidic components and it was demonstrated that the components working in series yielded a significantly improved result over each working independently. Next, methods from the microelectronics industry were applied to microfluidics to fabricate a novel lab-on-PCB. Printed circuit boards, a mainstay in electronics fabrication, can greatly reduce the difficulty and cost associated with integrating a large number of microfluidic components onto a single platform, and should soon supplant the unwieldly photolithography-based methods used today. Finally, pick-and-place methods developed in the field of surface mount technologies, long used to rapidly and precisely populate printed circuit boards, were adapted towards rapidly incorporating microelectronic components into microfluidic devices.

Microfluidic particle sorting technologies have finally approached the maturity required to move beyond proof-of-concept and into clinics, biotech laboratories, and homes. Indeed, very soon will come the day when a physician or a patient might perform a quick assay with some ubiquitous microfluidic gizmo and chuckle, "How did we ever get along without these things?" The technological developments presented in this work, while modest in the face of the revolutionary work of Moldavan, Herzenberg, Terry, and Whitesides, and almost certainly destined for a relatively minor place in the annals of biomedical engineering, nonetheless represent a few tiny advancements in that direction.

Chapter 7: Appendices

7.1 *Appendix A*

As discussed in Chapter 6, this project began as a perhaps overly-optimistic attempt at applying existing dielectrophoresis technology for performing a complete blood count. As such, very initial DEP experiments were conducted using traditional planarized gold electrodes patterned on a 1”x3” glass slide, with PDMS microchannels plasma-bonded over them. The device soon proved too impractical for general use, and soon after, the project expanded beyond it towards adapting microfluidics of all types for greater manufacturability and user friendliness. Nonetheless it did serve its original purpose and still retains a useful tool for a microfluidics engineer, and is presented here for the record.

7.1.1 Device

The electrodes consist of 50µm wide interdigitated bars spaced 50µm apart. An AC signal is applied to the electrodes in such a way that every other electrode is at the same potential at any moment in time; as a result, an equivalent electric field exists between every electrode bar, and the field is strongest at the electrode edges and weakest away from them. As particles are flowed over the array of electrodes, those undergoing pDEP are drawn to the electrode edges, where the electric field is strongest, while those undergoing nDEP are repelled and exit the device through the outlet.

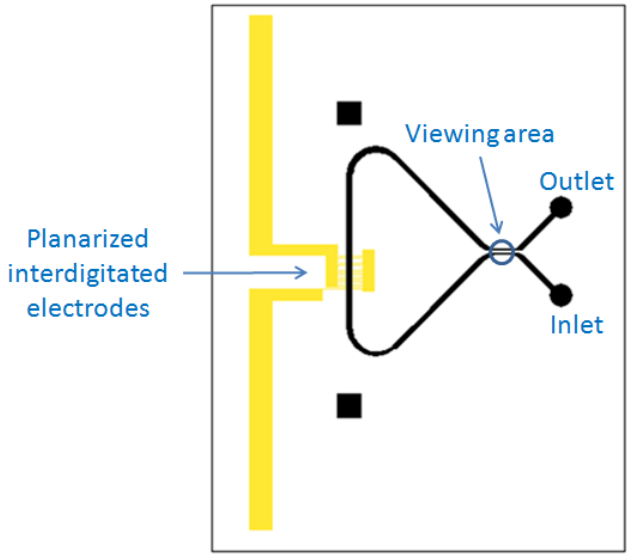

Figure 7.1.1 Device schematic
The device consists of a microfluidic channel that carries a cell suspension along a triangular-shaped path. Halfway through the path, the suspension passes over interdigitated electrodes. Particles experiencing pDEP are trapped at the edges of the electrodes, while particles experiencing nDEP remain in suspension and flow to the device outlet.

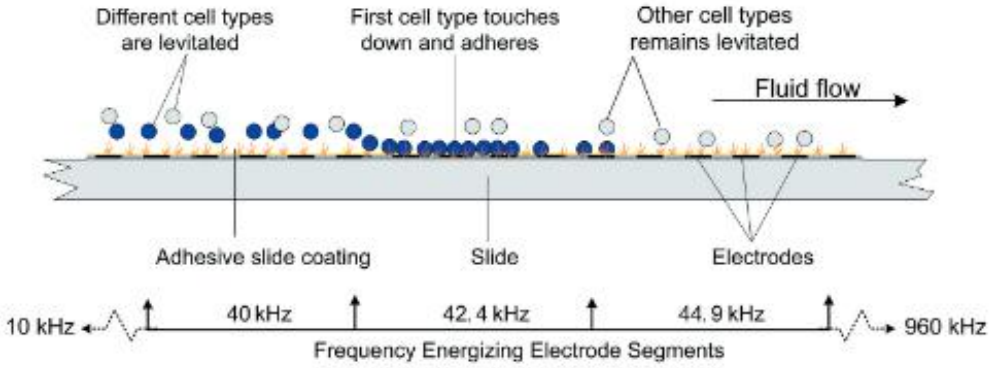

Figure 7.1.2 Device operating principle
Trapping particles as they pass over interdigitated electrodes is perhaps the most common form of DEP-based particle sorting. The signal frequency can be tuned to have a strong pDEP force, shown in blue in the schematic, in which case they move quickly to the electrodes and land relatively upstream, a weak pDEP force, shown in gray in the schematic, in which they made move slowly to the electrodes and land further downstream, or a nonexistent or nDEP force, in which case they remain in suspension and exit the device. Reprinted from [123] with permission from John Wiley and Sons. Copyright 2008.

7.1.2 Cell Prep

10ml of whole blood was collected from donors through UCI GCRC and processed using a routine protocol. Briefly, blood was diluted in a 1:1 ratio with PBS and gently layered over Ficoll-Paque, a density separation medium. Upon centrifugation, layers were separated by gentle aspiration, and batches of PBMCs, granulocytes, and platelets were collected. Residual erythrocytes were eliminated using lysis buffer. All cells were washed in PBS, suspended in DEP buffer (recipe as in Chapter 3, minus RPMI, $\sigma_m = 40\mu S/cm$) , and flowed through the device under positive pressure in a manner identical the methods described in Chapter 3.

7.1.3 Results

Video footage of cells passing through the viewing area was collected using brightfield microscopy; cells were videoed across a wide range of frequencies, from 50kHz to 3MHz. To quantify a cell population's response as a function of frequency, particles entering and exiting the device were enumerated using a MATLAB-based image processing packaged developed in-house. Trapping efficiency was defined as the percent of particles that did not exit the device through the outlet.

Figure 7.1.3 Automated particle enumeration
Video footage of particles entering and exiting the device was analyzed using a custom MATLAB program. Image processing techniques were used to compare adjacent frames, identify uncounted particles, and count them.

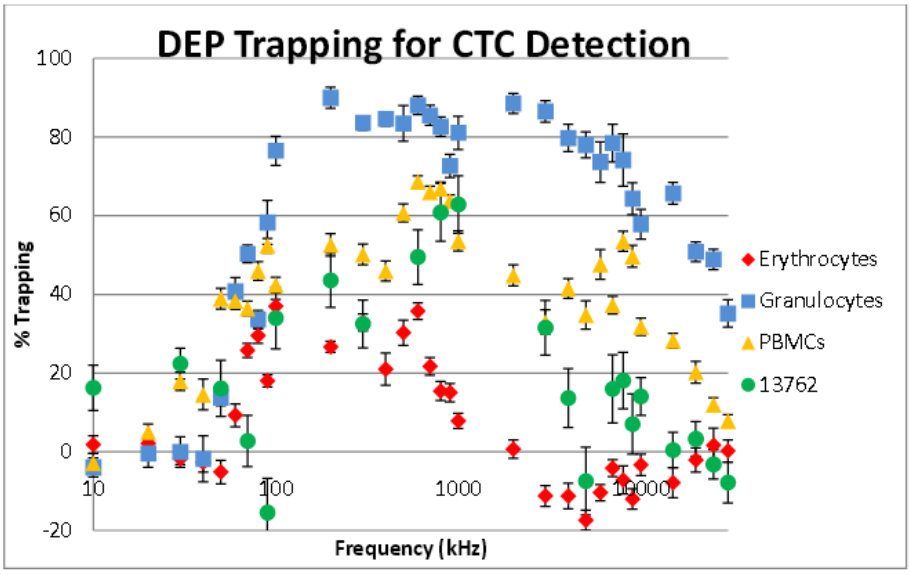

Figure 7.1.4 Particle trapping data
As shown above, granulocytes displayed a relatively dramatic pDEP force around the 1MHz mark, whereas erythrocytes displayed either no DEP force or a weak pDEP force at best, across the entire range of frequencies. Tumor cells and PBMCs fell somewhere in the middle.

7.1.4 Other Applications for Device

This DEP device, while simple and somewhat limited on its own, has proven useful as an auxiliary tool for quickly approximating a particle's C-M curve at a certain buffer. It is a simple matter of flowing particles over the planarized electrodes and performing a frequency sweep from Hz to MHz ranges.

Figure 7.1.5 Preliminary measurement of particles' dielectric properties
Particles passed over the interdigitated electrodes at a certain frequency and voltage can be settle at the electrode edge (pDEP). Particles undergoing nDEP will either pass over the electrodes completely or become trapped on top of the bulk of the electrode, caught between the field maxima at each of an electrode's two edges.

7.1.5 Conclusions

This early device, based heavily on designs from the literature, was intended to quickly test the potential for DEP to allow patients to perform at-home complete blood counts using a handheld device. The project soon evolved well beyond that initial scope, but the device remains a viable method for quickly approximating a particle's dielectric properties and for performing simple particle sorts.

7.2 *Appendix B*

Building on the trials detailed in Appendix A, attempts were made to perform a label-based DEP sort of tumor cells against a leukocyte background. This assay would be of interest to both the oncology diagnostics community as well as to researchers studying the mechanisms of metastasis. However, according to the literature and the data presented in Appendix A, it is a very delicate tuning process distinguishing one particle type from another based solely on size and dielectric properties, DEP's two testable parameters. The objective was thus to selectively tag the target cells using polystyrene microspheres via immunological methods. Because polystyrene particles' dielectric constants differ greatly from all mammalian cells, it was hypothesized that a wide range of frequencies existed at which the polymer particles would experience a DEP force in one direction while all mammalian cells experience a DEP force in the opposite direction. Following from this, a mammalian cell tagged with several polystyrene beads would experience a net DEP force somewhere in between the two extremes, and could be separated from untagged cells. In this scenario, a wide range of frequencies could be used to isolate cells of interest, instead of a very specific signal whose effect on the cell type of interest differs slightly than on other cells. In other words, the immunochemistry, a very specific tool, and not DEP, a less specific tool, does the majority of the targeting. The DEP force is relegated to primarily a particle retrieval role.

7.2.1 Device

This trial was conducted using an early prototype of the device presented in Chapter 3. While fundamentally similar in that electric field lines are guided by insulating structures normal to the walls of the main flow channel, for this trial, an attempt was made to avoid the use of any

conductive materials altogether, and rely entirely on channel geometry to create electric field gradients. This technology, which would subsequently be further developed by others, would come to be known in the literature as insulator-based dielectrophoresis (iDEP). Additionally, this device predates the development of the prefocusing technology, and particles enter the DEP sorting region dispersed across the entire width of the channel.

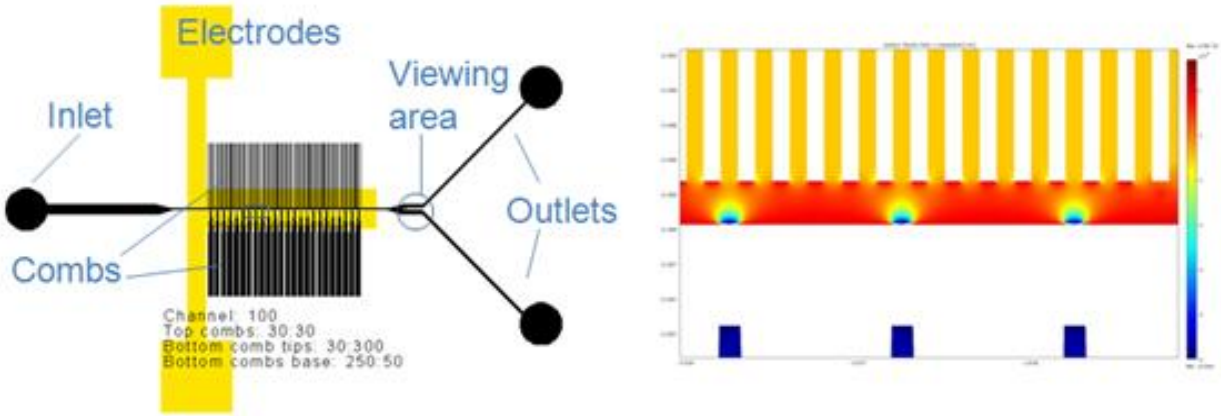

Figure 7.2.1 Schematic of early iDEP-type device
Left: Device Schematic. PDMS microchannels (black) are aligned over planarized electrodes (gold). **Right:** COMSOL simulation of operating principle. The electric field across the main flow channel contains several strong bumps at the bottom edge (three depicted), which diffuse towards the top edge.

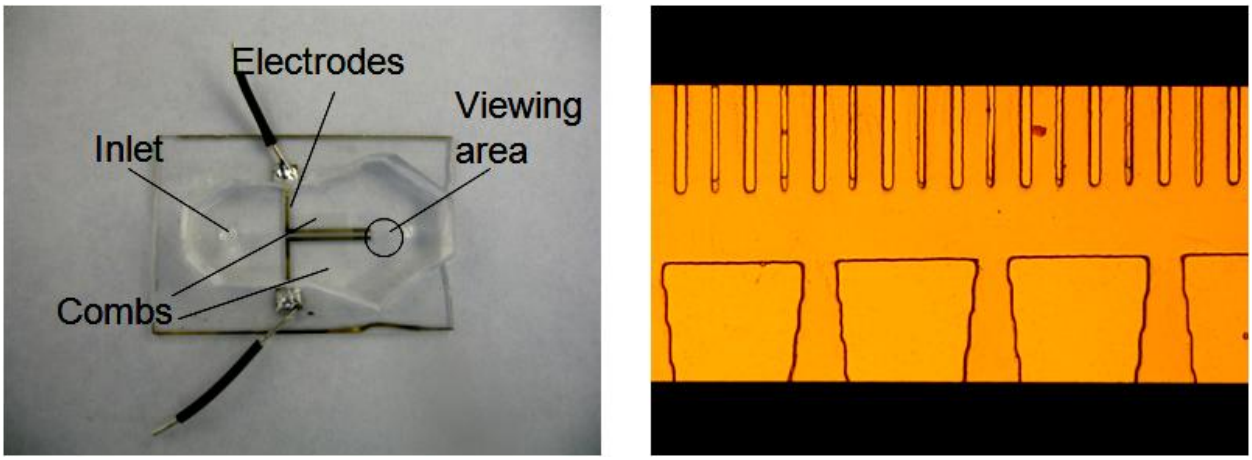

Figure 7.2.2 Fabricated iDEP-type device
Left: Device consists of PDMS microchannels plasma bonded over gold electrodes photolithographically patterned onto a 1"x1.5" piece of glass. **Right:** DEP sorting region. Electrode geometry is similar to those of the devices in Chapters 3 and 4, but no conductive material bridges the gold electrodes (black) and the main flow channel. As a result, although the DEP functioned in accordance with theory, a large voltage was required to compensate for the resistive losses in the side channels.

7.2.2 Cell Prep

Leukocytes were obtained using the protocol described in Appendix 7.1. To prepare the model CTCs, freshly detached SK-BR-3 cells were washed in PBS and incubated at a concentration of 10^6 cells/ml in FACS buffer containing 20µg/ml of biotinylated anti-EpCAM (Abcam, Cambridge, MA, USA) for thirty minutes at room temperature. Cells were washed and subsequently resuspended with streptavinated fluorescent polystyrene microspheres with a diameter of 6µm at a ratio of five beads per cell and again allowed to incubate for thirty minutes at room temperature under mild agitation. Finally, tagged cells were washed and suspended in DEP buffer.

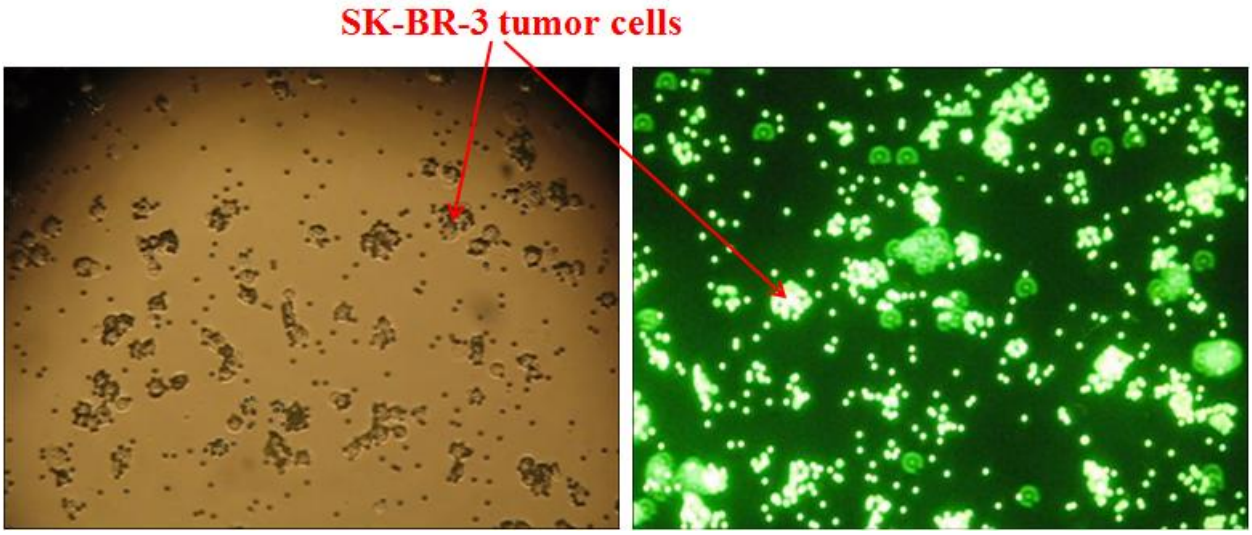

Figure 7.2.3 Tagged SK-BR-3 cells
Left: Brightfield image of tagged SK-BR-3s and loose fluospheres. **Right:** Same particles, viewed under 488nm illumination.

7.2.3 Results

Tagged cells and PBMCs were suspended at a 1:1 ratio in DEP buffer and flowed through the device at 1µL/min. A sinusoidal signal AC signal at 50kHz and 112V_{pp} was applied. Theoretically, at this frequency, the polystyrene beads experience a strong nDEP force and will be repelled towards the top channel, dragging the SK-BR-3 with it, while according to the data in Appendix 7.1, the PBMCs should display a more mixed response, with perhaps a slight tendency towards the bottom channel. Results are shown in the figure below. Imaging was performed using brightfield and fluorescent microscopy, and enumeration was performed manually.

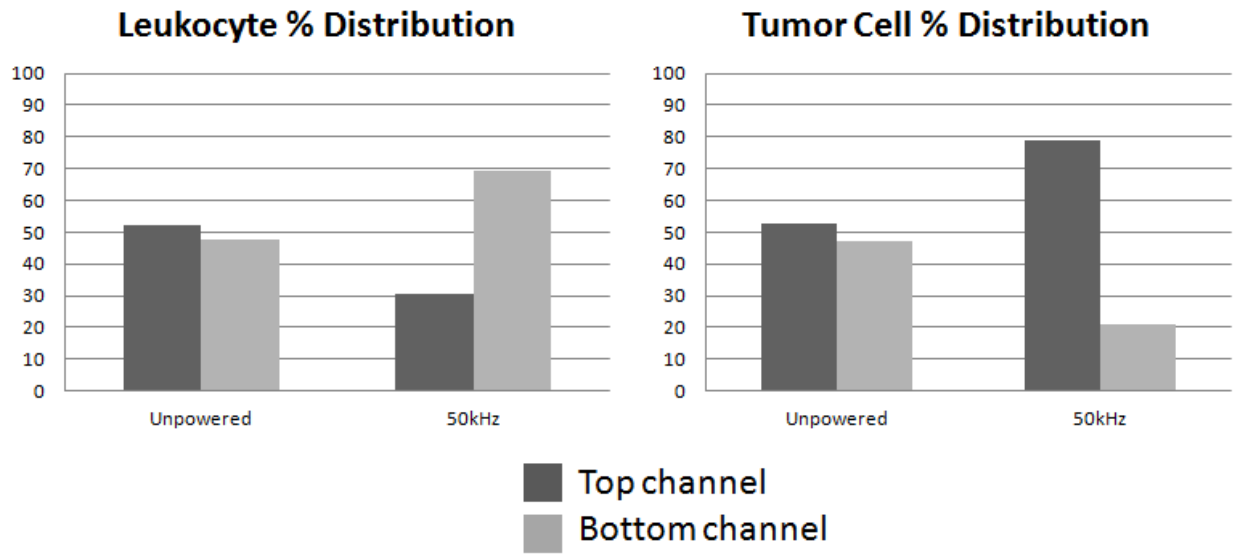

Figure 7.2.4 Leukocyte vs. Tumor Cell Distribution
Particle distribution before and after activation of DEP sorter is plotted. as expected, particles were randomly distributed when the device was off. However, activation of the device at 50kHz drove bead-tagged SK-BR-3 cells away from areas of high field strength and towards the upper outlet, whereas PBMCs were relatively unaffected.

As shown, particles were randomly distributed between both channels in an unpowered device. However, upon application of the electric field gradient, the polystyrene beads indeed drag their attached tumor cells into one channel, while PBMCs favor the other channel.

7.2.4 Conclusions

In this work, it was demonstrated that immunologically tagging target cells with polystyrene beads could yield interesting DEP-based separations. Specifically, while mammalian cells display similar DEP properties regardless of cell type, thus muddling any DEP-based sort, cells conjugated with polystyrene particles display dielectric properties very unlike those of just cells alone. As a result, the sensitivity and specificity of the DEP sort is greatly enhanced, and is dependent more on the accuracy of the tagging process than on the dielectric response. In this

particular assay, the tagging process is very high, given that it relied on the use of EpCAM, a marker commonly found on solid tumors, including those from which SK-BR-3 was derived, but not on leukocytes. This process can be adapted to other cell types and the possibilities are indeed exciting; however, care should be taken to ensure that the tagging accuracy remains relatively high.

REFERENCES

[1] N. Pamme, "Continuous flow separations in microfluidic devices," *Lab. Chip*, vol. 7, no. 12, p. 1644, 2007.

[2] M. Wintrobe, *Blood, Pure and Eloquent: A Story of Discovery, of People, and of Ideas*. 1980.

[3] H. W. Hou, A. A. S. Bhagat, A. G. Lin Chong, P. Mao, K. S. Wei Tan, J. Han, and C. T. Lim, "Deformability based cell margination-A simple microfluidic design for malaria-infected erythrocyte separation," *Lab Chip*, vol. 10, no. 19, pp. 2605–2613, 2010.

[4] M. Yu, S. Stott, M. Toner, S. Maheswaran, and D. A. Haber, "Circulating tumor cells: approaches to isolation and characterization," *J. Cell Biol.*, vol. 192, no. 3, pp. 373–382, Feb. 2011.

[5] P. Paterlini-Brechot and N. L. Benali, "Circulating tumor cells (CTC) detection: Clinical impact and future directions," *Cancer Lett.*, vol. 253, no. 2, pp. 180–204, Aug. 2007.

[6] W. Sheng, O. O. Ogunwobi, T. Chen, J. Zhang, T. J. George, C. Liu, and Z. H. Fan, "Capture, release and culture of circulating tumor cells from pancreatic cancer patients using an enhanced mixing chip," *Lab. Chip*, vol. 14, no. 1, pp. 89–98, Nov. 2013.

[7] A. L. Kierszenbaum and L. Tres, *Histology and Cell Biology: An Introduction to Pathology*. Elsevier Health Sciences, 2015.

[8] J. Zhang, R. E. Campbell, A. Y. Ting, and R. Y. Tsien, "Creating new fluorescent probes for cell biology," *Nat. Rev. Mol. Cell Biol.*, vol. 3, no. 12, pp. 906–918, Dec. 2002.

[9] C. M. Baum, I. L. Weissman, A. S. Tsukamoto, A. M. Buckle, and B. Peault, "Isolation of a candidate human hematopoietic stem-cell population," *Proc. Natl. Acad. Sci.*, vol. 89, no. 7, pp. 2804–2808, Apr. 1992.

[10] S. W. Levison, C. Chuang, B. J. Abramson, and J. E. Goldman, "The migrational patterns and developmental fates of glial precursors in the rat subventricular zone are temporally regulated," *Development*, vol. 119, no. 3, pp. 611–622, Nov. 1993.

[11] A. A. Neurauter, M. Bonyhadi, E. Lien, L. Nøkleby, E. Ruud, S. Camacho, and T. Aarvak, *Cell Isolation and Expansion Using Dynabeads ®*. Springer Berlin Heidelberg, 2007.

[12] S. Miltenyi, W. Muller, W. Weichel, and A. Radbruch, "High gradient magnetic cell separation with MACS," *Cytometry*, vol. 11, no. 2, pp. 231–238, 1990.

[13] S.-Y. Teh, R. Lin, L.-H. Hung, and A. P. Lee, "Droplet microfluidics," *Lab. Chip*, vol. 8, no. 2, pp. 198–220, 2008.

[14] L. L. Lanier, "Just the FACS," *J. Immunol.*, vol. 193, no. 5, pp. 2043–2044, Sep. 2014.

[15] B. J. Bain, *Blood Cells: A Practical Guide*. John Wiley & Sons, 2015.

[16] F. Piccinini, A. Tesei, G. Paganelli, W. Zoli, and A. Bevilacqua, "Improving reliability of live/dead cell counting through automated image mosaicing," *Comput. Methods Programs Biomed.*, vol. 117, no. 3, pp. 448–463, Dec. 2014.

[17] T. Sato and H. Clevers, "Primary Mouse Small Intestinal Epithelial Cell Cultures," in *Epithelial Cell Culture Protocols*, vol. 945, S. H. Randell and M. L. Fulcher, Eds. Humana Press, 2013, pp. 319–328.

[18] D. English and B. R. Andersen, "Single-step separation of red blood cells, granulocytes and mononuclear leukocytes on discontinuous density gradients of Ficoll-Hypaque," *J. Immunol. Methods*, vol. 5, no. 3, pp. 249–252, Aug. 1974.

[19] L. A. Herzenberg, D. Parks, B. Sahaf, O. Perez, M. Roederer, and L. A. Herzenberg, “The History and Future of the Fluorescence Activated Cell Sorter and Flow Cytometry: A View from Stanford,” *Clin. Chem.*, vol. 48, no. 10, pp. 1819–1827, Oct. 2002.
[20] A. Moldavan, “Photo-Electric Technique For The Counting Of Microscopical Cells,” *Science*, vol. 80, no. 2069, pp. 188–189, Aug. 1934.
[21] R. G. Sweet, “High Frequency Recording with Electrostatically Deflected Ink Jets,” *Rev. Sci. Instrum.*, vol. 36, no. 2, pp. 131–136, Feb. 1965.
[22] P. J. Crosland-Taylor, “A Device for Counting Small Particles suspended in a Fluid through a Tube,” *Nature*, vol. 171, no. 4340, pp. 37–38, Jan. 1953.
[23] C. W. H and C. W. H, *Means for counting particles suspended in a fluid*. 1949.
[24] M. J. Fulwyler, “Electronic Separation of Biological Cells by Volume,” *Science*, vol. 150, no. 3698, pp. 910–911, Nov. 1965.
[25] M. H. Julius, T. Masuda, and L. A. Herzenberg, “Demonstration That Antigen-Binding Cells Are Precursors of Antibody-Producing Cells After Purification with a Fluorescence-Activated Cell Sorter,” *Proc. Natl. Acad. Sci. U. S. A.*, vol. 69, no. 7, p. 1934, Jul. 1972.
[26] H. R. Hulett, W. A. Bonner, J. Barrett, and L. A. Herzenberg, “Cell Sorting: Automated Separation of Mammalian Cells as a Function of Intracellular Fluorescence,” *Science*, vol. 166, no. 3906, pp. 747–749, Nov. 1969.
[27] W. A. Bonner, H. R. Hulett, R. G. Sweet, and L. A. Herzenberg, “Fluorescence Activated Cell Sorting,” *Rev. Sci. Instrum.*, vol. 43, no. 3, pp. 404–409, Mar. 1972.
[28] L. A. Herzenberg, R. G. Sweet, and L. A. Herzenberg, “Fluorescence-activated cell sorting,” *Sci Am*, vol. 234, no. 3, pp. 108–117, 1976.
[29] M. R. Melamed, “A brief history of flow cytometry and sorting,” *Cytometry*, p. 1, 2000.
[30] J. Haron, “Flow Cytometry and Cell Sorting: A Practical Guide,” *Mater. Methods*, Mar. 2015.
[31] R. R. Jahan-Tigh, C. Ryan, G. Obermoser, and K. Schwarzenberger, “Flow Cytometry,” *J. Invest. Dermatol.*, vol. 132, no. 10, p. e1, Oct. 2012.
[32] T. Rowley, “Flow Cytometry - A Survey and the Basics,” *Mater. Methods*, Mar. 2015.
[33] S. C. Terry, “A gas chromatography system fabricated on a silicon wafer using integrated circuit technology,” 1975.
[34] S. C. Terry, J. H. Jerman, and J. B. Angell, “A gas chromatographic air analyzer fabricated on a silicon wafer,” *IEEE Trans. Electron Devices*, vol. 26, no. 12, pp. 1880–1886, Dec. 1979.
[35] A. Manz, N. Graber, and H. M. Widmer, “Miniaturized total chemical analysis systems: A novel concept for chemical sensing,” *Sens. Actuators B Chem.*, vol. 1, no. 1–6, pp. 244–248, Jan. 1990.
[36] D. C. Duffy, J. C. McDonald, O. J. Schueller, and G. M. Whitesides, “Rapid prototyping of microfluidic systems in poly (dimethylsiloxane),” *Anal. Chem.*, vol. 70, no. 23, pp. 4974–4984, 1998.
[37] P. J. A. Kenis, R. F. Ismagilov, and G. M. Whitesides, “Microfabrication Inside Capillaries Using Multiphase Laminar Flow Patterning,” *Science*, vol. 285, no. 5424, pp. 83–85, Jul. 1999.
[38] G. M. Whitesides, “The origins and the future of microfluidics,” *Nature*, vol. 442, pp. 368–373, 2006.
[39] E. K. Sackmann, A. L. Fulton, and D. J. Beebe, “The present and future role of microfluidics in biomedical research,” *Nature*, vol. 507, no. 7491, pp. 181–189, Mar. 2014.

[40] J. West, M. Becker, S. Tombrink, and A. Manz, “Micro Total Analysis Systems: Latest Achievements,” *Anal. Chem.*, vol. 80, no. 12, pp. 4403–4419, Jun. 2008.
[41] L. Yang, P. P. Banada, M. R. Chatni, K. S. Lim, A. K. Bhunia, M. Ladisch, and R. Bashir, “A multifunctional micro-fluidic system for dielectrophoretic concentration coupled with immuno-capture of low numbers of Listeria monocytogenes,” *Lab. Chip*, vol. 6, no. 7, pp. 896–905, Jun. 2006.
[42] D. E. Hertzog, B. Ivorra, B. Mohammadi, O. Bakajin, and J. G. Santiago, “Optimization of a Microfluidic Mixer for Studying Protein Folding Kinetics,” *Anal. Chem.*, vol. 78, no. 13, pp. 4299–4306, Jul. 2006.
[43] Q. Ramadan, V. Samper, D. Poenar, Z. Liang, C. Yu, and T. M. Lim, “Simultaneous cell lysis and bead trapping in a continuous flow microfluidic device,” *Sens. Actuators B Chem.*, vol. 113, no. 2, pp. 944–955, Feb. 2006.
[44] F. Lacharme and M. A. M. Gijs, “Single potential electrophoresis microchip with reduced bias using pressure pulse injection,” *ELECTROPHORESIS*, vol. 27, no. 14, pp. 2924–2932, Jul. 2006.
[45] J. G. Shackman, M. S. Munson, and D. Ross, “Gradient Elution Moving Boundary Electrophoresis for High-Throughput Multiplexed Microfluidic Devices,” *Anal. Chem.*, vol. 79, no. 2, pp. 565–571, Jan. 2007.
[46] B. Cordovez, D. Psaltis, and D. Erickson, “Trapping and storage of particles in electroactive microwells,” *Appl. Phys. Lett.*, vol. 90, no. 2, p. 024102, 2007.
[47] C. C. Chen, J. S. Wang, and O. Solgaard, “Micromachined bubble-jet cell sorter with multiple operation modes,” *Sens. Actuators B Chem.*, vol. 117, no. 2, pp. 523–529, 2006.
[48] D. Sud, G. Mehta, K. Mehta, J. Linderman, S. Takayama, and M.-A. Mycek, “Optical imaging in microfluidic bioreactors enables oxygen monitoring for continuous cell culture,” *J. Biomed. Opt.*, vol. 11, no. 5, pp. 050504–050504–3, 2006.
[49] D. S. Kim, S. H. Lee, C. H. Ahn, J. Y. Lee, and T. H. Kwon, “Disposable integrated microfluidic biochip for blood typing by plastic microinjection moulding,” *Lab. Chip*, vol. 6, no. 6, pp. 794–802, 2006.
[50] J. Ziegler, M. Zimmermann, P. Hunziker, and E. Delamarche, “High-Performance Immunoassays Based on Through-Stencil Patterned Antibodies and Capillary Systems,” *Anal. Chem.*, vol. 80, no. 5, pp. 1763–1769, Mar. 2008.
[51] M. Hashimoto, F. Barany, and S. A. Soper, “Polymerase chain reaction/ligase detection reaction/hybridization assays using flow-through microfluidic devices for the detection of low-abundant DNA point mutations,” *Biosens. Bioelectron.*, vol. 21, no. 10, pp. 1915–1923, Apr. 2006.
[52] N. N. Watkins, U. Hassan, G. Damhorst, H. Ni, A. Vaid, W. Rodriguez, and R. Bashir, “Microfluidic CD4+ and CD8+ T Lymphocyte Counters for Point-of-Care HIV Diagnostics Using Whole Blood,” *Sci. Transl. Med.*, vol. 5, no. 214, pp. 214ra170–214ra170, Dec. 2013.
[53] A. W. Martinez, S. T. Phillips, G. M. Whitesides, and E. Carrilho, “Diagnostics for the Developing World: Microfluidic Paper-Based Analytical Devices,” *Anal. Chem.*, vol. 82, no. 1, pp. 3–10, Jan. 2010.
[54] K. Eun Sung, N. Yang, C. Pehlke, P. J. Keely, K. W. Eliceiri, A. Friedl, and D. J. Beebe, “Transition to invasion in breast cancer: a microfluidic in vitro model enables examination of spatial and temporal effects,” *Integr. Biol.*, vol. 3, no. 4, pp. 439–450, 2011.

[55] A. M. Taylor, M. Blurton-Jones, S. W. Rhee, D. H. Cribbs, C. W. Cotman, and N. L. Jeon, "A microfluidic culture platform for CNS axonal injury, regeneration and transport," *Nat. Methods*, vol. 2, no. 8, pp. 599–605, Aug. 2005.
[56] X. Mao and T. Jun Huang, "Microfluidic diagnostics for the developing world," *Lab. Chip*, vol. 12, no. 8, pp. 1412–1416, 2012.
[57] L. R. Volpatti and A. K. Yetisen, "Commercialization of microfluidic devices," *Trends Biotechnol.*, vol. 32, no. 7, pp. 347–350, Jul. 2014.
[58] Y. Xia and G. M. Whitesides, "Soft Lithography," *Annu. Rev. Mater. Sci.*, vol. 28, no. 1, pp. 153–184, 1998.
[59] G. M. Whitesides, E. Ostuni, S. Takayama, X. Jiang, and D. E. Ingber, "SOFT LITHOGRAPHY IN BIOLOGY AND BIOCHEMISTRY," *Annu. Rev. Biomed. Eng.*, vol. 3, no. 1, pp. 335–373, 2001.
[60] W. C. Teach and G. C. Kiessling, *Polystyrene*, vol. 18. Reinhold Publishing Corporation, 1960.
[61] C.-W. Tsao and D. L. DeVoe, "Bonding of thermoplastic polymer microfluidics," *Microfluid. Nanofluidics*, vol. 6, no. 1, pp. 1–16, Nov. 2008.
[62] M. L. Hupert, W. J. Guy, S. D. Llopis, H. Shadpour, S. Rani, D. E. Nikitopoulos, and S. A. Soper, "Evaluation of micromilled metal mold masters for the replication of microchip electrophoresis devices," *Microfluid. Nanofluidics*, vol. 3, no. 1, pp. 1–11, Jun. 2006.
[63] V. N. Goral, Y.-C. Hsieh, O. N. Petzold, R. A. Faris, and P. K. Yuen, "Hot embossing of plastic microfluidic devices using poly(dimethylsiloxane) molds," *J. Micromechanics Microengineering*, vol. 21, no. 1, p. 017002, Jan. 2011.
[64] E. W. K. Young, E. Berthier, D. J. Guckenberger, E. Sackmann, C. Lamers, I. Meyvantsson, A. Huttenlocher, and D. J. Beebe, "Rapid Prototyping of Arrayed Microfluidic Systems in Polystyrene for Cell-Based Assays," *Anal. Chem.*, vol. 83, no. 4, pp. 1408–1417, Feb. 2011.
[65] E. Berthier, E. W. K. Young, and D. Beebe, "Engineers are from PDMS-land, Biologists are from Polystyrenia," *Lab. Chip*, vol. 12, no. 7, pp. 1224–1237, Apr. 2012.
[66] A. S. Curtis, J. V. Forrester, C. McInnes, and F. Lawrie, "Adhesion of cells to polystyrene surfaces.," *J. Cell Biol.*, vol. 97, no. 5, pp. 1500–1506, 1983.
[67] L. Martynova, L. E. Locascio, M. Gaitan, G. W. Kramer, R. G. Christensen, and W. A. MacCrehan, "Fabrication of Plastic Microfluid Channels by Imprinting Methods," *Anal. Chem.*, vol. 69, no. 23, pp. 4783–4789, Dec. 1997.
[68] A. W. Browne, M. J. Rust, W. Jung, S. H. Lee, and C. H. Ahn, "A rapid prototyping method for polymer microfluidics with fixed aspect ratio and 3D tapered channels," *Lab. Chip*, vol. 9, no. 20, pp. 2941–2946, Oct. 2009.
[69] A. C. Henry, T. J. Tutt, M. Galloway, Y. Y. Davidson, C. S. McWhorter, S. A. Soper, and R. L. McCarley, "Surface Modification of Poly(methyl methacrylate) Used in the Fabrication of Microanalytical Devices," *Anal. Chem.*, vol. 72, no. 21, pp. 5331–5337, Nov. 2000.
[70] J. Zhang, C. Das, and Z. H. Fan, "Dynamic coating for protein separation in cyclic olefin copolymer microfluidic devices," *Microfluid. Nanofluidics*, vol. 5, no. 3, pp. 327–335, Dec. 2007.
[71] E. Piccin, W. K. T. Coltro, J. A. Fracassi da Silva, S. C. Neto, L. H. Mazo, and E. Carrilho, "Polyurethane from biosource as a new material for fabrication of microfluidic devices by rapid prototyping," *J. Chromatogr. A*, vol. 1173, no. 1–2, pp. 151–158, Nov. 2007.

[72] Y. Lu, W. Shi, L. Jiang, J. Qin, and B. Lin, “Rapid prototyping of paper-based microfluidics with wax for low-cost, portable bioassay,” *Electrophoresis*, vol. 30, no. 9, pp. 1497–1500, May 2009.
[73] A. Nilghaz, D. H. B. Wicaksono, D. Gustiono, F. A. A. Majid, E. Supriyanto, and M. R. A. Kadir, “Flexible microfluidic cloth-based analytical devices using a low-cost wax patterning technique,” *Lab. Chip*, vol. 12, no. 1, pp. 209–218, 2012.
[74] Y. Lu, W. Shi, J. Qin, and B. Lin, “Fabrication and Characterization of Paper-Based Microfluidics Prepared in Nitrocellulose Membrane By Wax Printing,” 11-Dec-2009. [Online]. Available: http://pubs.acs.org/doi/abs/10.1021/ac9020193. [Accessed: 15-Jul-2015].
[75] R. Fobel, A. E. Kirby, A. H. Ng, R. R. Farnood, and A. R. Wheeler, “Paper microfluidics goes digital,” *Adv. Mater.*, vol. 26, no. 18, pp. 2838–2843, 2014.
[76] R. Pelton, “Bioactive paper provides a low-cost platform for diagnostics,” *TrAC Trends Anal. Chem.*, vol. 28, no. 8, pp. 925–942, Sep. 2009.
[77] C. D. Chin, V. Linder, and S. K. Sia, “Commercialization of microfluidic point-of-care diagnostic devices,” *Lab. Chip*, vol. 12, no. 12, pp. 2118–2134, 2012.
[78] N. Blow, “Microfluidics: the great divide,” *Nat. Methods*, vol. 6, no. 9, pp. 683–686, Sep. 2009.
[79] P. N. Nge, C. I. Rogers, and A. T. Woolley, “Advances in Microfluidic Materials, Functions, Integration, and Applications,” *Chem. Rev.*, vol. 113, no. 4, pp. 2550–2583, Apr. 2013.
[80] C. Gartner, H. Becker, B. Anton, and O. Roetting, “Microfluidic toolbox: tools and standardization solutions for microfluidic devices for life sciences applications,” 2004, vol. 5345, pp. 159–162.
[81] D. R. Gossett, W. M. Weaver, A. J. Mach, S. C. Hur, H. T. K. Tse, W. Lee, H. Amini, and D. Di Carlo, “Label-free cell separation and sorting in microfluidic systems,” *Anal. Bioanal. Chem.*, vol. 397, no. 8, pp. 3249–3267, Apr. 2010.
[82] S. Nagrath, L. V. Sequit, S. Maheswaran, D. W. Bell, D. Irimia, L. Ulkus, M. R. Smith, E. L. Kwak, S. Digumarthy, A. Muzikansky, P. Ryan, U. J. Balis, R. G. Tompkins, D. A. Haber, and M. Toner, “Isolation of rare circulating tumor cells in cancer patients by microchip technology,” *Nature*, vol. 450, pp. 1235 – 1239, 2007.
[83] A. A. S. Bhagat, H. Bow, H. W. Hou, S. J. Tan, J. Han, and C. T. Lim, “Microfluidics for cell separation,” *Med. Biol. Eng. Comput.*, vol. 48, no. 10, pp. 999–1014, Apr. 2010.
[84] S. S. Kuntaegowdanahalli, A. A. S. Bhagat, G. Kumar, and I. Papautsky, “Inertial microfluidics for continuous particle separation in spiral microchannels,” *Lab. Chip*, vol. 9, no. 20, p. 2973, 2009.
[85] W. Sheng, T. Chen, R. Kamath, X. Xiong, W. Tan, and Z. H. Fan, “Aptamer-Enabled Efficient Isolation of Cancer Cells from Whole Blood Using a Microfluidic Device,” *Anal. Chem.*, vol. 84, no. 9, pp. 4199–4206, May 2012.
[86] H. Morgan, M. P. Hughes, and N. G. Green, “Separation of Submicron Bioparticles by Dielectrophoresis,” *Biophys. J.*, vol. 77, no. 1, pp. 516–525, Jul. 1999.
[87] S. Zheng, H. Lin, J.-Q. Liu, M. Balic, R. Datar, R. J. Cote, and Y.-C. Tai, “Membrane microfilter device for selective capture, electrolysis and genomic analysis of human circulating tumor cells,” *J. Chromatogr. A*, vol. 1162, no. 2, pp. 154–161, Aug. 2007.

[88] H. M. Ji, V. Samper, Y. Chen, C. K. Heng, T. M. Lim, and L. Yobas, "Silicon-based microfilters for whole blood cell separation," *Biomed. Microdevices*, vol. 10, no. 2, pp. 251–257, Oct. 2007.
[89] A. Williams, S. Rawal, Z. Ao, J. Torres-Munoz, M. Balic, M. Zhou, S. Zheng, Y.-C. Tai, R. J. Cote, and R. Datar, "Clinical translation of a novel microfilter technology Capture, characterization and culture of circulating tumor cells," in *2013 IEEE Point-of-Care Healthcare Technologies (PHT)*, 2013, pp. 220–223.
[90] V. VanDelinder and A. Groisman, "Perfusion in Microfluidic Cross-Flow: Separation of White Blood Cells from Whole Blood and Exchange of Medium in a Continuous Flow," *Anal. Chem.*, vol. 79, no. 5, pp. 2023–2030, Mar. 2007.
[91] V. VanDelinder and A. Groisman, "Separation of Plasma from Whole Human Blood in a Continuous Cross-Flow in a Molded Microfluidic Device," *Anal. Chem.*, vol. 78, no. 11, pp. 3765–3771, Jun. 2006.
[92] V. VanDelinder and A. Groisman, "Perfusion in Microfluidic Cross-Flow: Separation of White Blood Cells from Whole Blood and Exchange of Medium in a Continuous Flow," *Anal. Chem.*, vol. 79, no. 5, pp. 2023–2030, Mar. 2007.
[93] M. Yamada, M. Nakashima, and M. Seki, "Pinched Flow Fractionation: Continuous Size Separation of Particles Utilizing a Laminar Flow Profile in a Pinched Microchannel," *Anal. Chem.*, vol. 76, no. 18, pp. 5465–5471, 2004.
[94] J. B. Knight, A. Vishwanath, J. P. Brody, and R. H. Austin, "Hydrodynamic Focusing on a Silicon Chip: Mixing Nanoliters in Microseconds," *Phys. Rev. Lett.*, vol. 80, no. 17, pp. 3863–3866, Apr. 1998.
[95] X. Mao, S.-C. Steven Lin, C. Dong, and T. Jun Huang, "Single-layer planar on-chip flow cytometer using microfluidic drifting based three-dimensional (3D) hydrodynamic focusing," *Lab. Chip*, vol. 9, no. 11, pp. 1583–1589, 2009.
[96] G.-B. Lee, C.-C. Chang, S.-B. Huang, and R.-J. Yang, "The hydrodynamic focusing effect inside rectangular microchannels," *J. Micromechanics Microengineering*, vol. 16, no. 5, p. 1024, 2006.
[97] N. Sundararajan, M. S. Pio, L. P. Lee, and A. Berlin, "Three-dimensional hydrodynamic focusing in polydimethylsiloxane (PDMS) microchannels," *Microelectromechanical Syst. J. Of*, vol. 13, no. 4, pp. 559–567, 2004.
[98] J. Takagi, M. Yamada, M. Yasuda, and M. Seki, "Continuous particle separation in a microchannel having asymmetrically arranged multiple branches," *Lab. Chip*, vol. 5, no. 7, pp. 778–784, 2005.
[99] L. R. Huang, E. C. Cox, R. H. Austin, and J. C. Sturm, "Continuous Particle Separation Through Deterministic Lateral Displacement," *Science*, vol. 304, no. 5673, pp. 987–990, May 2004.
[100] D. W. Inglis, J. A. Davis, R. H. Austin, and J. C. Sturm, "Critical particle size for fractionation by deterministic lateral displacement," *Lab. Chip*, vol. 6, no. 5, pp. 655–658, 2006.
[101] J. P. Beech, S. H. Holm, K. Adolfsson, and J. O. Tegenfeldt, "Sorting cells by size, shape and deformability," *Lab. Chip*, vol. 12, no. 6, pp. 1048–1051, Feb. 2012.
[102] D. D. Carlo, D. Irimia, R. G. Tompkins, and M. Toner, "Continuous inertial focusing, ordering, and separation of particles in microchannels," *Proc. Natl. Acad. Sci.*, vol. 104, no. 48, pp. 18892–18897, Nov. 2007.

[103] S. C. Jacobson, R. Hergenroder, L. B. Koutny, and J. M. Ramsey, “High-Speed Separations on a Microchip,” *Anal. Chem.*, vol. 66, no. 7, pp. 1114–1118, Apr. 1994.
[104] A. J. Hughes and A. E. Herr, “Microfluidic Western blotting,” *Proc. Natl. Acad. Sci.*, vol. 109, no. 52, pp. 21450–21455, Dec. 2012.
[105] A. E. Herr, A. K. Singh, and D. J. Throckmorton, *Microchannel gel electrophoretic separation systems and methods for preparing and using*. Google Patents, 2015.
[106] S. Saedinia, K. L. Nastiuk, J. J. Krolewski, G. P. Li, and M. Bachman, “Laminated microfluidic system for small sample protein analysis,” *Biomicrofluidics*, vol. 8, no. 1, p. 014107, Jan. 2014.
[107] M. He and A. E. Herr, “Microfluidic Polyacrylamide Gel Electrophoresis with in Situ Immunoblotting for Native Protein Analysis,” *Anal. Chem.*, vol. 81, no. 19, pp. 8177–8184, Oct. 2009.
[108] A. Lenshof and T. Laurell, “Continuous separation of cells and particles in microfluidic systems,” *Chem. Soc. Rev.*, vol. 39, no. 3, pp. 1203–1217, 2010.
[109] H. Lee, L. Xu, B. Ahn, K. Lee, and K. W. Oh, “Continuous-flow in-droplet magnetic particle separation in a droplet-based microfluidic platform,” *Microfluid. Nanofluidics*, vol. 13, no. 4, pp. 613–623, 2012.
[110] N. Pamme, J. C. T. Eijkel, and A. Manz, “On-chip free-flow magnetophoresis: Separation and detection of mixtures of magnetic particles in continuous flow,” *J. Magn. Magn. Mater.*, vol. 307, no. 2, pp. 237–244, Dec. 2006.
[111] J. D. Adams, U. Kim, and H. T. Soh, “Multitarget magnetic activated cell sorter,” *Proc. Natl. Acad. Sci.*, vol. 105, no. 47, pp. 18165–18170, Nov. 2008.
[112] Y. Liu and K.-M. Lim, “Particle separation in microfluidics using a switching ultrasonic field,” *Lab. Chip*, vol. 11, no. 18, pp. 3167–3173, 2011.
[113] J. Nam, H. Lim, C. Kim, J. Y. Kang, and S. Shin, “Density-dependent separation of encapsulated cells in a microfluidic channel by using a standing surface acoustic wave,” *Biomicrofluidics*, vol. 6, no. 2, p. 024120, 2012.
[114] S. Gupta, D. L. Feke, and I. Manas-Zloczower, “Fractionation of mixed particulate solids according to compressibility using ultrasonic standing wave fields,” *Chem. Eng. Sci.*, vol. 50, no. 20, pp. 3275–3284, 1995.
[115] A. Ashkin, J. M. Dziedzic, J. E. Bjorkholm, and S. Chu, “Observation of a single-beam gradient force optical trap for dielectric particles,” *Opt. Lett.*, vol. 11, no. 5, pp. 288–290, 1986.
[116] M. M. Wang, E. Tu, D. E. Raymond, J. M. Yang, H. Zhang, N. Hagen, B. Dees, E. M. Mercer, A. H. Forster, I. Kariv, P. J. Marchand, and W. F. Butler, “Microfluidic sorting of mammalian cells by optical force switching,” *Nat. Biotechnol.*, vol. 23, no. 1, pp. 83–87, Jan. 2005.
[117] A. Ashkin, “Optical trapping and manipulation of neutral particles using lasers,” *Proc. Natl. Acad. Sci.*, vol. 94, no. 10, pp. 4853–4860, May 1997.
[118] E. B. Cummings and A. K. Singh, “Dielectrophoresis in Microchips Containing Arrays of Insulating Posts: Theoretical and Experimental Results,” *Anal. Chem.*, vol. 75, no. 18, pp. 4724–4731, Sep. 2003.
[119] T. Schnelle, T. Müller, G. Gradl, S. G. Shirley, and G. Fuhr, “Dielectrophoretic manipulation of suspended submicron particles,” *Electrophoresis*, vol. 21, no. 1, pp. 66–73, 2000.

[120] H. A. Pohl, "The Motion and Precipitation of Suspensoids in Divergent Electric Fields," *J. Appl. Phys.*, vol. 22, no. 7, pp. 869–871, Jul. 1951.
[121] R. Zhou, P. Wang, and H.-C. Chang, "Bacteria capture, concentration and detection by alternating current dielectrophoresis and self-assembly of dispersed single-wall carbon nanotubes," *Electrophoresis*, vol. 27, no. 7, pp. 1376–1385, Apr. 2006.
[122] M. Frénéa, S. P. Faure, B. Le Pioufle, P. Coquet, and H. Fujita, "Positioning living cells on a high-density electrode array by negative dielectrophoresis," *Mater. Sci. Eng. C*, vol. 23, no. 5, pp. 597–603, Oct. 2003.
[123] M. Cristofanilli, S. Krishnamurthy, C. M. Das, J. M. Reuben, W. Spohn, J. Noshari, F. Becker, and P. R. Gascoyne, "Dielectric cell separation of fine needle aspirates from tumor xenografts," *J. Sep. Sci.*, vol. 31, no. 21, pp. 3732–3739, 2008.
[124] L. A. Flanagan, J. Lu, L. Wang, S. A. Marchenko, N. L. Jeon, A. P. Lee, and E. S. Monuki, "Unique Dielectric Properties Distinguish Stem Cells and Their Differentiated Progeny," *Stem Cells*, vol. 26, no. 3, pp. 656–665, Mar. 2008.
[125] P. R. C. Gascoyne and J. Vykoukal, "Particle separation by dielectrophoresis," *Electrophoresis*, vol. 23, no. 13, pp. 1973–1983, Jul. 2002.
[126] K.-H. Han and A. B. Frazier, "Lateral-driven continuous dielectrophoretic microseparators for blood cells suspended in a highly conductive medium," *Lab. Chip*, vol. 8, no. 7, pp. 1079–1086, 2008.
[127] N.-C. Chen, C.-H. Chen, M.-K. Chen, L.-S. Jang, and M.-H. Wang, "Single-cell trapping and impedance measurement utilizing dielectrophoresis in a parallel-plate microfluidic device," *Sens. Actuators B Chem.*, vol. 190, pp. 570–577, Jan. 2014.
[128] M. P. Hughes, *Nanoelectromechanics in Engineering and Biology*. CRC Press, 2010.
[129] S. Park, M. Koklu, and A. Beskok, "Particle Trapping in High-Conductivity Media with Electrothermally Enhanced Negative Dielectrophoresis," *Anal. Chem.*, vol. 81, no. 6, pp. 2303–2310, Mar. 2009.
[130] R. Pethig and G. H. Markx, "Applications of dielectrophoresis in biotechnology," *Trends Biotechnol.*, vol. 15, no. 10, pp. 426–432, Oct. 1997.
[131] P. Sajeesh and A. K. Sen, "Particle separation and sorting in microfluidic devices: a review," *Microfluid. Nanofluidics*, vol. 17, no. 1, pp. 1–52, Nov. 2013.
[132] J. Luo, E. L. Nelson, G. P. Li, and M. Bachman, "Microfluidic dielectrophoretic sorter using gel vertical electrodes," *Biomicrofluidics*, vol. 8, no. 3, p. 034105, May 2014.
[133] P. R. C. Gascoyne, J. Noshari, T. J. Anderson, and F. F. Becker, "Isolation of rare cells from cell mixtures by dielectrophoresis," *Electrophoresis*, vol. 30, no. 8, pp. 1388–1398, 2009.
[134] Lisen Wang, L. Flanagan, and A. P. Lee, "Side-Wall Vertical Electrodes for Lateral Field Microfluidic Applications," *Microelectromechanical Syst. J. Of*, vol. 16, no. 2, pp. 454–461, 2007.
[135] B. Y. Park and M. J. Madou, "3-D electrode designs for flow-through dielectrophoretic systems," *Electrophoresis*, vol. 26, no. 19, pp. 3745–3757, Oct. 2005.
[136] F. E. H. Tay, L. Yu, A. J. Pang, and C. Iliescu, "Electrical and thermal characterization of a dielectrophoretic chip with 3D electrodes for cells manipulation," *Electrochimica Acta*, vol. 52, no. 8, pp. 2862–2868, Feb. 2007.
[137] D. Holmes, M. E. Sandison, N. G. Green, and H. Morgan, "On-chip high-speed sorting of micron-sized particles for high-throughput analysis," *Nanobiotechnology IEE Proc. -*, vol. 152, no. 4, pp. 129–135, Aug. 2005.

[138] I.-F. Cheng, H.-C. Chang, D. Hou, and H.-C. Chang, "An integrated dielectrophoretic chip for continuous bioparticle filtering, focusing, sorting, trapping, and detecting," *Biomicrofluidics*, vol. 1, no. 2, p. 021503, Jun. 2007.
[139] R. Martinez-Duarte, "Microfabrication technologies in dielectrophoresis applications—A review," *Electrophoresis*, vol. 33, no. 21, pp. 3110–3132, Nov. 2012.
[140] R. Martinez-Duarte, R. A. Gorkin III, K. Abi-Samra, and M. J. Madou, "The integration of 3D carbon-electrode dielectrophoresis on a CD-like centrifugal microfluidic platform," *Lab. Chip*, vol. 10, no. 8, pp. 1030–1043, 2010.
[141] M. del C. Jaramillo, E. Torrents, R. Martínez-Duarte, M. J. Madou, and A. Juárez, "On-line separation of bacterial cells by carbon-electrode dielectrophoresis," *Electrophoresis*, vol. 31, no. 17, pp. 2921–2928, Sep. 2010.
[142] R. Martinez-Duarte, P. Renaud, and M. J. Madou, "A novel approach to dielectrophoresis using carbon electrodes," *Electrophoresis*, vol. 32, no. 17, pp. 2385–2392, Sep. 2011.
[143] R. Martinez-Duarte, F. Camacho-Alanis, P. Renaud, and A. Ros, "Dielectrophoresis of lambda-DNA using 3D carbon electrodes," *Electrophoresis*, vol. 34, no. 7, pp. 1113–1122, Apr. 2013.
[144] L. Wang, L. A. Flanagan, N. L. Jeon, E. Monuki, and A. P. Lee, "Dielectrophoresis switching with vertical sidewall electrodes for microfluidic flow cytometry," *Lab. Chip*, vol. 7, no. 9, pp. 1114–1120, 2007.
[145] J. Vykoukal, D. M. Vykoukal, S. Freyberg, E. U. Alt, and P. R. C. Gascoyne, "Enrichment of putative stem cells from adipose tissue using dielectrophoretic field-flow fractionation," *Lab. Chip*, vol. 8, no. 8, p. 1386, 2008.
[146] R. Pethig, Y. Huang, X. Wang, and J. P. H. Burt, "Positive and negative dielectrophoretic collection of colloidal particles using interdigitated castellated microelectrodes," *J. Phys. Appl. Phys.*, vol. 25, no. 5, p. 881, May 1992.
[147] S. Fiedler, S. Shirley, T. Schnelle, and G. Fuhr, *Anal Chem*, vol. 70, no. 9, p. 1909, 1998.
[148] L. Wang, J. Lu, S. A. Marchenko, E. S. Monuki, L. A. Flanagan, and A. P. Lee, "Dual frequency dielectrophoresis with interdigitated sidewall electrodes for microfluidic flow-through separation of beads and cells," *Electrophoresis*, vol. 30, no. 5, pp. 782–791, Mar. 2009.
[149] A. Jahn, W. N. Vreeland, M. Gaitan, and L. E. Locascio, "Controlled Vesicle Self-Assembly in Microfluidic Channels with Hydrodynamic Focusing," *J. Am. Chem. Soc.*, vol. 126, no. 9, pp. 2674–2675, Mar. 2004.
[150] J. Yang, Y. Huang, X.-B. Wang, F. F. Becker, and P. R. C. Gascoyne, "Cell Separation on Microfabricated Electrodes Using Dielectrophoretic/Gravitational Field-Flow Fractionation," *Anal. Chem.*, vol. 71, no. 5, pp. 911–918, Mar. 1999.
[151] X.-B. Wang, J. Vykoukal, F. F. Becker, and P. R. C. Gascoyne, "Separation of Polystyrene Microbeads Using Dielectrophoretic/Gravitational Field-Flow-Fractionation," *Biophys. J.*, vol. 74, no. 5, pp. 2689–2701, May 1998.
[152] V. Gupta, I. Jafferji, M. Garza, V. O. Melnikova, D. K. Hasegawa, R. Pethig, and D. W. Davis, "ApoStream™, a new dielectrophoretic device for antibody independent isolation and recovery of viable cancer cells from blood," *Biomicrofluidics*, vol. 6, no. 2, p. 024133, Jun. 2012.
[153] R. D. Sochol, S. Li, L. P. Lee, and L. Lin, "Continuous flow multi-stage microfluidic reactors via hydrodynamic microparticle railing," *Lab. Chip*, vol. 12, no. 20, pp. 4168–4177, Sep. 2012.

[154] C. Kantak, S. Beyer, L. Yobas, T. Bansal, and D. Trau, "A 'microfluidic pinball' for on-chip generation of Layer-by-Layer polyelectrolyte microcapsules," *Lab. Chip*, vol. 11, no. 6, pp. 1030–1035, Mar. 2011.
[155] R. D. Sochol, R. Ruelos, V. Chang, M. E. Dueck, L. P. Lee, and L. Lin, "Continuous flow layer-by-layer microbead functionalization via a micropost array railing system," in *Solid-State Sensors, Actuators and Microsystems Conference (Transducers), 2011 16th International*, June, pp. 1761–1764.
[156] H. Shafiee, J. L. Caldwell, M. B. Sano, and R. V. Davalos, "Contactless dielectrophoresis: a new technique for cell manipulation," *Biomed. Microdevices*, vol. 11, no. 5, pp. 997–1006, May 2009.
[157] H. Shafiee, M. B. Sano, E. A. Henslee, J. L. Caldwell, and R. V. Davalos, "Selective isolation of live/dead cells using contactless dielectrophoresis (cDEP)," *Lab. Chip*, vol. 10, no. 4, pp. 438–445, Feb. 2010.
[158] G. Mernier, N. Piacentini, T. Braschler, N. Demierre, and P. Renaud, "Continuous-flow electrical lysis device with integrated control by dielectrophoretic cell sorting," *Lab. Chip*, vol. 10, no. 16, p. 2077, 2010.
[159] C.-P. Jen and W.-F. Chen, "An insulator-based dielectrophoretic microdevice for the simultaneous filtration and focusing of biological cells," *Biomicrofluidics*, vol. 5, no. 4, p. 044105, 2011.
[160] A. Salmanzadeh, H. Kittur, M. B. Sano, P. C. Roberts, E. M. Schmelz, and R. V. Davalos, "Dielectrophoretic differentiation of mouse ovarian surface epithelial cells, macrophages, and fibroblasts using contactless dielectrophoresis," *Biomicrofluidics*, vol. 6, no. 2, p. 024104, Jun. 2012.
[161] C.-F. Chou, J. O. Tegenfeldt, O. Bakajin, S. S. Chan, E. C. Cox, N. Darnton, T. Duke, and R. H. Austin, "Electrodeless Dielectrophoresis of Single- and Double-Stranded DNA," *Biophys. J.*, vol. 83, no. 4, pp. 2170–2179, Oct. 2002.
[162] S. Bhattacharya, T.-C. Chao, N. Ariyasinghe, Y. Ruiz, D. Lake, R. Ros, and A. Ros, "Selective trapping of single mammalian breast cancer cells by insulator-based dielectrophoresis," *Anal. Bioanal. Chem.*, vol. 406, no. 7, pp. 1855–1865, Mar. 2014.
[163] N. Demierre, T. Braschler, R. Muller, and P. Renaud, "Focusing and continuous separation of cells in a microfluidic device using lateral dielectrophoresis," *Sens. Actuators B Chem.*, vol. 132, no. 2, pp. 388–396, Jun. 2008.
[164] R. C. Gallo-Villanueva, V. H. Pérez-González, R. V. Davalos, and B. H. Lapizco-Encinas, "Separation of mixtures of particles in a multipart microdevice employing insulator-based dielectrophoresis," *Electrophoresis*, vol. 32, no. 18, pp. 2456–2465, 2011.
[165] B. H. Lapizco-Encinas, B. A. Simmons, E. B. Cummings, and Y. Fintschenko, "Dielectrophoretic Concentration and Separation of Live and Dead Bacteria in an Array of Insulators," *Anal. Chem.*, vol. 76, no. 6, pp. 1571–1579, Mar. 2004.
[166] Y.-K. Cho, S. Kim, K. Lee, C. Park, J.-G. Lee, and C. Ko, "Bacteria concentration using a membrane type insulator-based dielectrophoresis in a plastic chip," *Electrophoresis*, vol. 30, no. 18, pp. 3153–3159, Sep. 2009.
[167] N. Demierre, T. Braschler, P. Linderholm, U. Seger, H. van Lintel, and P. Renaud, "Characterization and optimization of liquid electrodes for lateral dielectrophoresis," *Lab. Chip*, vol. 7, no. 3, pp. 355–365, 2007.
[168] F. Gielen, A. J. deMello, and J. B. Edel, "Dielectric Cell Response in Highly Conductive Buffers," *Anal. Chem.*, vol. 84, no. 4, pp. 1849–1853, Feb. 2012.

[169] J. Chen, M. Abdelgawad, L. Yu, N. Shakiba, W.-Y. Chien, Z. Lu, W. R. Geddie, M. A. S. Jewett, and Y. Sun, "Electrodeformation for single cell mechanical characterization," *J. Micromechanics Microengineering*, vol. 21, no. 5, p. 054012, May 2011.
[170] Y. Huang, R. Holzel, R. Pethig, and X.-B. Wang, "Differences in the AC electrodynamics of viable and non-viable yeast cells determined through combined dielectrophoresis and electrorotation studies," *Phys. Med. Biol.*, vol. 37, no. 7, p. 1499, Jul. 1992.
[171] Y. Shi, D. D. Ryu, and R. Ballica, "Rheological properties of mammalian cell culture suspensions: Hybridoma and HeLa cell lines," *Biotechnol. Bioeng.*, vol. 41, no. 7, pp. 745–754, Mar. 1993.
[172] R. Pethig, "Dielectric Properties of Biological Materials: Biophysical and Medical Applications," *IEEE Trans. Electr. Insul.*, vol. EI-19, no. 5, pp. 453–474, Oct. 1984.
[173] A. Goldup, S. Ohki, and J. F. Danielli, "Recent Progress in Surface Science," *Danielli JF Riddiford AC Rosenb. MD Ed*, vol. 3, p. 193, 1970.
[174] J. Luo, E. Nelson, G.-P. Li, and M. Bachman, "Electronic-microfluidic system for sorting particles and whole blood using gel electrodes," in *Electronic Components and Technology Conference (ECTC), 2013 IEEE 63rd*, 2013, pp. 1905–1911.
[175] G. M. Whitesides, "Cool, or simple and cheap? Why not both?," *Lab. Chip*, vol. 13, no. 1, pp. 11–13, Nov. 2012.
[176] L. Altomare, M. Borgatti, G. Medoro, N. Manaresi, M. Tartagni, R. Guerrieri, and R. Gambari, "Levitation and movement of human tumor cells using a printed circuit board device based on software-controlled dielectrophoresis," *Biotechnol. Bioeng.*, vol. 82, no. 4, pp. 474–479, May 2003.
[177] L. A. Marshall, L. L. Wu, S. Babikian, M. Bachman, and J. G. Santiago, "Integrated printed circuit board device for cell lysis and nucleic acid extraction," *Anal. Chem.*, vol. 84, no. 21, pp. 9640–9645, 2012.
[178] T. W. Herling, T. Müller, L. Rajah, J. N. Skepper, M. Vendruscolo, and T. P. J. Knowles, "Integration and characterization of solid wall electrodes in microfluidic devices fabricated in a single photolithography step," *Appl. Phys. Lett.*, vol. 102, no. 18, p. 184102, May 2013.
[179] J. F. Hainfeld, D. N. Slatkin, T. M. Focella, and H. M. Smilowitz, "Gold nanoparticles: a new X-ray contrast agent," *Br. J. Radiol.*, 2014.
[180] E. W. Kemna, L. I. Segerink, F. Wolbers, I. Vermes, and A. van den Berg, "Label-free, high-throughput, electrical detection of cells in droplets," *Analyst*, vol. 138, no. 16, pp. 4585–4592, 2013.
[181] Á. Ríos, M. Zougagh, and M. Avila, "Miniaturization through lab-on-a-chip: Utopia or reality for routine laboratories? A review," *Anal. Chim. Acta*, vol. 740, pp. 1–11, Aug. 2012.
[182] R. Prasad, *Surface Mount Technology: Principles and Practice*. Springer Science & Business Media, 2013.
[183] P. Neužil, C. D. M. Campos, C. C. Wong, J. B. W. Soon, J. Reboud, and A. Manz, "From chip-in-a-lab to lab-on-a-chip: towards a single handheld electronic system for multiple application-specific lab-on-a-chip (ASLOC)," *Lab. Chip*, vol. 14, no. 13, pp. 2168–2176, 2014.
[184] L. F. Capitan-Vallvey and A. J. Palma, "Recent developments in handheld and portable optosensing—A review," *Anal. Chim. Acta*, vol. 696, no. 1, pp. 27–46, 2011.
[185] J. G. Bralla, "Design for manufacturability handbook," 1997.

[186] B. W. An, K. Kim, H. Lee, S.-Y. Kim, Y. Shim, D.-Y. Lee, J. Y. Song, and J.-U. Park, "High-Resolution Printing of 3D Structures Using an Electrohydrodynamic Inkjet with Multiple Functional Inks," *Adv. Mater.*, 2015.
[187] S. E. Chung, W. Park, S. Shin, S. A. Lee, and S. Kwon, "Guided and fluidic self-assembly of microstructures using railed microfluidic channels," *Nat. Mater.*, vol. 7, no. 7, pp. 581–587, 2008.
[188] C. D. Chin, T. Laksanasopin, Y. K. Cheung, D. Steinmiller, V. Linder, H. Parsa, J. Wang, H. Moore, R. Rouse, G. Umviligihozo, E. Karita, L. Mwambarangwe, S. L. Braunstein, J. van de Wijgert, R. Sahabo, J. E. Justman, W. El-Sadr, and S. K. Sia, "Microfluidics-based diagnostics of infectious diseases in the developing world," *Nat. Med.*, vol. 17, no. 8, pp. 1015–1019, Aug. 2011.